FACULTAD DE CIENCIAS

Departamento de Química Física Aplicada

CATALIZADORES BIFUNCIONALES ACTIVOS EN LA CONVERSIÓN DIRECTA DE ÁCIDO LEVULÍNICO A VALERATO DE ETILO

Memoria para aspirar al

grado de DOCTOR

Martín Muñoz Olasagasti

Instituto de Catálisis y
Petroleoquímica, C.S.I.C. Madrid,
2022

Martín Muñoz Olasagasti

CATALIZADORES BIFUNCIONALES ACTIVOS EN LA CONVERSIÓN DIRECTA DE ÁCIDO LEVULÍNICO A VALERATO DE ETILO

Memoria para aspirar al

grado de DOCTOR

Director:

Dr. D. Rafael Mariscal López

Investigador Científico

Instituto de Catálisis y Petroleoquímica (CSIC)

UNIVERSIDAD AUTÓNOMA DE

MADRID FACULTAD DE

CIENCIAS

Dpto. Química Física Aplicada

Madrid, 2022

AGRADECIMIENTOS

En primer lugar, quería agradecer al Dr. Rafael Mariscal, mi director y tutor por haber hecho posible el desarrollo de esta Tesis, por haber confiado en mí desde un principio. Por haberme seguido apoyando cuando, por motivos profesionales, se hizo más difícil encontrar el momento para encontrarnos y seguir adelante con este proyecto.

Al Dr. Manuel López Granados, por todas las horas que ha dedicado a apoyar este trabajo, las horas de discusión de resultados y la ayuda para el desarrollo experimental del mismo. Por todas las sugerencias que ha hecho para la mejora de esta Tesis.

Quería agradecer también al Grupo de Ingeniería Química y Ambiental, al Dr. Gabriel Morales y al Dr. José Iglesias por su colaboración. A la Unidad Asociada Laboratorio de Materiales para Catálisis en la Universidad de Málaga y en especial al Dr. Pedro Maireles-Torres y al Dr. Juan A. Cecilia por haberme recibido en su laboratorio y por haber contribuido a este trabajo. Y finalmente al profesor J. Dumesic de la UW-Madison (USA) por su apoyo y contribución a esta investigación.

También quería mencionar mi agradecimiento al director del Instituto de Catálisis y Petroleoquímica, al Dr. Enrique Sastre, así como al Personal Administrativo y de Servicios del Instituto. Agradecer también a Irene Salazar por todo su trabajo especialmente en esta última etapa y a Yolanda Ródenas por su colaboración en los primeros momentos de trabajo.

Esta Tesis tampoco habría sido posible sin el apoyo de Aran, sin su ánimo, sin su comprensión y su generosidad.

No podía dejarme en estos agradecimientos a la tía Uge, por sus consejos en tantas ocasiones.

Por último, quería agradecer a mi madre, por todo.

TABLA DE CONTENIDOS

1. RESUMEN

El desarrollo industrial ha supuesto una mayor demanda de combustibles fósiles para la obtención de energía. Éstos son también de gran interés como fuente de partida para obtener productos químicos con diversas aplicaciones. Existe un gran desarrollo en el uso de **energías alternativas a estos combustibles fósiles,** pero debe buscarse aún fuentes que cubran las necesidades tanto energéticas como de moléculas plataforma para la obtención de diferentes productos químicos. En las primeras etapas de la búsqueda de estas alternativas, se empleaba el etanol proveniente de cereales, así como los ésteres metílicos de ácidos grasos de origen vegetal. El mayor inconveniente de esta primera generación de biocombustibles consistía en la competencia con la alimentación humana y animal, distorsionando los mercados de estas materias primas. El uso de lignocelulosa procedente de la biomasa subsana este problema al ser ésta no comestible, barata, abundante, ampliamente distribuida geográficamente y renovable.

El **uso de lignocelulosa** como materia prima de partida plantea el reto de obtener a partir de ella **compuestos plataforma** desde los que obtener un amplio abanico de biocombustibles y productos químicos. El **ácido levulínico (AL)** ha demostrado ser una molécula plataforma que puede obtenerse desde la lignocelulosa. La funcionalidad del AL lo convierte en un compuesto plataforma. Solo mencionar como ejemplo que mediante la hidrogenación del AL puede obtenerse un amplio abanico de productos con muy diversas aplicaciones como el 2-metiltetrahidrofurano (MTHF), el 1,4-pentanodiol, la gamma-valerolactona (GVL), o el ácido valérico (AV) y los ésteres valéricos.

Los **combustibles valéricos**, como se denomina al ácido valérico y ciertos ésteres valéricos, han despertado un gran interés ya que sus propiedades hacen que se trate de combustibles líquidos compatibles con los motores de combustión actuales, especialmente el valerato de etilo (VE) y el valerato de pentilo. La obtención de combustibles valéricos a partir de AL es una reacción conocida y a la que en la última década se ha prestado mucha atención, tanto desde el punto de vista académico como industrial.

El gran interés por esta reacción ha promovido la búsqueda de **catalizadores bifuncionales ácido e hidrogenantes** capaces de completar la reacción en un sólo reactor con altos rendimientos, evitando así las separaciones intermedias

y la necesidad de dos o más catalizadores para obtener los productos de interés. Se ha logrado identificar sistemas catalíticos capaces de llevar a cabo esta reacción, sin embargo un estudio pormenorizado de las necesidades catalíticas que deben cubrir estos catalizadores bifuncionales se hace necesario.

El **objetivo del presente trabajo** ha sido el desarrollo de sistemas catalíticos bifuncionales activos en la conversión directa del AL en combustibles valéricos. Además, la modificación y análisis de los catalizadores que se realiza en el mismo, persigue la comprensión del proceso y de las características que son necesarias para la obtención de catalizadores activos, selectivos y estables en este proceso.

Las dos primeras publicaciones "*Direct Conversion of Levulinic Acid into Valeric Biofuels Using Pd Supported Over Zeolites as Catalysts*" y "*Elucidating the roles of acid site nature and strength in the direct conversion of levulinic acid into ethyl valerate: the case of Zr-modified Beta zeolite-supported Pd catalysts"* se empleó un reactor tipo *batch* (sistema discontinuo y fase líquida) y catalizadores basados en Pd como fuente de centros hidrogenantes. En el **primero de los trabajos** se impregnó Pd sobre una serie de soportes comerciales de tipo aluminosilicatos. Se trata de dos zeolitas con estructura ZSM5 y beta así como una sílica alúmina amorfa. Cuentan, por tanto, con propiedades texturales y ácidas distintas que dan lugar a una familia de catalizadores con diferentes características. Los resultados determinan la importancia de la estructura del soporte, así como a la necesidad de acidez superficial en cantidad y fortaleza concretas. Centros ácidos demasiado débiles se mostraron incapaces de abrir el anillo de gamma-valerolactona (GVL) mientras que, catalizadores con centros suficientemente ácidos reducían el balance de carbono incrementando la proporción de subproductos no identificados.

En el **segundo artículo**, se incorporó una misma cantidad de Pd (2 % en peso) sobre una familia de zeolitas. En este caso, se trabajó con una zeolita beta comercial como punto de partida para sustituir en ella proporciones variables del Al por átomos de Zr en la estructura. Con esta estrategia, se persigue el análisis del efecto que tiene la naturaleza de los centros ácidos sobre la actividad de los catalizadores. Se busca que la estructura y textura de todos los soportes sea la misma, con la misma carga de metal hidrogenante y que los cambios

observados en la actividad tengan su origen en las diferencias de acidez de los soportes. Los resultados obtenidos permiten afirmar que tanto los centros ácidos fuertes de tipo Brønsted como Lewis son capaces de catalizar esta reacción. Sin embargo, los centros débiles Lewis no lo son bajo nuestras condiciones de reacción y, en caso de una gran cantidad de centros ácidos Brønsted fuertes, éstos son capaces de descomponer los productos de interés además de provocar la desactivación del catalizador al producir depósitos carbonosos sobre ellos. La estabilidad del catalizador se ve afectada por la desactivación reversible con residuos carbonosos e irreversible por la ligera formación de fase Al_2O_3 a partir del Al de red del soporte.

El **tercer trabajo**, titulado "*The relevance of the Lewis acid sites on gas phase reaction of levulinic acid into ethyl valerate using CoSBA-xAl bifunctional catalysts"* busca sustituir los metales nobles como el Pd empleado en los dos trabajos anteriores por el Co ensayando su actividad en un reactor de lecho fijo (sistema continuo). Este artículo estudia una familia de soportes basados en la SBA-15 sobre el que se incorpora una cantidad creciente de Al con el objetivo de modular la naturaleza, fortaleza y cantidad de centros ácidos en este soporte. En todos ellos se ha mantenido el contenido en Co constante en un 10 % en peso tratando de no influir en la función reductora. La acidez del catalizador se deriva de la presencia de Al en el soporte y por tanto es mayor con la concentración del mismo. Los resultados catalíticos muestran una tendencia en la actividad que se comporta de forma paralela al grado de sustitución del Si por Al. Así, cuando el contenido en Al está por debajo de un umbral, el producto mayoritario es la GVL. Esto es debido a que la acidez del sistema es insuficiente para catalizar la apertura del anillo de GVL. Sin embargo, superado cierto contenido en Al, sí se cataliza esta apertura y se logran los combustibles valéricos con alta selectividad y rendimiento.

En conclusión, se ha trabajado con dos metales y diferentes tipos de soportes ácidos para lograr una mayor comprensión sobre las necesidades catalíticas del proceso. Se ha encontrado relaciones entre las propiedades de los catalizadores empleados y la actividad obtenida. Los resultados obtenidos para algunos de los sistemas catalíticos han superado el rendimiento del 90 % a los productos de interés y con catalizadores suficientemente estables.

2. INTRODUCCIÓN

2.1 Aspectos generales

2.1.1 Escenario socio-económico de los recursos energéticos.

El crecimiento de la población y el desarrollo industrial, especialmente en los países emergentes, ha incrementado el consumo de combustibles fósiles. Este crecimiento ha comprometido su suministro y generado tensiones en su precio por la oferta insuficiente para satisfacer la demanda. Además, el consumo de éstos emite gases de combustión a la atmósfera que tienen efectos nocivos para el medioambiente. Desde hace décadas, la consciencia de este problema ha impulsado la investigación sobre fuentes de energía alternativas. La energía solar, eólica o hidroeléctrica entre otras, se han denominado energías renovables por su capacidad de aprovecharse sin ser consumida su fuente. Además, se mitiga el problema de la emisión de gases perjudiciales al no generarse éstos durante su uso.

Sin embargo, son dos los principales problemas que plantean las fuentes renovables arriba mencionadas. Por un lado, y pese a que su desarrollo haya evolucionado significativamente en las últimas décadas, existe aún aplicaciones en las que no han sido capaces de reemplazar por completo a las fuentes tradicionales. Un ejemplo de esto es el que se presenta en el transporte, en el que, por el momento, siguen predominando los combustibles fósiles por las dificultades para la adaptación de las energías renovables a estas aplicaciones móviles.

La Directiva Europea 2018/2001[1], *relativa al fomento del uso de energía procedente de fuentes renovables*, marca objetivos para el uso de energías renovables en la UE con los horizontes de 2020 y 2030. En ella, se establece que el 32 % de la energía consumida en la UE deberá tener origen renovable en 2030. Además de este objetivo global, la Directiva define un objetivo específico del 14 % de origen renovable para la energía del sector transporte. El riesgo de que el cumplimiento de este objetivo conduzca a un cambio de uso del suelo en que prime la obtención de biocarburantes frente al uso alimentario, llevó a establecer, dentro de esta misma Directiva, una limitación a la proporción de biocarburantes, biolíquidos o combustibles de biomasa con riesgo elevado de cambio indirecto del uso de la tierra.

Por otro lado, el uso de combustibles fósiles no tiene por único objetivo la obtención de energía. Los combustibles fósiles son fuente de gran cantidad de moléculas empleadas en síntesis de productos químicos de alto valor añadido. Algunas fuentes como las arriba mencionadas (eólica, solar, hidroeléctrica…) sí suponen una alternativa energética renovable, pero carecen de la capacidad de proporcionar los productos que se obtienen también de los recursos fósiles.

El uso de la biomasa presenta la ventaja de servir como fuente de compuestos plataforma que pueden transformarse para obtener gran variedad de productos. Además, algunos de los derivados que pueden obtenerse de la biomasa son capaces de emplearse en aplicaciones como el transporte, dando lugar a biocarburantes y contribuyendo por tanto al cumplimiento del 14 % de carburantes con origen renovable establecido por la UE para 2030.

2.1.2 Combustibles líquidos derivados de la biomasa

La búsqueda de biocombustibles líquidos para el transporte ha dado lugar a diferentes alternativas. Entre ellos, el bioetanol es el que mayor desarrollo ha vivido, siendo el que tiene una mayor implantación en la actualidad. La obtención del bioetanol puede llevarse a cabo mediante la fermentación de la biomasa[2]. Sin embargo, las propiedades del etanol no son las ideales para un combustible por su menor densidad energética, y su miscibilidad con el agua[3].

Una alternativa a este bioetanol consiste en el uso de biodiesel obtenido por transesterificación de los triglicéridos presentes en la biomasa para obtener ésteres metílicos de ácidos grasos. Las propiedades de éstos los hacen compatibles con los motores de combustión de diésel actuales, reducen las emisiones de CO_2 y mejoran la lubricación de los motores[4]. Algunos de los inconvenientes que presentan estos biocombustibles son su menor compatibilidad con las temperaturas bajas y sus propiedades corrosivas para algunos metales. Sin embargo, sí son una alternativa viable para su combinación con el diésel. El uso de diésel verde, el derivado hidrogenado de los ésteres metílicos de ácidos grasos, es capaz de solucionar algunos de los inconvenientes arriba descritos, reduciendo su corrosión sobre los metales, reduciendo la temperatura a la que puede ser empleado y haciendo viable su uso, en estado puro o diluido, en los motores de combustión actuales[5].

La búsqueda de carburantes alternativos también ha recurrido a la reacción de Fischer-Tropsch. Con este fin, la biomasa debe ser convertida en gas de síntesis, compuesto mayoritariamente por H_2 y CO y posteriormente, ser transformada en los productos de interés, fundamentalmente hidrocarburos líquidos. El gas de síntesis obtenido a partir de la biomasa debe ser tratado para reducir su contenido en especies que resultan perjudiciales para los catalizadores como son los compuestos sulfurados o nitrogenados. Este proceso de Fischer-Tropsch permite obtener hidrocarburos de diferente longitud y, por tanto, diferentes propiedades físicas. Los parámetros fundamentales para dirigir la reacción hacia unos productos u otros son la relación entre el hidrógeno y el monóxido de carbono, la temperatura a la que tiene lugar el proceso y la naturaleza del catalizador[6–8].

Este gas de síntesis puede ser empleado también para la obtención de metanol o de dimetil-éter, ambos compuestos con propiedades que los hacen adecuados como biocombustibles[8].

Otra de las líneas que se ha desarrollado para la obtención de biocarburantes es la obtención de combustibles valéricos dentro de los denominados biocombustibles avanzados. Éstos, han demostrado su capacidad para combinarse con los combustibles actuales e incluso reemplazarlos por completo. Por sus propiedades, el valerato de etilo ha mostrado su capacidad de añadirse a la gasolina y el valerato de pentilo al diésel pudiendo emplearse ambos en los motores de combustión actuales[9,10].

A pesar de las ventajas mostradas, la biomasa presenta potenciales problemas que han quedado de manifiesto con su desarrollo. En caso de que las fuentes de la biomasa compitan con la alimentación humana, éstas pueden agravar la falta de alimento, elevando el precio de ciertos alimentos o desplazando cultivos enfocados a la alimentación humana por otros de mayor rendimiento para la obtención de biomasa. La primera generación de fuentes de biomasa como el etanol procedente del maíz o caña de azúcar o los ésteres metílicos procedentes de aceites vegetales presentaban este inconveniente. En una siguiente etapa de desarrollo, se ha trabajado con fuentes que no compitan con la alimentación humana desarrollándose así una segunda generación de biocarburantes[11]. Este paso busca la aplicación de fuentes de biomasa que sean abundantes, baratas y

que incluso podrían considerarse un residuo para obtener energía y moléculas de las que pueda obtenerse productos de alto valor añadido. Esta transición hacia los biocombustibles de segunda generación también está impulsada por la normativa europea, que limitará, desde 2023, el cómputo de los primeros biocombustibles para el cumplimiento de los objetivos de la Directiva 2018/2001.

2.1.3 Producción de ácido levulínico desde azúcares derivados de lignocelulosa

La lignocelulosa, presente en la biomasa vegetal, cumple con la característica de ser abundante y no interferir con la alimentación humana y, por tanto, ha despertado gran interés como fuente primaria para la sustitución de los combustibles fósiles. La lignocelulosa se compone en un 38 a 50 % de celulosa, un 23 a 32 % de hemicelulosa y en un 15 a 30 % de lignina[12]. La celulosa es un polímero lineal de glucosa unido por enlaces β-1,4 y enlaces de hidrógeno entre cadenas adyacentes confiriéndole estructura cristalina y dificultando su degradación. La hemicelulosa es un heteropolímero ramificado mayoritariamente constituido por unidades de xilosa. La lignina es también un heteropolímero ramificado, pero en este caso compuesto fundamentalmente de alcoholes aromáticos, principalmente alcohol p-cumarílico, alcohol coniferílico y alcohol sinapílico. La lignocelulosa se plantea como fuente alternativa al petróleo, pero, al igual que sucede con el petróleo, debe procesarse para el aprovechamiento de esta fuente primaria.

A partir de la lignocelulosa puede obtenerse diferentes moléculas de las denominadas moléculas plataforma por su capacidad para ser transformadas en otros productos de alto valor añadido. Entre ellas cabe destacar las doce que el Departamento de Energía de EEUU identificó, de entre las derivadas de la biomasa,[13] con capacidad de generar sustancias alternativas a las obtenidas del petróleo. El ácido levulínico se encuentra en la lista de estas moléculas por la gran cantidad de productos que pueden derivarse de él[14].

Como queda patente tras lo descrito en el apartado anterior, existen diferentes opciones para la obtención de biocombustibles. Sin embargo, la presente Tesis se centra en la transformación del AL, uno de los posibles productos de ésta, para la obtención de biocombustibles a partir de la lignocelulosa y, más

concretamente de la biomasa celulósica y hemicelulósica. El ácido levulínico, o ácido 4-oxopentanóico, es un cetoácido líquido entre los 306 K y los 518 K, soluble en agua y en disolventes polares como el etanol[15].

Como ya se ha mencionado, la hemicelulosa se trata de un polímero mayoritariamente compuesto por xilosa y así, por medio de su hidrólisis, puede descomponerse el polímero y recuperar la xilosa. La deshidratación de la xilosa, por ser una pentosa, proporcionará furfural; la hidrogenación de la xilosa dará lugar al xilitol, otra de las doce moléculas plataforma consideradas por el Departamento de Energía de EEUU. Por otro lado, la celulosa, el componente mayoritario de la lignocelulosa, es un polímero formado por monómeros de glucosa e igualmente, de su hidrólisis podrá obtenerse los monómeros de glucosa[16]. La deshidratación de ésta, sin embargo, proporcionará 5-hidroximetilfurfural. La hidrólisis ácida de este 5-hidroximetilfurfural proporciona ácido levulínico[17–19] además de ácido fórmico.

El ácido levulínico también puede obtenerse a partir del furfural obtenido de las pentosas, siendo necesario en este caso una etapa adicional de hidrogenación. Este proceso se ha llevado a cabo empleando primero catalizadores metálicos con los que hidrogenar el furfural a ácido furfurílico que es transformado posteriormente por medio de una hidrólisis catalizada por ácidos como la zeolita HZSM-5 o la Amberlyst 15[20,21]. Así, se puede obtener el ácido levulínico tanto de la fracción proveniente de los azúcares C-6 de la celulosa como de los C-5 provenientes de la hemicelulosa, como puede observarse en la Figura 1.[22,23]

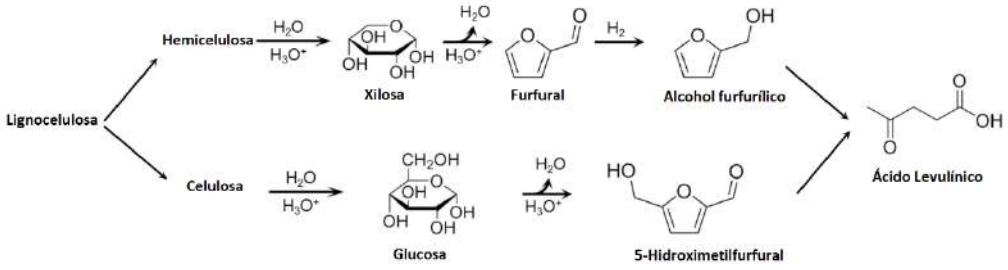

Figura 1. Rutas de obtención del AL a partir de la lignocelulosa.

La obtención a escala industrial del ácido levulínico a partir de la celulosa y hemicelulosa presente en la lignocelulosa se ha descrito previamente en la literatura[3,24–26]. Para ello, se propone un tratamiento de la fuente de lignocelulosa con ácidos fuertes inorgánicos como el clorhídrico o el sulfúrico a temperaturas sobre los 373 K para lograr la hidrólisis de los polisacáridos y obtener los monómeros correspondientes. Posteriormente, este hidrolizado se trataría en ácidos diluidos durante 20 a 48 horas si bien incrementando temperatura y presión podría reducirse el tiempo de esta segunda etapa. La purificación del ácido levulínico así obtenido podría llevarse a cabo o bien por extracción con disolventes orgánicos o bien por destilación[17]. Uno de los inconvenientes de procesar la biomasa en su conjunto y que dificulta el proceso de separación es la gran variedad de productos obtenidos de la biomasa si se lleva a cabo procesos inespecíficos y sin separación previa de los componentes de la biomasa.

Es por esto por lo que se ha propuesto etapas previas para la separación de las fracciones de la lignocelulosa, así como la reacción en condiciones menos agresivas. Se busca obtener así, a partir de los azúcares, moléculas intermedias menos reactivas que las de partida y que puedan funcionalizarse posteriormente para alcanzar las moléculas plataforma de interés[27]. El uso de tratamiento mecánico previo ha demostrado facilitar el proceso de obtención de los azúcares a partir de la lignocelulosa[28,29]. Con este procesado mecánico previo se ha logrado reducir la cantidad de ácido necesaria para impregnar la biomasa y que se alcance rendimientos similares con una importante reducción de uso de ácidos con el consiguiente ahorro económico.

También se ha recurrido a otros enfoques como el uso de una bifase agua gamma-valerolactona para llevar a cabo la reacción[30]. El uso de gamma-valerolactona en este proceso plantea ventajas significativas al favorecer la solubilización de la celulosa además de ahorrar la separación del ácido levulínico de la fase orgánica al ser la gamma-valerolactona un producto de la propia hidrogenación del ácido levulínico.

La obtención a escala industrial del ácido levulínico a partir de la lignocelulosa ya se alcanzó en 2015 por la compañía Biofine.[28] Su proceso parte de residuos urbanos aunque podría partir de corrientes de lignocelulosa de diferentes

orígenes. Emplean temperaturas de 483 K y tiempos de residencia cortos en reactores en flujo en los que, en cuestión de segundos, se obtiene furfural e hidroximetilfurfural. En una segunda etapa, el hidroximetilfurfural se trata durante 20 minutos a 463 K para lograr obtener ácido levulínico con rendimientos del 75 %. Para trabajar en continuo debe molturarse la corriente de alimentación hasta tener tamaños de entre 0,5 y 1 cm. La importancia de este proceso reside en que la obtención de ácido levulínico partiendo de la biomasa es ya una realidad a escala industrial y que permite continuar con el desarrollo de las etapas que permitan valorizar el ácido levulínico que así se obtiene.

2.1.4 Biocombustibles valéricos: ácido valérico y valerato de etilo

El ácido levulínico, presenta una gran versatilidad en su reactividad por ser un ácido γ-ceto-carboxílico[31]. El propio ácido levulínico tiene múltiples aplicaciones entre las que cabe destacar su uso en la industria farmacéutica[32] o como disolvente. Sin embargo, el mayor interés de esta molécula reside en su gran versatilidad química que permite transformarla en productos con propiedades muy diversas[33].

Una reacción que ha centrado un gran interés por la variedad de productos que puede proporcionar a partir del ácido levulínico es la hidrogenación de éste. A partir de ella, puede obtenerse gamma-valerolactona que puede emplearse como disolvente o aditivo alimentario[34], 2-metiltetrahidrofurano con aplicación como carburante[35], 1,4-pentanodiol con aplicación como monómero en la síntesis de poliésteres[36] o ácido valérico y ésteres valéricos con aplicación como combustibles liquidos[37] a los que ya se ha hecho referencia en apartados anteriores.

Los ésteres valéricos han despertado un interés creciente ya que sus propiedades los hacen compatibles con los motores de combustión actuales. La naturaleza del alcohol con el que se lleva a cabo la esterificación del ácido valérico condiciona las propiedades fisicoquímicas de los ésteres derivados. Así, el valerato de etilo comparte las propiedades de ignición con la gasolina mientras que el valerato de pentilo es semejante al diésel. Presentan éstos una densidad energética superior a otros biocombustibles por la mayor relación C/O

con la que cuentan. Por otro lado, la esterificación del ácido valérico a los ésteres reduce la polaridad de la molécula reduciendo su reactividad, evitando así que ataque a los materiales con los que entrarán en contacto en los motores de combustión. Esta modulación de la polaridad también incrementa su miscibilidad con los hidrocarburos, haciendo viable su mezcla con los carburantes actuales[22,38–40].

2.1.5 Caminos de reacción para transformar el AL a biocombustibles valéricos

El presente trabajo se centra en la transformación directa, en un único reactor o "one-pot", del ácido levulínico en combustibles valéricos. Tal y como muestra la Figura 2, el proceso transcurre a través de una cascada de reacciones que comienzan por la transformación del ácido levulínico en gamma-valerolactona. Para el caso en que la reacción se produzca en medio acuoso, esta primera etapa, en caso de transcurrir a temperaturas inferiores a 473 K transcurre a través de una hidrogenación del ácido levulínico para dar lugar al ácido 4-hidroxivalérico que posteriormente es deshidratado en gamma-valerolactona. Por el contrario, si la reacción transcurre por encima de estos 473 K la reacción comienza por la deshidratación del ácido levulínico en angélica lactona que posteriormente se hidrogena en gamma-valerolactona. En ambos casos, la transformación transcurre vía hidrogenación catalizada por un metal y deshidratación catalizada por un centro ácido, aunque en orden inverso. Una vez se ha obtenido la gamma-valerolactona, se produce la apertura del anillo catalizada por centros ácidos dándose el ácido pentenoico que será hidrogenado en una etapa posterior en ácido valérico. En caso de llevarse a cabo la reacción en medio acuoso, en una etapa posterior podría llevarse a cabo la esterificación con el alcohol correspondiente y un catalizador ácido. El uso de un alcohol como disolvente permite obtener, en lugar del ácido valérico, el éster valérico correspondiente a la esterificación del ácido valérico con éste y ahorraría este paso posterior. La descripción del proceso muestra la necesidad

de un catalizador bifuncional para tratar de llevar a cabo la reacción en cascada[41].

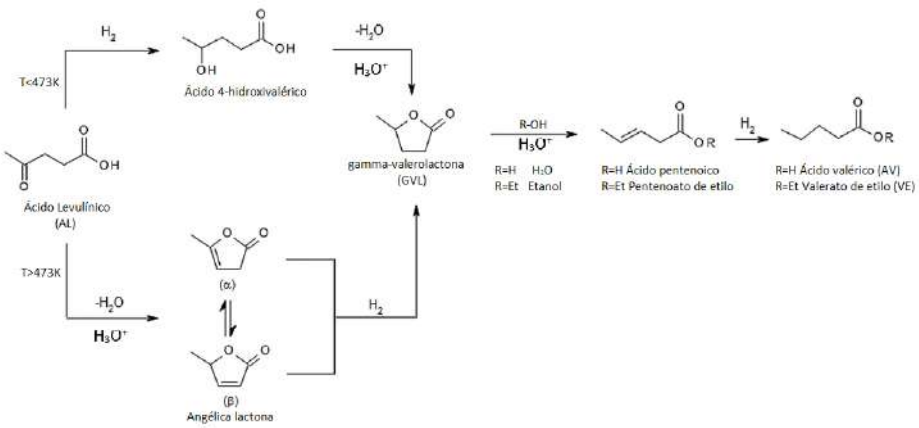

Figura 2. Mecanismo de la conversión del AL en AV y VE.

Desde que Lange y colaboradores[37] planteasen en 2010 la idoneidad de los ésteres valéricos para su incorporación a los carburantes sin necesidad de modificar los sistemas de distribución ni los motores de combustión actuales, son muchos los pasos que se han dado en la comprensión de la reacción para la obtención de los combustibles valéricos a partir del ácido levulínico. En aquellos primeros pasos, se partía del desarrollo de la reacción empleando diferentes catalizadores para cada una de las etapas en las que se desglosaba el proceso. Partiendo desde la hidrólisis de la lignocelulosa para obtener el ácido levulínico, continuaba con la hidrogenación de éste para obtener la gamma-valerolactona. Le seguía la apertura del anillo y la hidrogenación de ésta dando lugar al ácido valérico que posteriormente se esterificaba para dar lugar a los ésteres valéricos de interés. En su propuesta, se planteaba una serie de catalizadores con los que llevar a cabo cada una de las etapas, comenzando por el ácido sulfúrico para la hidrólisis de la lignocelulosa y su transformación en ácido levulínico, seguida del Pt/TiO_2 con la que hidrogenar en gamma-valerolactona el ácido levulínico; el Pt sobre zeolita ZSM-5 para la transformación de la gamma-valerolactona en ácido valérico y una resina de intercambio catiónico con la que esterificar el ácido valérico en el éster valérico.

2.2 Catalizadores para la transformación directa de ácido levulínico (AL) a valerato de etilo (VE)

2.2.1 Sistemas catalíticos basados en metales nobles en fase líquida (*batch*)

El hecho de realizar la reacción en tres etapas tal y como fue descrito por Lange, suponía un gran hándicap para el proceso. Una idea que ya quedaba plasmada en aquel momento era la importancia del diseño del catalizador, con el equilibro entre las capacidades hidrogenante y ácida para conducir la reacción hacia los productos de interés. Estos autores también publicaron una patente[9] en la que describían aquellos catalizadores susceptibles de ser empleados en cada una de las diferentes etapas. Dumesic y col.[42] también trabajaron empleando un enfoque similar, llevando a cabo por un lado la transformación del ácido levulínico en gamma-valerolactona con catalizadores hidrogenantes y empleando en una segunda etapa catalizadores bifuncionales para la obtención de combustibles valéricos. El uso de Ru/C era capaz de proporcionar gamma-valerolactona a partir de una disolución acuosa al 50 % en ácido levulínico. Posteriormente, y sin tratamiento intermedio, el efluente de la reacción anterior se trataba con catalizadores de Pd/Nb_2O_5 para que la reacción continuase. Modulando la carga metálica, y, por tanto, la capacidad hidrogenante del catalizador, se lograba que la reacción llegase a proporcionar mayoritariamente ácido valérico, con selectividades de hasta el 92 %. En caso de que el contenido en Pd fuese superior, las condiciones de reacción eran tales que la reducción llegaba a proporcionar hidrocarburos.

Entre los primeros autores en realizar la reacción en cascada de manera directa, Weckhuysen[43], ya apuntaba a la apertura del anillo como el paso limitante de la reacción. Los catalizadores empleados en la conversión directa por parte de Weckhuysen se basaban en Ru soportado sobre zeolitas de tipo beta y ZSM-5. Pese a lograr alcanzar la reacción en un único reactor cuando empleaba dioxano como disolvente, observaron una fuerte desactivación por desaluminación del catalizador. Sus resultados demostraban la necesidad de la función ácida para la apertura del anillo, logrando, en ausencia de acidez, gamma-valerolactona como producto de la reacción. Por otro lado, la relevancia del disolvente en que se llevaba a cabo la reacción es clara. Ésta iba más allá de la obtención de ácido

valérico o el éster valérico correspondiente. Demostraba que la reacción progresaba en dioxano mientras que apenas lo hacía más allá de la gamma-valerolactona cuando el disolvente era ácido 2-etilhexanóico.

Los resultados, si bien abrían la posibilidad de llevar a cabo la reacción de interés en cascada y permitían integrar la reacción por etapas en un solo reactor, no eran capaces de superar el 45,8 % en rendimiento a los productos de interés. Por otro lado, los catalizadores empleados, si bien apenas sufrían lixiviado y sinterizado del Ru, sí sufrían de desaluminación del soporte y, por tanto, pérdida de la acidez. Estudios posteriores de este mismo grupo[44] y empleando de nuevo el Ru sobre la HZSM-5 por ser la que menor pérdida de acidez había demostrado sufrir, lograron un rendimiento a ácido valérico de un 91,3 %. Para ello, se centraron en la forma de preparación del catalizador variando el precursor con el que se incorporaba el Ru, comparando la zeolita que se encontraba en la forma ácida o amónica y la ratio Si/Al. Cabe destacar que, pese a la optimización lograda, la primera reutilización sufría una caída del rendimiento hasta el 66,4 % y la calcinación de éste no era capaz de recuperar el rendimiento inicial a los productos de interés.

De forma paralela a lo anterior, se lograba un rendimiento del 94 % a combustibles valéricos empleando un catalizador de Ru soportado sobre una SBA modificada con grupos sulfónico para proporcionarle acidez[29]. En este trabajo, el uso de etanol como disolvente tenía como consecuencia la obtención de la mezcla del valerato de etilo y ácido valérico como productos de reacción. Además de la constatación de que una mayor cantidad de grupos sulfónico, y por tanto una mayor acidez, contribuía a mejorar el rendimiento a los productos de interés, se analizaba otras variables como la temperatura de reacción o la presión de hidrógeno. De ello, cabe destacar la presencia de una temperatura óptima que en este caso se trataba de los 513 K a los que se alcanzaba el rendimiento óptimo. Las temperaturas superiores demostraron hacer posible la descomposición de los productos de interés perjudicando por tanto a balances de carbono y a la selectividad a los productos de interés. Además, estas temperaturas superiores y las condiciones de reacción resultaron suficientes para dañar la estructura de los soportes. De los ensayos alterando la presión inicial de hidrógeno puede concluirse que, si se aportaba la presión inicial suficiente, se alcanzaba el resultado óptimo y que, a partir de él, los incrementos

de presión no redundaban en mejoras en la selectividad del proceso. En cuanto a la carga metálica, de nuevo hay un óptimo ya que a cantidades inferiores no se logra la capacidad hidrogenante suficiente y, por encima de ella, el exceso de capacidad hidrogenante favorece rutas no selectivas como aquella de la que se deriva el 2-metiltetrahidrofurano. Otro punto que se concluía de este trabajo consistía en que la etapa limitante del proceso era la apertura del anillo de gamma-valerolactona y que, tras ella, la hidrogenación del pentenoato de etilo, era rápida. El principal escollo planteado en el trabajo consiste en la desactivación sufrida por el catalizador dado el lixiviado de los grupos sulfónicos. También enfrenta el inconveniente de que, al tratar de reemplazar el Ru por metales no nobles encuentra rendimientos muy inferiores a los productos de interés.

Kon y colaboradores[45] fueron capaces de alcanzar rendimientos del 99 % a ácido valérico empleando el ácido levulínico sin disolvente. Estos resultados se alcanzaron con catalizadores de Pd sobre zeolita HMFI en condiciones *batch* y aportaban, además de un rendimiento superior, condiciones menos exigentes en cuanto a la presión de hidrógeno necesaria y la ventaja de la ausencia de disolvente. Otro de los inconvenientes mostrados por el sistema catalítico presentado se encontraba en la desactivación que se producía en el sistema, que perdía actividad alcanzando solo un 52 % de rendimiento a ácido valérico en el tercer ciclo de reutilización.

Otra aproximación experimental para la síntesis de los catalizadores, la *atomic layer deposition* (ALD), se empleó para preparar un sistema de Pt sobre una zeolita ZSM5[46] que era capaz de obtener rendimientos del 91,4 % de ácido valérico a partir de ácido levulínico en medio acuoso a 473 K. Se ha obtenido rendimientos similares cuando se ha empleado como catalizador Pd sobre carbono y triflatos metálicos para aportar la acidez[47] con la ventaja de que la temperatura necesaria en este caso era incluso inferior, de 423 K. La naturaleza del triflato resultaba también clave en la actividad del sistema catalítico, resultando el Hf el que mejor rendimiento proporcionaba. Este sistema catalítico mostraba además una buena estabilidad manteniéndose el rendimiento a ácido valérico por encima de 80 % incluso tras 5 ciclos.

Un resultado de interés es el obtenido por Villa y col.[48]. El sistema catalítico empleado consiste en la modificación de carbono mesoporoso para incluirle acidez, bien sea mediante la modificación con ácido sulfúrico o bien con ácido fosfórico. Lo que cabe destacar de esta referencia es que, dependiendo de las condiciones de presión y temperatura empleadas en el proceso, la reacción progresa hasta los productos de interés o bien queda bloqueada en la apertura del anillo de gamma-valerolactona. Así, cuando las condiciones de reacción son más severas, 473 K y 40 bars de presión, se obtiene ácido valérico con rendimientos próximos al 90 %. Sin embargo, con condiciones menos severas, a 303 K y 7 bars de presión, lo que se obtiene es gamma-valerolactona con rendimientos superiores al 90 %. Estos resultados, permiten apuntar a la mayor exigencia de la etapa de la apertura del anillo de gamma-valerolactona, siendo ésta la etapa limitante de la cascada de reacciones. Otro dato de interés que cabe destacar de los resultados de Villa es la gran estabilidad que se alcanza cuando las condiciones son menos exigentes. Así, apenas se aprecia desactivación del catalizador a 303 K tras cinco ciclos de reutilización mientras que, cuando se emplea 473 K como temperatura de reacción, el rendimiento cae significativamente tras solo tres ciclos de reutilización.

2.2.2 Sistemas catalíticos basados en metales no nobles (Co, Ni) en fase gaseosa (continuo)

La mayoría de los resultados presentados hasta el momento empleaban reactores *batch* en lugar de los reactores en flujo, más favorables para su aplicación industrial. Por otro lado, el uso de metales nobles supone un elevado coste para el proceso. Los primeros ensayos para realizar la reacción en flujo y evitando además los metales nobles son aquellos en que se empleaba el proceso electrocatalítico para la conversión directa del ácido levulínico en ácido valérico[49,50] empleando un electrodo de Pb.

Otro de los hitos en el desarrollo de la conversión directa de ácido levulínico en combustibles valéricos también en flujo y en ausencia de metales nobles consistió en el uso de Ni como metal hidrogenante, permitiendo sustituir los metales nobles empleados hasta entonces[51]. En este caso, el Ni depositado sobre óxido de titanio era modificado con W para proporcionar la acidez necesaria al catalizador. Se mostraba que la incorporación del W estabilizaba el

Ni^{2+} y las sinergias establecidas entre Ni y W favorecían la apertura del anillo de gamma-valerolactona. La reacción era llevada a cabo en un reactor de lecho fijo en condiciones en que el flujo a través del lecho catalítico se producía en fase gaseosa. Sin embargo, estos catalizadores no eran capaces de alcanzar la conversión completa del ácido levulínico y la selectividad a ácido valérico no superaba el 24 %. La incorporación del W daba como resultado mejora en la selectividad al ácido valérico al mismo tiempo que se producía una disminución en la conversión de ácido levulínico.

El Co también ha demostrado su capacidad como metal hidrogenante[52] en la transformación del ácido levulínico en combustibles valéricos. Soportado sobre zeolita ZSM-5 por impregnación húmeda, ha logrado un rendimiento superior al 94 % en un reactor *batch*. Sin embargo, en medio etanol y en las condiciones de reacción, se producía la desactivación del catalizador. La síntesis de una zeolita ZSM-5 que integre en sus canales las partículas de Co ha sido el enfoque con el que se ha logrado, no tanto una mejora de los resultados catalíticos, como la estabilización del catalizador. Esta estrategia ha sido capaz de preparar un catalizador para el que, incluso tras 8 ciclos de reutilización, el rendimiento siga encontrándose por encima del 90 %. Los ensayos con estos catalizadores en un reactor en flujo sin embargo muestran una desactivación significativa de los mismos antes de alcanzarse 30 horas de flujo. La regeneración que empleaba la calcinación y la posterior reducción era capaz de recuperar la actividad original si bien la desactivación se volvía a producir.

Otro catalizador basado en metales no nobles y con rendimientos superiores al 99 % es el obtenido a base de Cu dopado con Nb soportado sobre una sílice modificada con Zr.[53] El uso del Nb se ha demostrado capaz de proporcionar la acidez necesaria para la apertura del anillo de GVL además de evitar el lixiviado del Cu en las condiciones de reacción. Tanto es así que, en ausencia de Nb el producto mayoritario que se obtenía era la GVL.

2.2.3 Importancia de la función ácida en el comportamiento catalítico

A lo largo de la bibliografía, se ha prestado atención a la necesidad de acidez en los sistemas catalíticos. La constatación de que la etapa limitante del proceso consistía en la apertura del anillo de gamma-valerolactona, un proceso

catalizado por centros ácidos, determinaba la importancia de la acidez de los catalizadores.

Sun y col.[54] partían de un catalizador de Ni sobre HZSM5 capaz de convertir el ácido levulínico en ácido valérico y valerato de etilo en un reactor en flujo. A éste se le incorporaba cantidades crecientes de K con el fin de neutralizar los centros ácidos más fuertes. El resultado en este caso, más que a un patrón diferente en la actividad que se producía, respondía a un cambio en el patrón de desactivación del catalizador. En este caso, según los resultados, la incorporación de K neutralizaba primero los centros Brønsted más fuertes y esto tenía como consecuencia que los depósitos de coque generados fuesen más ligeros y tardasen más en producirse, proporcionando una mejor estabilidad del catalizador.

También se ha considerado el efecto que causa sobre la acidez del catalizador la incorporación de los metales.[55] Así sucedía al impregnar cantidades equivalentes de Ru y Ni sobre una zeolita; se observaba que la impregnación con Ru daba lugar a acideces mucho más fueres que el Ni. El efecto sobre la acidez que causaba el uso de diferentes metales se traducía de manera directa en los productos obtenidos a partir del ácido levulínico. Así como en el caso del Ru sí se lograba que la reacción llegase a formar combustibles valéricos, para el caso de que el metal fuese Ni, la acidez resultaba insuficiente y la reacción quedaba bloqueada en la gamma-valerolactona. Este efecto no era debido a una falta de capacidad hidrogenante de los catalizadores si no a que el uso de diferentes metales impactaba sobre la acidez del sistema.

Sin embargo, y pese a lo descrito hasta el momento, un estudio más en profundidad del papel que tiene la función ácida (naturaleza, fortaleza y densidad de centros ácidos) en el comportamiento catalítico tanto en sistemas en fase líquida como gaseosa se hace necesaria.

2.2.4 Estabilidad de los catalizadores en el sistema de reacción

La descripción del estado del arte ha dejado patente que una de las limitaciones que han encontrado los catalizadores ensayados ha consistido en la desactivación que se produce en ellos. La búsqueda de catalizadores activos se ha encontrado en muchas ocasiones con sistemas catalíticos que, en las

condiciones de reacción, daban lugar al lixiviado de la función ácida[29]. Se ha tratado de mejorar la estabilidad de los sistemas mediante diferentes técnicas, como puede ser el uso del ALD[46] para proteger del lixiviado y el uso de contra iones potasio que redujesen la actividad ácida para mitigar la formación de depósitos de naturaleza carbonosa sobre los centros con una acidez más fuerte[54]. Sin embargo, la exigencia de las condiciones de reacción necesarias para alcanzar los combustibles valéricos a partir del ácido levulínico de manera directa potencian la desactivación de los catalizadores. El uso de temperaturas y presiones elevadas así como el disolvente o el propio ácido levulínico contribuyen por un lado al lixiviado del catalizador y a la formación de depósitos carbonáceos.

2.3 Objetivos y metodología

El **objetivo principal** de la presente Tesis es desarrollar catalizadores sólidos activos, selectivos y estables para la conversión directa del ácido levulínico en combustibles valéricos. En cualquier caso, se requiere para ello catalizadores bifuncionales ácidos e hidrogenantes para cubrir la necesidad de las diferentes etapas catalíticas (ver figura 2).

Existe en bibliografía diversos ejemplos de este tipo de sistemas y se ha estudiado el mecanismo de la reacción, como se ha expuesto previamente. Sin embargo, en esta Tesis se persigue profundizar en el efecto que tiene la acidez del catalizador sobre la actividad catalítica. Esta variable resulta clave al ser la que determina la velocidad de la apertura del anillo de GVL. Una acidez insuficiente imposibilita el progreso de la reacción y una acidez excesiva, favorece la deposición de coque y, por tanto, la desactivación del catalizador.

La consecución de este objetivo principal requiere de una serie de hitos u objetivos secundarios como son:

- **Preparar catalizadores bifuncionales** con las propiedades requeridas para la consecución de la reacción de manera directa, especialmente las propiedades ácidas e hidrogenantes.
- **Definir las condiciones de reacción** para que los resultados catalíticos obtenidos sean favorables.

- **Hallar sistemas catalíticos robustos** y que soporten las condiciones de reacción en lo que respecta especialmente al medio de reacción; el uso de etanol como disolvente facilita el proceso al permitir la esterificación *in situ* ahorrando una etapa posterior, pero puede favorecer la desactivación de los sistemas catalíticos.
- **Contar con sistemas estables en las condiciones de reacción** o, en su defecto, que la actividad pueda recuperarse mediante un procedimiento simple de regeneración del catalizador desactivado.

La **metodología** que se ha seguido en el presente trabajo ha consistido en la preparación de soportes en los que se ha modulado la acidez sustituyendo Si por Al en el caso de la familia de la SBA-15 o Al por Zr en el caso de las BEA. Realizada dicha sustitución, se ha llevado a cabo la impregnación del metal correspondiente, Pd o Co sobre el soporte, empleando la impregnación incipiente de una solución acuosa. Con esto, se ha logrado preparar los catalizadores a estudiar.

A las familias de catalizadores así obtenidas se les ha realizado la caracterización, centrándose especialmente en la **acidez** por diversas técnicas. Por medio de la **espectroscopia infrarroja de transformada de Fourier de reflectancia difusa** (**DRIFT**) se ha caracterizado la acidez. La **desorción a temperatura programada del amoniaco (TPD-NH_3)** también ha permitido cuantificar y analizar la acidez presente en estos catalizadores. Igualmente, se ha atendido al efecto de la acidez sobre el metal, su interacción y el efecto en la reducibilidad o grado de dispersión.

Obtenida una caracterización preliminar, se ha procedido a ensayar la actividad catalítica de los mismos. Los ensayos de actividad se han llevado a cabo bien en **condiciones de flujo o en *batch***. Respecto de los ensayos en flujo, se han ensayado en un reactor de lecho fijo en que se ha presurizado empleando H_2 y se ha circulado una disolución de ácido levulínico en etanol en el sistema termostatizado. El uso de estas condiciones conduce a la trasformación de la corriente de alimentación a fase gaseosa, previniendo el lixiviado del catalizador. En estas condiciones se han ensayado los diferentes catalizadores analizando el efluente por cromatografía de gases para caracterizar la actividad de cada catalizador, la conversión y selectividad a los diferentes productos.

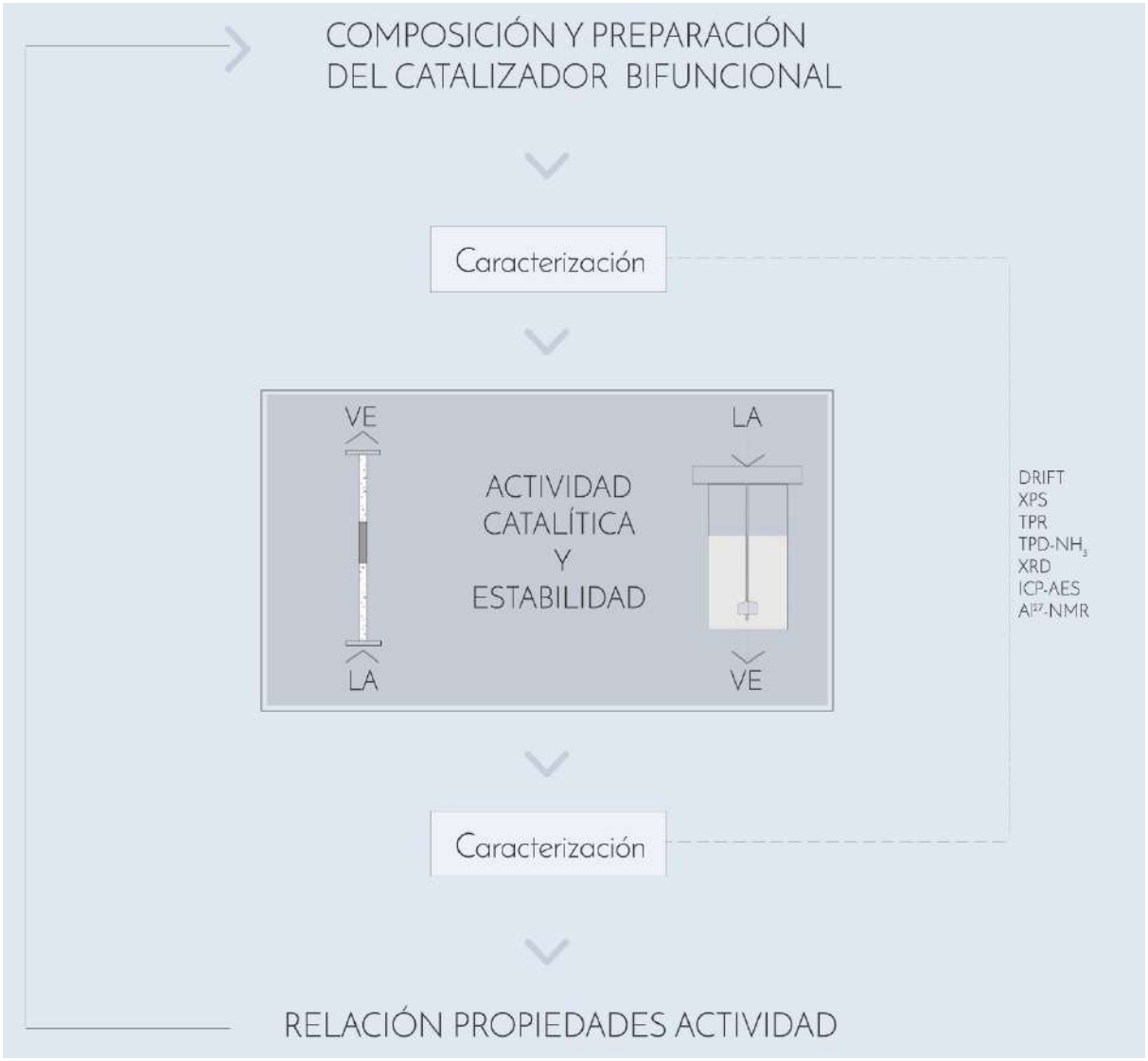

Figura 3. Esquema de la metodología seguida en la Tesis.

También se ha modificado el tiempo de contacto del catalizador con el sustrato para evaluar el efecto sobre la actividad. Estos ensayos permiten además evaluar la estabilidad de los catalizadores.

Por otro lado, los ensayos de actividad en condiciones *batch*, han empleado un reactor discontinuo en que se ha cargado el catalizador, el disolvente y el sustrato. Tras ello, se ha purgado para eliminar el aire contenido en su interior

y reemplazarlo por H_2 que además se ha empleado para presurizarlo. De nuevo, al calentar, se ha generado una presión autógena que se suma a la introducida por el hidrógeno. En este caso, el sistema se ha mantenido en las condiciones de reacción durante el periodo de tiempo que duraba el experimento tras lo que se ha enfriado. Se ha analizado una alícuota del crudo de reacción mediante cromatografía de gases.

Otra etapa que se ha llevado a cabo al valorar la actividad catalítica ha consistido en **estudiar la estabilidad.** Para ello, en los ensayos en flujo, simplemente se prolonga el tiempo de reacción para evaluar si el efluente de productos se mantiene estable en el tiempo. En el caso de las reacciones en *batch*, la valoración de la estabilidad se lleva a cabo ensayando el catalizador en reacciones sucesivas para valorar si la actividad permanece a través de los ciclos.

Se ha realizado también la **caracterización de los catalizadores tras la reacción** para estudiar los cambios sufridos por éstos. Se busca con ello comprender posibles causas de desactivación y tratar de mitigarlas o evitarlas.

Los resultados catalíticos obtenidos, unidos a la caracterización realizada de los catalizadores, deben llevar a establecer la relación entre las variables modificadas en el catalizador y las diferencias en actividad catalítica. La comprensión de estas relaciones es clave para alcanzar el objetivo de la presente Tesis. Es necesario entender las necesidades catalíticas del proceso de trasformación del ácido levulínico en combustibles valéricos para el diseño de un sistema catalítico para dicho proceso. Igualmente, los resultados obtenidos para cada familia han servido para proponer otros soportes que modificar y ensayar siguiendo este mismo proceso.

2.4 Aportaciones de la presente Tesis a la conversión directa del AL en VE

Como ya se ha indicado, la obtención de combustibles líquidos para el transporte a partir de la biomasa es un campo de estudio prometedor y que ha recibido gran atención. El AL, que puede obtenerse partiendo de lignocelulosa, es susceptible de transformarse en combustibles valéricos a través de una reacción consistente en diferentes etapas catalizadas por centros ácidos e hidrogenantes. Uno de los retos de esta reacción es su consecución de manera

directa, llevando a cabo las diferentes etapas en un único reactor. Se han descrito en la bibliografía diferentes catalizadores capaces de llevar a cabo este proceso tal y como se ha detallado en los apartados anteriores.

A lo largo de los diferentes trabajos se ha constatado que la **etapa limitante** de esta reacción es la **apertura del anillo de GVL**. Se sabe que esta etapa es catalizada por los centros ácidos. Sin embargo, los centros hidrogenantes han centrado gran parte de la atención en los trabajos previos. Un estudio centrado especialmente en las propiedades ácidas de los sistemas catalíticos es pertinente por ser ésta la función encargada del desarrollo de la etapa limitante.

El presente estudio, teniendo en cuenta esta carencia de atención sobre los centros ácidos, busca precisamente emplear diferentes centros ácidos y analizar el efecto de esta variación sobre la actividad y la selectividad del proceso. Por tanto, lo novedoso de la presente Tesis se centra en la búsqueda de catalizadores activos en la transformación directa de ácido levulínico en valerato de etilo tales que permitan una mejor **comprensión de las necesidades catalíticas del proceso**. Modulando las propiedades ácidas de los catalizadores, caracterizándolos y evaluando los resultados de la actividad catalítica, se busca comprender los requisitos que debe cumplir un catalizador para ser activo y selectivo en este proceso.

El primero de los trabajos realizados en la Tesis[56] emplea tres soportes comerciales (zeolita ZSM5, zeolita beta y sílica alúmina amorfa) depositando sobre ellos el Pd por impregnación acuosa incipiente. El primer paso consiste en impregnar una cantidad idéntica de Pd sobre los tres soportes y ensayar su actividad en la reacción de interés en condiciones *batch*. El punto de partida, la reacción llevada a cabo a 4 horas da como resultado actividades muy diferentes. En el caso del catalizador con soporte sílica alúmina amorfa el rendimiento logrado es muy bajo, inferior al 5 %, mientras que para las dos zeolitas se logra un rendimiento similar, alrededor del 60 %.

Sin embargo, la distribución de los productos obtenidos con estos catalizadores es significativamente diferente y es que, además de este 60 % de ácido valérico y valerato de etilo, el catalizador basado en zeolita beta apenas tiene aún productos intermedios de reacción llegando el balance de carbono apenas al 70 %. Esto hace plantear que la reacción ya haya atravesado un máximo a los

productos de interés y que éstos han seguido degradando en las condiciones de reacción, lo que queda descartado realizando una cinética de la reacción.

Por contra, el catalizador basado en zeolita ZSM5, además del 60 % de productos de interés, muestra aún más de un 30 % de productos intermedios lo que hace posible que la reacción continúe y se logre un rendimiento mejor. Así se comprueba al realizar la cinética de reacción y lograr un **rendimiento del 92 %** a las 8 horas de reacción.

La caracterización de las propiedades ácidas de los tres catalizadores muestra que todos ellos presentan centros ácidos muy débiles de tipo Brønsted asociados a los grupos silanol. Además de ello, el catalizador soportado sobre la zeolita beta es el que muestra acidez Lewis de mayor fortaleza, seguido por el basado en zeolita ZSM5 y siendo el más débil de los tres el de soporte sílica alúmina amorfa. Estos resultados sugieren que la acidez del soporte amorfo resulta insuficiente para llevar a cabo la apertura del anillo de GVL. Este hecho se comprueba llevando a cabo la reacción empleando como catalizadores los soportes libres de metal y como sustrato la propia GVL. Para estos ensayos se observa que la sílica alúmina amorfa no es capaz de abrir la GVL más allá de un 10 % tras 4 horas de reacción mientras que las dos zeolitas lo hacen por encima de un 60 %.

Una vez determinado el efecto de los diferentes tipos de acidez, el estudio de la dispersión del Pd se lleva a cabo con el fin de determinar cuál es el efecto de la acidez sobre ésta. Los resultados obtenidos son significativamente diferentes para los tres catalizadores, mostrando claramente una relación entre la acidez y la dispersión del Pd. Así los tamaños de partícula para el catalizador soportado sobre la zeolita beta son los menores, seguidos de los de la zeolita ZSM5 y de los de la sílica alúmina amorfa.

Los resultados de este primer artículo muestran que, como ya se ha indicado en la bibliografía, la tipología y fortaleza de la acidez, son clave en el diseño de catalizadores para la conversión del AL en VE y AV. Sin embargo, en el artículo, al emplear diferentes soportes, se han introducido variables como la superficie específica del catalizador o las propiedades texturales. En el segundo de los artículos[57], tratando de superar la limitación que acaba de exponerse, se trabaja con una zeolita beta de partida que se modifica para obtener una familia de

soportes en los que se ha reemplazado parcial o totalmente el **Al por Zr para lograr modular las propiedades ácidas** sin interferir en la estructura de la zeolita beta[58–60]. Una vez sintetizada esta familia de soportes se ha impregnado en todos ellos la misma cantidad de Pd, un 2 %, para asegurar que muestran la capacidad hidrogenante suficiente y se pueda así evaluar el efecto de la acidez de manera aislada.

Los ensayos de actividad en este segundo artículo muestran por un lado que todos los catalizadores que conservan algo de Al en su estructura son capaces de alcanzar un **rendimiento del 70 %** a los productos de interés. Sin embargo, aquel catalizador en el que el Al ha sido totalmente reemplazado por Zr no es capaz de alcanzar el 20 % en cuatro horas de reacción. Por otro lado, para el catalizador basado en la zeolita beta comercial, se observa que la reacción atraviesa un máximo de rendimiento a los productos de interés a las dos horas y que, a partir de ese momento, el rendimiento comienza a disminuir al continuar la reacción más allá del punto de interés.

Los resultados de caracterización de la acidez de esta familia de catalizadores mostraban para todos ellos la señal propia de los ácidos Brønsted débiles asociados al silanol. Además de ello, el catalizador con todo su Al sustituido por Zr, **Pd/ZAB-0.0 mostraba una acidez Lewis débil**. En el otro extremo, el catalizador con todo el Al, el **Pd/HBEA, mostraba acidez tipo Brønsted fuerte y dos señales de acidez Lewis de fortaleza mayor**. Los intermedios de la serie, Pd/ZAB-1.6 y Pd/ZAB-0.1, mostraban una combinación de las señales descritas para los extremos de la serie. De estos resultados, cabe señalar que la acidez Lewis débil y la propia de los grupos silanol son insuficientes para llevar a cabo la reacción. Son necesarios centros ácidos de mayor fortaleza. Además, una mayor cantidad de centros ácidos se ha traducido en una mayor velocidad de reacción, alcanzando el máximo a tiempos más cortos en aquellos catalizadores con mayor cantidad de centros ácidos. Los resultados muestran la **necesidad de los centros ácidos Brønsted fuertes así como los Lewis fuertes** para la catálisis de las diferentes etapas catalizadas por centros ácidos en la reacción. El hecho de que la variación de los centros fuertes de los dos tipos sea paralela complica el análisis en cuanto a la capacidad de desarrollo de la reacción en ausencia de alguno de los tipos de acidez fuerte.

En los dos artículos que se han presentado se lleva a cabo también ensayos sobre la estabilidad de los catalizadores. Se emplea en el primero de ellos un sistema de lecho fijo apreciándose **que la actividad permanece estable durante al menos 90 horas de reacción**. Los resultados de caracterización de los catalizadores tras la reacción muestran sin embargo que los centros ácidos quedan cubiertos por depósitos carbonosos que pueden ser recuperados con la calcinación de los catalizadores tras su uso. En el segundo de los artículos, los ensayos de estabilidad se llevaron a cabo en condiciones *batch*, reutilizando el catalizador en reacciones sucesivas. Se observó que **la actividad del catalizador decrecía ligeramente a lo largo de tres ciclos de reacción** y que, tras calcinarlo, si bien se interrumpía la tendencia decreciente y había una recuperación parcial de la actividad, no se recuperaba los valores del catalizador fresco. La caracterización del catalizador tras la reacción mostró también los depósitos carbonosos sobre los centros ácidos e hidrogenantes y se pudo observar que, si bien la calcinación era capaz de recuperar la totalidad de los centros ácidos, el Pd había sufrido sinterizado y se encontraba parcialmente oxidado. Estos resultados explicaban la pérdida de actividad que se producía en el catalizador incluso tras su calcinación. Por otro lado, para el catalizador reutilizado se observaba la presencia de una fase Al_2O_3 (XRD) que contribuía a la desactivación.

Una segunda línea de trabajo consistió en el uso de catalizadores que **empleasen Co para reemplazar el Pd y evitar así el uso de metales nobles**.[61] Para ello, se empleó como soporte una familia de SBA-15 a la que se le incorporó una cantidad creciente de Al buscando incrementar la acidez de los mismos[62]. Posteriormente, se incorporaba, por medio de la impregnación acuosa incipiente, el Co a estos soportes. La caracterización de los catalizadores así preparados ha mostrado que la sustitución del Al por Si no ha alcanzado la extensión deseada y que, por tanto, el contenido en Al real es inferior al nominal. A pesar de ello, la tendencia sí es idéntica a la nominal y el crecimiento es tal que casi duplica el contenido en Al entre un miembro de la familia y el siguiente con lo que el efecto logrado es el que se pretendía. La incorporación de Al ha mostrado además un efecto de disminución en la superficie de los catalizadores así como del volumen de poro. Sin embargo, el diámetro del poro

permanece estable pudiendo afirmarse que la estructura no se ha visto significativamente afectada, tal y como se confirma por difracción de rayos X.

La incorporación del Al ha mostrado mejorar la dispersión y dificultar la reducción del Co, especialmente para los tres catalizadores con un mayor contenido en Al. Incluso en las condiciones de reducción a las que se activa el catalizador, parte del Co permanece en su forma oxidada. Una activación con temperaturas de reducción superiores, sin embargo, podría deteriorar la estructura del soporte. La incorporación del Al a la estructura de la SBA-15 se produce inicialmente en posiciones tetraédricas y, a partir de cierta proporción de Al, la ocupación de posiciones octaédricas pasa a ganar importancia. La explicación a este fenómeno reside en que las sustituciones se producen inicialmente en las posiciones de la red (posiciones tetraédricas) y solo una vez que éstas no pueden seguir sustituyéndose comienza a incorporarse el Al en posiciones octaédricas.

Lo que se ha expuesto hasta ahora impacta en la acidez de la familia de catalizadores. La caracterización de la acidez de los soportes ha mostrado que todos los catalizadores muestran la acidez propia de los grupos silanol, acidez tipo Brønsted de intensidad similar en todos ellos[63]. Además de la anterior, en base a la caracterización puede concluirse que hay dos tipos de acidez Lewis en estos soportes, una más fuerte debida al Al en posición tetraédrica y otra más débil por el Al octaédrico. La incorporación del Co a los soportes altera la acidez de éstos ya que todos los catalizadores que contienen Al muestran acidez Lewis débil debida a la presencia de Co^{2+}. Además, la acidez debida al Al octaédrico disminuye significativamente por la interacción que se produce entre estos átomos de Al y el Co. La presencia de Al octaédrico refuerza así la presencia de acidez Lewis débil a la vez que favorece la dispersión del Co y dificulta su reducibilidad

Los ensayos catalíticos se han realizado en un **reactor en lecho fijo** siendo alimentando con una disolución de ácido levulínico en etanol e iniciándose a una velocidad espacial de $10h^{-1}$. Transcurridas aproximadamente 90 hora se ha reducido la velocidad a la que se alimenta el sustrato para aumentar el tiempo de contacto del catalizador con el ácido levulínico. Los resultados muestran que, a velocidades altas, los mejores resultados, en términos de valerato de etilo

producido por gramo de catalizador y por hora, se obtienen para los catalizadores con menor contenido en Al. Sin embargo, la desactivación en éstos es significativa y el VE que es el producto principal al inicio deja de serlo en favor de la GVL. Sin embargo, a tiempos de contacto mayores, **el catalizador con mayor contenido en Al es el que proporciona la mayor cantidad de VE** por gramo de catalizador y por hora. En estos tiempos de contacto largos es donde se aprecia una mayor cantidad de productos de la vía no selectiva de reducción de la GVL como el 2-metiltetrahidrofurano y el 1-pentanol para los catalizadores con baja cantidad de Al.

La explicación a estos resultados debe buscarse en el hecho de que, para el caso del catalizador con más Al, el Co encuentra más dificultades para reducirse y queda por tanto en mayor proporción en la forma oxidada, reduciendo la capacidad reductora a la par que proporciona acidez. La vía selectiva, que requiere que el anillo de GVL sea abierto por un centro ácido antes de ser reducida, se ve beneficiada por esta menor presencia de centros reductores.

Estos resultados evidencian que debe existir un **compromiso entre la naturaleza, fortaleza y cantidad de centros ácidos y la capacidad reductora del catalizador**.

2.5 Referencias

(1) Directiva (UE) 2018/2001 Relativa Al Fomento Del Uso de Energía Procedente de Fuentes Renovables. *D. Of. la Unión Eur.* **2018**, *2018* (87), 141–144.

(2) Limayem, A.; Ricke, S. C. Lignocellulosic Biomass for Bioethanol Production: Current Perspectives, Potential Issues and Future Prospects. *Prog. Energy Combust. Sci.* **2012**, *38* (4), 449–467.

(3) Rackemann, D. W.; Doherty, W. O. S. The Conversion of Lignocellulosics to Levulinic Acid. *Biofuels, Bioprod. Biorefiniering* **2011**, *5*, 198–214.

(4) Granados, M. L.; Poves, M. D. Z.; Alonso, D. M.; Mariscal, R.; Galisteo, F. C.; Moreno-Tost, R.; Santamaría, J.; Fierro, J. L. G. Biodiesel from Sunflower Oil by Using Activated Calcium Oxide. *Appl. Catal. B Environ.* **2007**, *73* (3), 317–326.

(5) Douvartzides, S. L.; Charisiou, N. D.; Papageridis, K. N.; Goula, M. A. Green Diesel: Biomass Feedstocks, Production Technologies, Catalytic Research, Fuel Properties and Performance in Compression Ignition Internal Combustion Engines. *Energies* **2019**, *12* (5), 809-849.

(6) Zhang, Y.; Sahir, A. H.; Tan, E. C. D.; Talmadge, M. S.; Davis, R.; Biddy, M. J.; Tao, L. Economic and Environmental Potentials for Natural Gas to Enhance Biomass-to-Liquid Fuels Technologies. *Green Chem.* **2018**, *20* (23), 5358–5373.

(7) Sun, X.; Sartipi, S.; Kapteijn, F.; Gascon, J. Effect of Pretreatment Atmosphere on the Activity and Selectivity of Co/: Meso HZSM-5 for Fischer-Tropsch Synthesis. *New J. Chem.* **2016**, *40* (5), 4167–4177.

(8) Huber, G. W.; Iborra, S.; Corma, A. Synthesis of Transportation Fuels from Biomass: Chemistry, Catalysts, and Engineering. *Chem. Rev.* **2006**, *106* (9), 4044–4098.

(9) Lange, J. P. US Patent 2011/0112326. *Shell Int. B.V.* **2011**.

(10) Dayma G. Foucher F., Togbé C., Mounaim-Rouselle C., Dagaut P., H. F. Experimental and Detailed Kinetic Modeling Study of Ethyl Pentanoate (Ethyl Valerate) Oxidation in a Jet Stirred Reactor and Laminar Burning Velocities in a Spherical Combustion Chamber. *Energy and Fuels* **2012**, *26*, 4735–4748.

(11) Mariscal, R.; Maireles-Torres, P.; Ojeda, M.; Sádaba, I.; López Granados, M. Furfural: A Renewable and Versatile Platform Molecule for the Synthesis of Chemicals and Fuels. *Energy and Environmental Science*. **2016**, 9 (4), 1144–1189.

(12) Pileidis, F. D.; Titirici, M. M. Levulinic Acid Biorefineries: New Challenges for

Efficient Utilization of Biomass. *ChemSusChem* **2016**, *9*, 562–582.

(13) Werpy, T.; Petersen, G. Top Value Added Chemicals from Biomass Volume I. Results of Screening for Potential Candidates from Sugars and Synthesis Gas *Us Nrel* **2004**

(14) Yan K. Gu J., Yan Y., J. C. Production and Catalytic Transformation of Levulinic Acid: A Platform for Speciality Chemicals and Fuels. *Renew. Sustain. Energy Rev.* **2015**, *51*, 986–997.

(15) Jakob, A.; Grilc, M.; Teržan, J.; Likozar, B. Solubility Temperature Dependence of Bio-Based Levulinic. *Processes* **2021**, *9*, 924-936.

(16) Shuai, L.; Questell-Santiago, Y. M.; Luterbacher, J. S. A Mild Biomass Pretreatment Using γ-Valerolactone for Concentrated Sugar Production. *Green Chem.* **2016**, *18* (4), 937–943.

(17) Corma Canos, A.; Iborra, S.; Velty, A. Chemical Routes for the Transformation of Biomass into Chemicals. *Chem. Rev.* **2007**, *107* (6), 2411–2502.

(18) L., L. Synthesis, Chemistry and Applications of 5-Hydroxymethylfurfural and Its Derivatives. *ARKIVOC* **2001**, 17–54.

(19) Antonetti, C.; Licursi, D.; Fulignati, S.; Valentini, G.; Raspolli Galletti, A. New Frontiers in the Catalytic Synthesis of Levulinic Acid: From Sugars to Raw and Waste Biomass as Starting Feedstock. *Catalysts* **2016**, *6* (12), 196.

(20) Mellmer, M. A.; Gallo, J. M. R.; Martin Alonso, D.; Dumesic, J. A. Selective Production of Levulinic Acid from Furfuryl Alcohol in THF Solvent Systems over H-ZSM-5. *ACS Catal.* **2015**, *5* (6), 3354–3359.

(21) González Maldonado, G. M.; Assary, R. S.; Dumesic, J.; Curtiss, L. A. Experimental and Theoretical Studies of the Acid-Catalyzed Conversion of Furfuryl Alcohol to Levulinic Acid in Aqueous Solution. *Energy Environ. Sci.* **2012**, *5* (5), 6981–6989.

(22) Dautzenberg, G.; Gerhardt, M.; Kamm, B. Bio Based Fuels and Fuel Additives from Lignocellulose Feedstock via the Production of Levulinic Acid and Furfural. *Holzforschung* **2011**, *65* (4), 439–451.

(23) Alonso Wettstein S., Mellmer M.A., Gurbuz E.I., Dumesic J.A., D. M. Integrated Conversion of Hemicellulose and Cellulose from Lignocellulosic Biomass. *Energy Environ. Sci. Technol.* **2013**, *6*, 76–80.

(24) Gürbüz, E. I.; Wettstein, S. G.; Dumesic, J. A. Conversion of Hemicellulose to Furfural and Levulinic Acid Using Biphasic Reactors with Alkylphenol Solvents.

ChemSusChem **2012**, *5* (2), 383–387.

(25) Yan, L.; Yao, Q.; Fu, Y. Conversion of Levulinic Acid and Alkyl Levulinates into Biofuels and High-Value Chemicals. *Green Chem.* **2017**, *19* (23), 5527–5547.

(26) Serrano-Ruiz J.C. Dumesic J.A., W. R. M. Catalytic Conversion of Renewable Biomass Resources to Fuels and Chemicals. *Annu. Rev. Chem. Biomol. Eng.* **2010**, *1*, 79–100.

(27) Alonso, D. M.; Wettstein, S.; Dumesic, J. A. Gamma-Valerolactone, a Sustainable Platform Molecule Derived from Lignocellulosic Biomass. *Green Chem.* **2013**, *15*, 584–595.

(28) Luterbacher, J. S.; Martin Alonso, D.; Dumesic, J. A. Targeted Chemical Upgrading of Lignocellulosic Biomass to Platform Molecules. *Green Chem.* **2014**, *16* (12), 4816–4838.

(29) Pan, T.; Deng, J.; Xu, Q.; Xu, Y.; Guo, Q. X.; Fu, Y. Catalytic Conversion of Biomass-Derived Levulinic Acid to Valerate Esters as Oxygenated Fuels Using Supported Ruthenium Catalysts. *Green Chem.* **2013**, *15* (10), 2967–2974.

(30) Wettstein, S. G.; Alonso, D. M.; Chong, Y.; Dumesic, J. A. Production of Levulinic Acid and Gamma-Valerolactone (GVL) from Cellulose Using GVL as a Solvent in Biphasic Systems. *Energy Environ. Sci.* **2012**, *5* (8), 8199–8203.

(31) Xue, Z.; Liu, Q.; Wang, J.; Mu, T. Valorization of Levulinic Acid over Non-Noble Metal Catalysts: Challenges and Opportunities. *Green Chem.* **2018**, *20* (19), 4391–4408.

(32) Morone, A.; Apte, M.; Pandey, R. A. Levulinic Acid Production from Renewable Waste Resources: Bottlenecks, Potential Remedies, Advancements and Applications. *Renew. Sustain. Energy Rev.* **2015**, *51*, 548–565.

(33) Serrano-Ruiz, J. C.; Luque, R.; Sepúlveda-Escribano, A. Transformations of Biomass-Derived Platform Molecules: From High Added-Value Chemicals to Fuels via Aqueous-Phase Processing. *Chem. Soc. Rev.* **2011**, *40* (11), 5266–5281.

(34) Yan K. Wu G., Liao J., Ceng C., Xie X., L. T. Highly Selective Production of Value-Added Gammavalerolactone Frombiomass-Derived Levulinic Acid Using the Robust Pd Nanoparticles. *Appl. Catal. A Gen.* **2013**, *468*, 52–58.

(35) Horváth I.T. Fábos V., Boda L., Mika L.T., M. H. GammValerolactone, a Sustainable Liquid for Energy and Carbon-Based Chemicals. *Green Chem.* **2008**, *10*, 238–242.

(36) Li, M.; Li, G.; Li, N.; Wang, A.; Dong, W.; Wang, X.; Cong, Y. Aqueous Phase Hydrogenation of Levulinic Acid to 1,4-Pentanediol. *Chem. Commun.* **2014**, *50* (12), 1414–1416.

(37) Lange, J. P.; Price, R.; Ayoub, P. M.; Louis, J.; Petrus, L.; Clarke, L.; Gosselink, H. Valeric Biofuels: A Platform of Cellulosic Transportation Fuels. *Angew. Chemie - Int. Ed.* **2010**, *49* (26), 4479–4483.

(38) Blanco-Sánchez, M.; Franco, A.; Pineda, A.; Balu, A.; Romero, A.; Luque, R. NH4F Modified Al-SBA-15 Materials for Esterification of Valeric Acid to Alkyl Valerates. *Proceedings* **2018**, *3* (1), 4-10.

(39) Yan K. Chai J., Lu Y., Y. Y. Catalytic Reactions of Gamma-Valerolactone: A Platform to Fuels and Value-Added Chemicals. *Appl. Catal. B Environ.* **2015**, *179*, 292–304.

(40) De S. Luque R., S. B. Hydrodeoxygenation Processes: Advances on Catalytic Transformations of Biomass-Derived Platform Chemicals into Hydrocarbon Fuels. *Bioresour. Technol.* **2015**, *178*, 108–118.

(41) Yu, Z.; Lu, X.; Xiong, J.; Ji, N. Transformation of Levulinic Acid to Valeric Biofuels: A Review on Heterogeneous Bifunctional Catalytic Systems. *ChemSusChem* **2019**, *12* (17), 3915–3930.

(42) Serrano-Ruiz, J. C.; Wang, D.; Dumesic, J. A. Catalytic Upgrading of Levulinic Acid to 5-Nonanone. *Green Chem.* **2010**, *12* (4), 574–577.

(43) Luo, W.; Deka, U.; Beale, A. M.; Van Eck, E. R. H.; Bruijnincx, P. C. A.; Weckhuysen, B. M. Ruthenium-Catalyzed Hydrogenation of Levulinic Acid: Influence of the Support and Solvent on Catalyst Selectivity and Stability. *J. Catal.* **2013**, *301*, 175–186.

(44) Luo, W.; Bruijnincx, P. C. A.; Weckhuysen, B. M. Selective, One-Pot Catalytic Conversion of Levulinic Acid to Pentanoic Acid over Ru/H-ZSM5. *J. Catal.* **2014**, *320* (1), 33–41.

(45) Kon, K.; Onodera, W.; Shimizu, K. I. Selective Hydrogenation of Levulinic Acid to Valeric Acid and Valeric Biofuels by a Pt/HMFI Catalyst. *Catal. Sci. Technol.* **2014**, *4* (9), 3227–3234.

(46) Gu, X. M.; Zhang, B.; Liang, H. J.; Ge, H. Bin; Yang, H. M.; Qin, Y. Pt/HZSM-5 Catalyst Synthesized by Atomic Layer Deposition for Aqueous-Phase Hydrogenation of Levulinic Acid to Valeric Acid. *Ranliao Huaxue Xuebao/Journal Fuel Chem. Technol.* **2017**, *45* (6), 714–722.

(47) Zhou, J.; Zhu, R.; Deng, J.; Fu, Y. Preparation of Valeric Acid and Valerate Esters

from Biomass-Derived Levulinic Acid Using Metal Triflates + Pd/C. *Green Chem.* **2018**, *20* (17), 3974–3980.

(48) Villa, A.; Schiavoni, M.; Chan-Thaw, C. E.; Fulvio, P. F.; Mayes, R. T.; Dai, S.; More, K. L.; Veith, G. M.; Prati, L. Acid-Functionalized Mesoporous Carbon: An Efficient Support for Ruthenium-Catalyzed γ-Valerolactone Production. *ChemSusChem* **2015**, *8* (15), 2520–2528.

(49) Xin, L.; Zhang, Z.; Qi, J.; Chadderdon, D. J.; Qiu, Y.; Warsko, K. M.; Li, W. Electricity Storage in Biofuels: Selective Electrocatalytic Reduction of Levulinic Acid to Valeric Acid or γ-Valerolactone. *ChemSusChem* **2013**, *6* (4), 674–686.

(50) Qiu, Y.; Xin, L.; Chadderdon, D. J.; Qi, J.; Liang, C.; Li, W. Integrated Electrocatalytic Processing of Levulinic Acid and Formic Acid to Produce Biofuel Intermediate Valeric Acid. *Green Chem.* **2014**, *16* (3), 1305–1315.

(51) Kumar, V. V.; Naresh, G.; Deepa, S.; Bhavani, P. G.; Nagaraju, M.; Sudhakar, M.; Chary, K. V. R.; Venugopal, A.; Tardio, J.; Bhargava, S. K. Influence of W on the Reduction Behaviour and Brønsted Acidity of Ni/TiO2catalyst in the Hydrogenation of Levulinic Acid to Valeric Acid: Pyridine Adsorbed DRIFTS Study. *Appl. Catal. A Gen.* **2017**, *531*, 169–176.

(52) Sun, P.; Gao, G.; Zhao, Z.; Xia, C.; Li, F. Stabilization of Cobalt Catalysts by Embedment for Efficient Production of Valeric Biofuel. *ACS Catal.* **2014**, *4* (11), 4136–4142.

(53) Karanwal, N.; Verma, D.; Butolia, P.; Kim, S. M.; Kim, J. One-Pot Direct Conversion of Levulinic Acid into High-Yield Valeric Acid over a Highly Stable Bimetallic Nb-Cu/Zr-Doped Porous Silica Catalyst. *Green Chem.* **2020**, *22* (3), 766–787.

(54) Sun, P.; Gao, G.; Zhao, Z.; Xia, C.; Li, F. Acidity-Regulation for Enhancing the Stability of Ni/HZSM-5 Catalyst for Valeric Biofuel Production. *Appl. Catal. B Environ.* **2016**, *189*, 19–25.

(55) Yi, Z.; Hu, D.; Xu, H.; Wu, Z.; Zhang, M.; Yan, K. Metal Regulating the Highly Selective Synthesis of Gamma-Valerolactone and Valeric Biofuels from Biomass-Derived Levulinic Acid. *Fuel* **2020**, *259*, 3–6.

(56) Muñoz-Olasagasti, M.; Sañudo-Mena, A.; Cecilia, J. A.; Granados, M. L.; Maireles-Torres, P.; Mariscal, R. Direct Conversion of Levulinic Acid into Valeric Biofuels Using Pd Supported Over Zeolites as Catalysts. *Top. Catal.* **2019**, *62* (5–6), 579–588.

(57) Muñoz-Olasagasti, M. .; Martínez-Salazar, I.; López Granados, M.; López-

Aguado, C.; Iglesias, J.; Morales, G.; Mariscal, R. Sustainable Energy & Fuels Elucidating the Roles of Acid Site Nature and Strength in the Direct Conversion of Levulinic Acid into Ethyl Valerate : The Case of Zr-Modi Fi Ed Beta. *Sustain. Energy Fuels* **2022**, *6*, 1164–1174.

(58) Hernández, B.; Iglesias, J.; Morales, G.; Paniagua, M.; López-Aguado, C.; García Fierro, J. L.; Wolf, P.; Hermans, I.; Melero, J. A. One-Pot Cascade Transformation of Xylose into γ-Valerolactone (GVL) over Bifunctional Brønsted-Lewis Zr-Al-Beta Zeolite. *Green Chem.* **2016**, *18* (21), 5777–5781.

(59) Paniagua, M.; Morales, G.; Melero, J. A.; Iglesias, J.; López-Aguado, C.; Vidal, N.; Mariscal, R.; López-Granados, M.; Martínez-Salazar, I. Understanding the Role of Al/Zr Ratio in Zr-Al-Beta Zeolite: Towards the One-Pot Production of GVL from Glucose. *Catal. Today* **2021**, 367, 228–238.

(60) Melero, J. A.; Morales, G.; Iglesias, J.; Paniagua, M.; López-Aguado, C.; Wilson, K.; Osatiashtiani, A. Efficient One-Pot Production of γ-Valerolactone from Xylose over Zr-Al-Beta Zeolite: Rational Optimization of Catalyst Synthesis and Reaction Conditions. *Green Chem.* **2017**, *19* (21), 5114–5121.

(61) Muñoz-Olasagasti, M.; López Granados, M.; Jiménez-Gómez, C. P.; Cecilia, J. A.; Maireles-Torres, P.; Dumesic, J. A.; Mariscal, R. The Relevance of Lewis Acid Sites on the Gas Phase Reaction of Levulinic Acid into Ethyl Valerate Using CoSBA-XAl Bifunctional Catalysts. *Catal. Sci. Technol.* **2021**, *11* (12), 4280–4293.

(62) Gómez-Cazalilla, M.; Mérida-Robles, J. M.; Gurbani, A.; Rodríguez-Castellón, E.; Jiménez-López, A. Characterization and Acidic Properties of Al-SBA-15 Materials Prepared by Post-Synthesis Alumination of a Low-Cost Ordered Mesoporous Silica. *J. Solid State Chem.* **2007**, *180* (3), 1130–1140.

(63) Mariscal, R.; López-Granados, M.; Fierro, J. L. G.; Sotelo, J. L.; Martos, C.; Van Grieken, R. Morphology and Surface Properties of Titania-Silica Hydrophobic Xerogels. *Langmuir* **2000**, *16* (24), 9460–9467.

3. PUBLICACIONES

3.1. Direct conversion of levulinic acid into valeric biofuels using Pd supported over zeolites as catalysts; Topics in Catalysis **62**, 579-588 (2019)

Topics in Catalysis (2019) 62:579–588
https://doi.org/10.1007/s11244-019-01147-4

ORIGINAL PAPER

Direct Conversion of Levulinic Acid into Valeric Biofuels Using Pd Supported Over Zeolites as Catalysts

M. Muñoz-Olasagasti[1] · A. Sañudo-Mena[1] · J. A. Cecilia[2] · M. López Granados[1] · P. Maireles-Torres[2] · R. Mariscal[1]

Published online: 23 February 2019

Abstract
A series of Pd-based catalysts was prepared by incipient wetness impregnation over different acidic supports: amorphous SiO_2-Al_2O_3, ZSM5 and beta zeolites. In addition to the effect of the support, other variables like the metal loading (0, 1, 2 and 4 wt%) on ZSM5 were tested in the direct conversion of levulinic acid (LA) to valeric biofuels (valeric acid/ester). The best result, a 92% yield of valeric biofuels, was obtained for a 2 wt% Pd supported on ZSM5 catalyst (2PdZSM5) after 8 h of reaction at 240 °C. Characterization techniques such as FTIR spectroscopy (using deuterated acetonitrile and CO as probe molecules), TEM and XPS were employed to explain this catalytic performance. FTIR spectra with deuterated acetonitrile evidenced the moderate acidity (in terms of concentration and strength) of the 2PdZSM5 catalyst, a desirable feature for the proper realization of this reaction. It has been observed that the acidity of the support favors the Pd dispersion, but it is less relevant for its catalytic properties. Finally, the stability of a representative catalyst was demonstrated under flow conditions for over 90 h, obtaining moderate but stable yields for the 2PdZSM5 catalyst.

Keywords Pd catalyst · Valeric biofuels · Levulinic acid · Stability · DRIFT · Deuterated acetonitrile

1 Introduction

The industrial development together with the increase of the world population has led to an excessive consumption of major crude oil reserves. There are many alternatives that are being studied, but biomass is the one that is capable to give rise to both energy and organic molecules of interest. Another advantage present in biomass is its abundance throughout the Earth. Among biomass sources, lignocellulose shows the additional characteristic of not interfering with the food chain [1] and it is present in the structure of plants. The process to exploit this lignocellulose involves its conversion to platform molecules, such as levulinic acid (LA), furfural or 5-hydroxymethylfurfural (HMF), by chemical processes [1, 2].

✉ R. Mariscal
r.mariscal@icp.csic.es

[1] Group of Sustainable Energy and Chemistry (EQS), Institute of Catalysis and Petrochemistry (IPC-CSIC), C/Marie Curie 2, Cantoblanco, 28049 Madrid, Spain

[2] Department of Inorganic Chemistry, Crystallography and Mineralogy (Associated Unit to ICP-CSIC), University of Málaga, Campus de Teatinos, 29071 Málaga, Spain

LA is a compound that can be used in the production of textiles, pharmaceuticals, plasticizers and rubbers [3, 4]. LA is a gamma-keto-carboxylic acid, which displays a rich chemistry to be transformed into fuel additives and commodity chemicals. In this sense, Dupont company has patented several LA-derivatives compounds, which have a great potential for the synthesis of Nylon intermediates, ionic liquids and biofuel additives [5].

Among the reactions that can proceed from the LA, its hydrogenation has shown increasing interest in recent years to obtain valuable products [1, 4]. The conversion of LA to γ-valerolactone (GVL) requires two steps. Some authors have pointed out that LA is hydrogenated to obtain hydroxyvaleric acid, which is subsequently dehydrated to (GVL) [6]; however, other authors have established that an acidic medium favors the dehydration and cyclization of the LA to form the angelica lactone, which is then hydrogenated to obtain GVL [7]. This latter compound is also considered as an attractive compound since it can be used as food additive, solvent or fuel additive [8–10]. In addition, GVL can be used as feedstock for the synthesis of valuable chemicals from biomass, such as valeric acid (VA), valeric esters, 5-nonanone, 2-methyltetrahydrofuran or α-methylene-γ-valerolactone [11–14].

In this way, Lange et al. established the synthesis of valeric biofuels from cellulosic biomass. They pointed out the conversion of LA to valeric esters takes place through three consecutive steps: (i) the hydrogenation of LA to GVL using Pt/TiO_2 as catalyst; (ii) the acid-catalyzed ring-opening of the GVL to form valeric acid (VA) over a Pt/HZSM5 catalyst; and (iii) the esterification of VA to valeric esters (VE) using an acidic ion exchange resin [15]. These valeric biofuels have showed better fuel performance than other products obtained from biomass, such as ethanol, *n*-butanol, ethyl levulinate (EL), GVL or 2-methyltetrahydrofuran (MTHF) [15, 16]. In recent years, studies to obtain valeric biofuels are focused on the catalytic processes from LA to VA and VE in one-pot reactions in the presence of bifunctional catalysts, which present an acid character and active hydrogenating sites. The solvent where the reaction takes place has relevance, since the obtained products depend on it. Scheme 1 shows a simple pathway of reaction considering the products when water or ethanol are used like solvent. In the present work ethanol is chosen in order to obtain ethyl valerate in one pot reaction. While if this reaction is conducted in water the main product of the reaction would be the valeric acid and it should subsequently be subjected to its esterification with ethanol in a second reactor. The use of ethanol also implies other differences with respect to water, such as its reactivity and lower boiling temperature.

Among the studies for this reaction, Weckhuysen et al. has reported the direct conversion of LA to VA using Ru-based catalysts supported on HZSM5 and HBEA zeolites, establishing a strong deactivation of the catalyst by the loss of acid sites by the partial dealumination under the catalytic conditions [17, 18]. In the same way, Pan et al. evaluated the one-pot conversion of LA to VA and VE using Ru/SBA-SO_3H, where the Brønsted acid sites associated to sulfonic groups favor the formation of VE [19]. Other authors have pointed out that Pt-species supported on zeolites, such as HZSM5, are highly selective to produce VA from LA [20, 21]. More recently, Kumar et al. evaluated the influence of the W-species in Ni/TiO_2 in the conversion of LA to VA [22]. On the other hand, Li et al. have evaluated the selective electrocatalytic reduction of LA to VA using an electrocatalytic cell reactor with a non-precious Pb-electrode in a single-polymer electrolyte membrane [23, 24].

Pd has shown a high hydrogenating capacity and it is quite resistant to its lixiviate in liquid phase [25]. The present research aims at the catalytic study of Pd supported catalysts in the direct conversion of LA to VA and EV using ethanol like solvent. As indicated above, this one-pot reaction also requires acid centers, so several commercial zeolites (HZSM5, HBEA) and an amorphous SiO_2-Al_2O_3 have been chosen as catalyst supports. This work has focused in an original way to study the acidity provided by the support and the dispersion of the Pd of the catalysts prepared in order to understand their effect on the catalytic behavior. In addition, the stability of one of the catalysts with the best catalytic behavior has been evaluated.

2 Experimental

2.1 Preparation of Catalysts

A series of supported Pd catalysts has been prepared by incipient wetness impregnation. Three different supports have been chosen due to their different acidic properties: amorphous silica-alumina (Sigma–Aldrich, Si/Al = 2.8 and $S_{BET} = 475\ m^2\ g^{-1}$), H-Beta zeolite (Zeolyst, Si/Al = 25 and $S_{BET} = 680\ m^2\ g^{-1}$) and HZSM5 zeolite (ACS Material, Si/Al = 38 and $S_{BET} = 295\ m^2\ g^{-1}$). For the incorporation of the Pd, an aqueous solution of $(NH_4)_2PdCl_4$ (Sigma-Aldrich, ≥ 99.995%) was used. After impregnation, the precursors were dried for 10 h at 120 °C and calcined at 550 °C for 5 h to obtain the metal oxide precursor.

Five catalysts have been prepared following this procedure: 2Pd/HBeta, 1Pd/HZSM5, 2Pd/HZSM5 4Pd/HZSM5 and 2Pd/SiO_2-Al_2O_3 where the number indicates the weight percentage of Pd. The catalysts and supports have been labelled as: 2PdBEA, 1PdZSM5, 2PdZSM5, 4PdZSM5, 2PdSA, BEA, ZSM5 and SA. These catalysts have been tested without further treatment, since the high reducibility of palladium oxide is well known and therefore it was expected that reduction happens under reaction conditions (4 MPa H_2 and 240 °C).

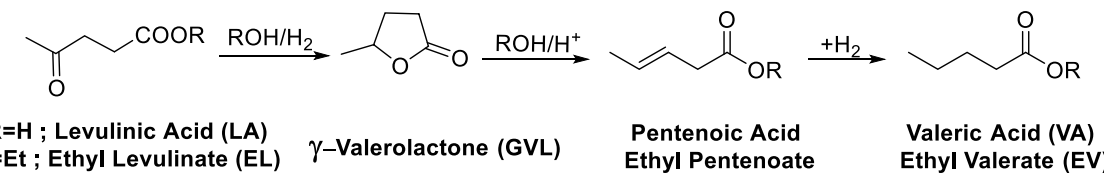

Scheme 1 Reaction pathway for LA/EL conversion to VA/EV

2.2 Activity Measurements

Reactions in batch conditions were carried out in a stainless-steel reactor (100 mL, Parr-series 4590 reactor) loaded with 15 g of ethanol, 2 g of levulinic acid and 0.2 g of catalyst (10 wt% of catalyst in relation to LA). Once loaded, the reactor was flushed several times first with nitrogen to remove the air, and later with hydrogen to replace the nitrogen. Then, the system was pressurized at 4.0 MPa of H_2 and heated to the reaction temperature (240 °C) that was measured with the thermocouple in direct contact with the reaction medium. When the reactor reached the set temperature, agitation at 700 rpm was applied. This was considered the starting time for the reaction (t = 0).

Reactants and products in the liquid were analyzed by gas chromatography (Agilent 6890 N) using a capillary column (ZB-WAX: 30 m × 0.32 mm × 0.50 µm) equipped with a flame ionization detector (FID). The detected products were ethyl levulinate (EL), gamma-valerolactone (GVL), ethyl valerate (EV), valeric acid (VA), methyltetrahydrofuran (MTHF), 1-pentanol (1-PeOH). The samples for analysis were prepared by adding a known amount of the internal standard (0.1 g of cyclohexanol) to 2 g of product sample. Conversion of LA is defined as the ratio of moles of LA consumed in the reaction to the total moles of LA initially present (Eq. 1). Yield is the ratio of moles of product formed to the total moles of LA initially present (Eq. 2), being the selectivity to the products the result of dividing the yield by the conversion calculated previously (Eq. 3).

$$Conversion\ (\%) = \frac{consumed\ LA\ (moles)}{initial\ LA\ (moles)} \times 100 \quad (1)$$

$$Yield\ (\%) = \frac{formed\ product\ (moles)}{initial\ LA\ \ (moles)} \times 100 \quad (2)$$

$$Selectivity\ (\%) = \frac{formed\ product\ (moles)}{consumed\ LA\ \ (moles)} \times 100 \quad (3)$$

Fixed-bed continuous reaction was carried out at 250 °C and 3.0 MPa of H_2. The catalyst (0.25 g) was loaded between two layers of quartz wool and filled with silica chips. The system was heated to 250 °C under a nitrogen flow and, when the temperature was achieved, nitrogen was changed by H_2 and it was pressurized to 3 MPa. The reaction starts when an ethanolic solution of LA (10 wt%) was fed at the desired rate. Samples were collected at regular time periods and analyzed using the same procedure as for the batch reactions.

2.3 Catalysts Characterization

The diffuse reflectance infrared Fourier transform (DRIFT) spectra were collected with a Nicolet 5700 spectrometer equipped with an Hg-Cd-Te cryodetector of high sensitivity, working in the spectral range of 4000–650 cm^{-1}. A diffuse reflectance accessory (Praying Mantis-Harrick Co) was used as mirror optical accessory. About 30 mg of samples, previously ground, were placed in a high temperature catalytic reaction chamber (HVC-DRP Harrick Scientific Products, NY) that allows treatment in situ at high temperature. The calcined sample was pretreated 120 °C during 1 h under a flow of Ar (50 ml min^{-1}) to clean the surface and then cooled to 25 °C. To evaluate the surface acidity deuterated acetonitrile (CD_3CN) was used like probe molecule. CD_3CN was dosed at room temperature passing the flow of Ar through a bubbler placed prior to DRIFT compartment during time sufficient to saturate the sample. Next and prior to the collection of the spectrum the physisorbed fraction of CD_3CN was removed by flushing with Ar flow at 100 °C for 5 min. Carbon monoxide (CO) was also used as a probe molecule to identify the state of oxidation and aggregation of palladium surface species. Prior to CO adsorption, calcined catalysts were reduced under a 10% H_2/Ar flow (50 ml min^{-1}) at 240 °C during 1 h. After that, H_2 was replaced by Ar (50 ml min^{-1}) and the sample was cooled to room temperature. Then a 5% CO/He flow (30 ml min^{-1}) was fed until adsorption. CO physisorbed was removed by flushing with Ar at this temperature for 2 min. In both case each spectrum was recorded with 128 scans accumulation and a resolution of 4 cm^{-1}.

HRTEM microscopy was performed in order to evaluate the morphology and the dispersion of the palladium particles by using a JEOL JEM-2100 F model, working with an acceleration voltage of 300 kV. Specimens were prepared by ultrasonically dispersing some powder sample in absolute ethanol and a droplet of the suspension was put on a Cu grid.

XPS spectra were obtained by using a Physical Electronics PHI 5700 spectrometer with non-monochromatic Mg Kα radiation (300 W, 15 kV, 1253.6 eV) with a multichannel detector. Spectra were recorded in the constant pass energy mode at 29.35 eV using a 720 µm diameter analysis area. The static charge of the samples was corrected by referencing all binding energies (BE) against adventitious carbon (C 1s at 284.8 eV). A PHI ACCESS ESCA-V6.0 F software package was used for acquisition and data analysis. A Shirley-type background was subtracted from the signals. All recorded spectra were fitted using Gaussian–Lorentzian curves to more accurately determine the BE of the different element core levels. The samples were outgassed at room temperature for 1 h at 10^{-7} mbar before being transferred to the ion-pumped analysis chamber, where the residual pressure was kept below 7×10^{-9} mbar during data acquisition. The XPS of Pd 3*d*, Si 2*p*, Al 2*p*, O 1*s* and C 1*s* spectra were scanned a number of times to obtain a good signal-to-noise ratio.

3 Results and Discussion

3.1 Catalytic Activity

Palladium supported over the three supports (HBEA, HZSM5 and SiO_2-Al_2O_3) have been assayed in the conversion of levulinic acid to obtain valeric biofuels. To make easy the description and discussion of the results of catalytic activity presented below, it is necessary to bear in mind the Scheme 1 with the reaction pathway. Figure 1 shows the catalytic behavior of catalysts containing 2 wt% of palladium, after 4 h of reaction. In the three cases, almost full LA conversion was reached, although the yield pattern differs between them. The 2PdSA catalyst displays the poorest results in terms of production of VA/EV, being ethyl levulinate (EL) the main product, followed by gamma-valerolactone (GVL) and the rest were basically unknown products, which is calculated as the subtraction of the levulinic acid conversion by the sum of the yields of identified products. This result indicates that this catalyst does not possess a sufficient amount of the required active sites to conduct the transformation of the EL and GVL intermediates, especially to give the ring-opening reaction of GVL. Thereby the reaction is retained in the first stages of tandem reactions. The amount of unknown products also reveals the existence of side reactions, while the yield towards the desired products (VA and EV) is only 3%. 2PdBEA and 2PdZSM5 catalysts, after 4 h of reaction, gave rise to comparable LA conversion and EV and VA yields. The main difference, in this case, can be found in the EL yield and unknown products. 2PdBEA leads to more than a 25% of unknown products, whereas 2PdZSM5 does not. With respect to the unknown compounds it has to say that some small peaks are present in our chromatograms, some of them have been identified such as methyltetrahydrofuran, 1-pentanol and ethyl pentenoate isomers but in any case it could mean less than 3–5% in total and is not enough to explain the loss in carbon balance. Therefore, other heavy products must be formed that are not detected by the gas chromatography.

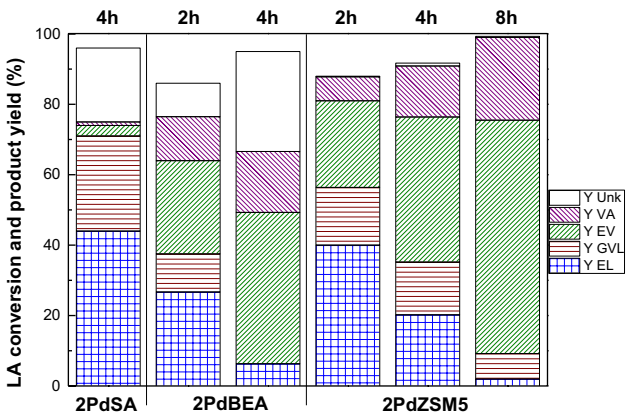

Fig. 1 Levulinic acid conversion and reaction product yields for the palladium supported catalysts at different reaction times. Reaction conditions: 15 g Ethanol, 2 g LA, 0.2 g catalyst, T = 240 °C, 4.0 MPa H_2 and 700 rpm

To further analyze the difference in the catalytic performance of 2PdBEA and 2PdZSM5, both active and selective catalysts, kinetic experiments have been carried out. For that, catalytic processes have been conducted at different reaction times and results are also represented in Fig. 1. For 2PdBEA catalyst, experiment at 2 h was also conducted and, as it could be expected, yield of the intermediate products, EL and GVL, were lower than after 4 h. The yield of unknown products, on the other side, is higher at 4 h than at 2 h. This information indicates that the reaction cannot evolve to desired EV and VA when employing longer reaction time. The two hours experiment was conducted to elucidate if the reaction passes through an optimum before 4 h, but it can be discarded. For the 2PdZSM5 catalyst, three experiments were conducted at 2, 4 and 8 h. After 4 h, the yield of unknown products is negligible. More than 30% of combined EL and GVL remains still capable to evolve to ethyl valerate and valeric acid. This result suggests that longer reaction times may be positive for 2PdZSM5. Extending reaction time to 8 h confirms this hypothesis obtaining a 92% of yield of combined EV and VA, the best performance for the three catalysts tested.

Back to the comparison between the different acid supports, Fig. 2 shows catalytic results for the three bare supports (palladium-free samples). The reactions were carried out under the same experimental conditions, but starting from a GVL instead than from a LA ethanolic solution. In these experiments, the objective was to evaluate the GVL ring-opening capacity, closely related to acidic properties of catalysts. Although the three supports are acidic, it is clearly shown that the SA support exhibits a much lower activity for the ring-opening reaction and this is the cause of the worse catalytic behavior of the 2PdSA with respect to 2PdBEA and 2PdZSM5 catalysts, where the difference concerning to ring opening capacity between them is minor.

Once ZSM5 support has been identified like the best for our purpose, the influence of the palladium content (0–4 wt% Pd) was also evaluated, since the palladium metal is responsible for the hydrogenating character. Figure 3 shows that ZSM5 palladium-free sample presents a low selectivity of VA and EV because it lacks from hydrogenating capacity. This result confirms the requirement of a metal to produce the hydrogenation reactions. When comparing 1PdZSM5, 2PdZSM5 and 4PdZSM5 catalysts, only slight differences are observed, indicating that the 1PdZSM5 already has enough exposed Pd centers to fulfill the hydrogenating role and that even lower Pd

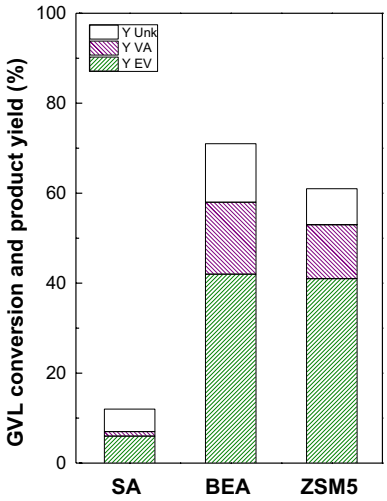

Fig. 2 GVL conversion and reaction product yields for the acid supports samples. Reaction conditions: 15 g ethanol, 2 g GVL, 0.2 g catalyst, T = 240 °C, 4.0 MPa H_2, 700 rpm and 4 h reaction time

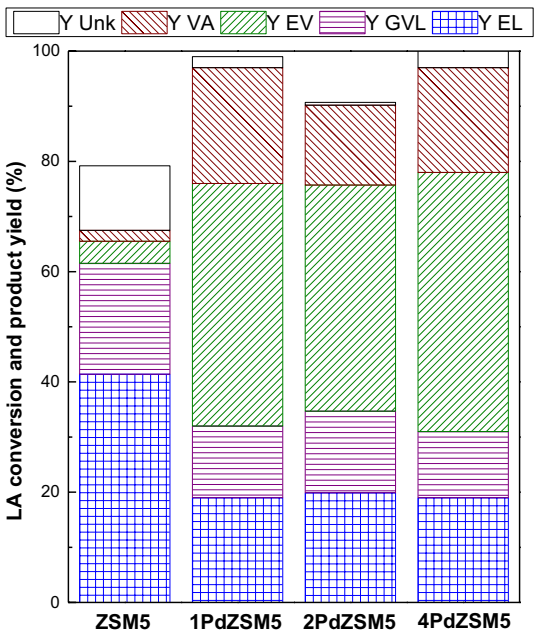

Fig. 3 Levulinic acid conversion and reaction product yields for palladium content ZSM-5 supported catalysts. Reaction conditions are same than Fig. 1

loading can be used. It suggests that the ring-opening of GVL is the rate determining step in agreement with Luo et al. have already reported using other solvent [17].

3.2 Characterization of the Catalysts

To explain this catalytic behavior the characterization of surface acidity and metal palladium has been conducted. Surface acidity of supports and catalysts was evaluated by the diffuse reflectance infrared Fourier transform (DRIFT) technique using deuterated acetonitrile as probe molecule to know the nature, strength and amount of acid centers. Acetonitrile chemisorbed on Lewis acids sites (LAS) displays a νCN vibration clearly distinguishable (> 2300 cm^{-1}) from that assigned to acetonitrile chemisorbed on Brønsted acid sites (BAS, < 2300 cm^{-1}). The dynamic diameter of this selected probe molecule is small and therefore diffusion problems within channels of the zeolite are not expected [26]. Figure 4 shows the spectra obtained for the different acid supports and catalysts with 2 wt% Pd. It is observed a vibration band around 2270 cm^{-1} associated to CD_3CN adsorbed on surface silanol groups, as previously described by other authors [27, 28]. This assignment was confirmed by the fact that, after CD_3CN outgassed by flushing at different temperatures and times, a clear increasing in the intensity of the free silanol groups at 3740 cm^{-1} was also observed (not shown here). The infrared bands at higher wavenumber (> 2300 cm^{-1}) are associated with deuterated acetonitrile adsorbed on Lewis acid sites. The shift of the LAS bands to higher wavenumbers indicates an increase of the strength of these acid sites.

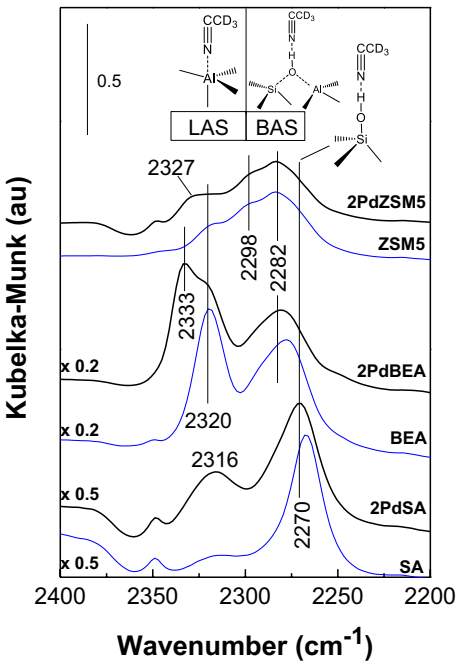

Fig. 4 DRIFT spectra for Pd supported catalysts with adsorbed CD_3CN as basic probe molecule

It can be observed that all samples present both silanol groups and Lewis acid sites. The acid strength of these type of centers is higher for 2PdBEA, showing a maximum at 2333 cm^{-1} slightly stronger than for the Pd-free BEA. For the ZSM5 support, the acid strength distribution is broader, with several maxima at 2282, 2298 (BAS) and 2327 cm^{-1} (LAS). Thus, it can be stated that BEA presents a stronger acidity and more homogeneous in their strength when compared with ZSM5. To end up the comparison, SA support shows the weakest acid sites at 2316 cm^{-1}. On the other hand, the amount of Lewis acid sites is associated with the amount of aluminum exposed in the surface. This aluminum follows the sequence BEA > SA > ZSM5 (see the multiply factor in the Fig. 4).

Summarizing, the catalysts containing the strongest acid sites, 2PdBEA and 2PdZSM5, are able to carry out the GVL ring-opening reaction, whereas 2PdSA has too weak acidity to accomplish it. Comparing 2PdBEA and 2PdZSM5, the 2PdZSM5 contains the weakest acid sites, minimizing the formation of heavy products but showing enough strength for the GVL ring-opening. It has been reported that, besides the acidic strength, it is also relevant the nature of acid centers [29] and the BAS/LAS ratio [30]. Moreover, the amount of surface exposed acid sites is also relevant since 2PdBEA gives more unknown products than 2PdZSM5 catalyst. It could be possibly due to the fact that the number of exposed acid centers is much higher in the 2PdBEA as well.

Since the Pd metal is responsible for the hydrogenating character of these catalysts, the palladium dispersion was studied by transmission electron microscopy (TEM). In the Fig. 5 some micrographs and Pd particle size distributions are shown as examples for the fresh and used catalysts. The data extracted from this technique are compiled in Table 1. The fresh 2PdBEA catalyst presents a very high dispersion of metal particles (average metal size of 2.9 nm.). The greatest acidic strength and the highest number of acid sites correspond to the 2PdBEA catalyst, the one that shows the best dispersion. On the other hand, 2PdZSM5 shows an average particle size of 8.0 nm, worse than the previous one. This

Table 1 Average Pd particle size (nm) calculated by TEM micrographies of fresh and used Pd supported catalysts

Catalysts	Fresh	Used
2PdSA	13.70 ± 0.49	14.80 ± 0.43
2PdBEA	2.87 ± 0.06	19.86 ± 1.01
1PdZSM5	8.33 ± 0.37	–
2PdZSM5	7.99 ± 0.33	7.59 ± 0.24
4PdZSM5	6.99 ± 0.22	–

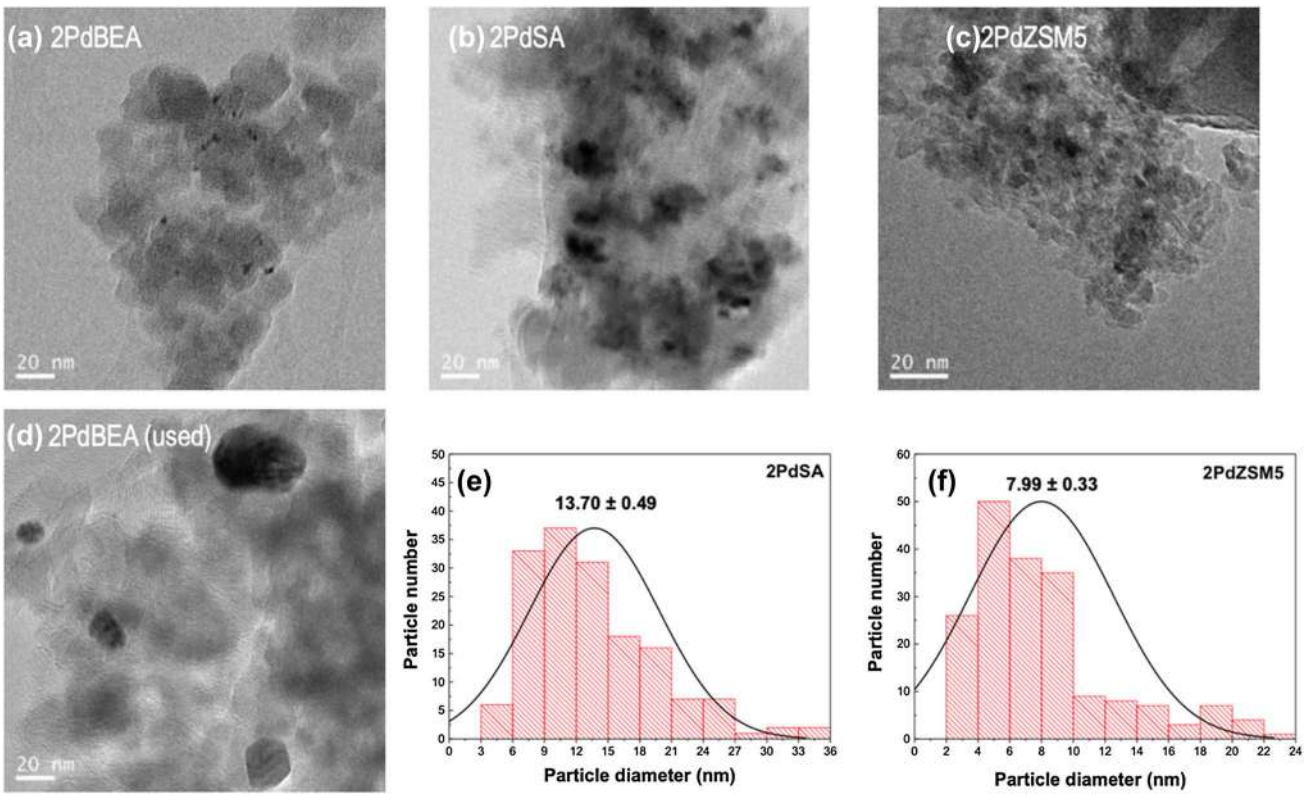

Fig. 5 TEM images of (**a**) 2PdBEA, (**b**) 2PdSA, (**c**) 2PdZSM5, (**d**) 2PdBEA (used) and particle size distribution of (**e**) 2PdSA and (**f**) 2PdZSM5 catalysts

also agrees with the lower amount and strength of acid sites. The poorest dispersion (average particle size of 13.7 nm.) was found for 2PdSA catalyst, the support with the lowest acidic strength, even if it shows a higher amount of acid centers than the previous ones. These data allow relating the strength of the acid sites and Pd dispersion, the lower the strength the larger the particle size and the lower the dispersion [31, 32]. Finally the comparison of the ZSM5 series with different Pd content was carried out and there are not significant differences between them.

The infrared spectroscopy using CO as probe molecule results to be useful to analyze the palladium species and their aggregation in different catalysts. DRIFT spectra corresponding to the different reduced catalysts are displayed in the Fig. 6. For all samples, a low intensity band in the range of 2100–2000 cm^{-1} was observed, which is attributed to the linear adsorption of CO on a Pd atom in its metallic state [33, 34]. The position of the maximum for this band changes for the different supports, shifting from 2073 cm^{-1} for BEA, 2057 cm^{-1} in the case of ZSM5 and up to 2048 cm^{-1} for the SA. This result indicates that longer shifts of linear CO band towards higher wavenumbers are observed in those supports displaying stronger acid centers. These stronger acid centers as mentioned above favor the dispersion of supported palladium.

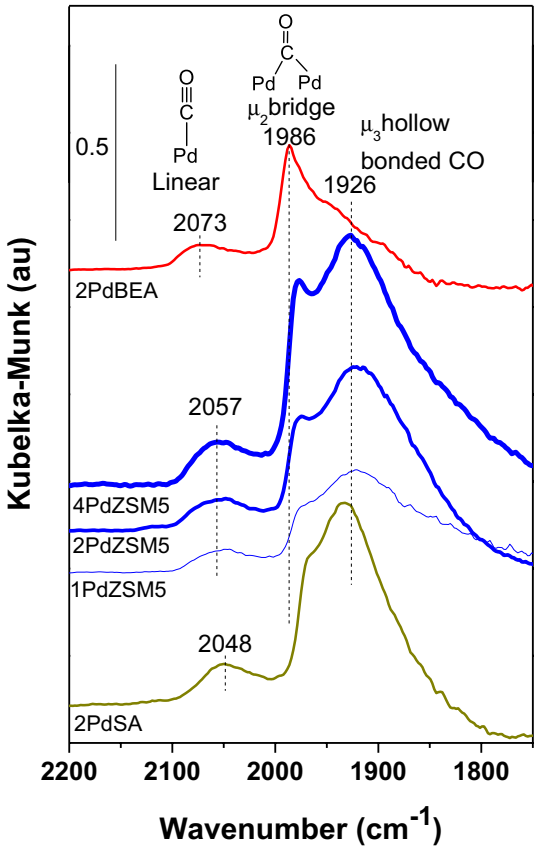

Fig. 6 DRIFT spectra for reduced Pd supported catalysts with CO as probe molecule

Below 2000 cm^{-1}, there are two bands: one narrow centered at 1986 cm^{-1} and another much wider at 1926 cm^{-1}. The former can be associated to twofold μ_2 bridged-bonded CO on Pd (100) faces and the second broad band to μ_3 hollow bonded CO or twofold bridged-bonded CO on (111) planes of palladium particles [34, 35]. The intensity and shift of the band at 1986 cm^{-1} follows the same trend as that previously described for the linear CO band. The maximum of the third infrared band at 1926 cm^{-1} shows no shift. However, there are significant differences in its intensity, being the most intense in the case of 2PdSA catalyst. All this indicates that the dispersion of palladium will depend on the strength of the acid sites present in the support [31, 32]. The order in terms of dispersion of Pd is as follows: BEA > ZSM5 > SA. These results are consistent with those found by TEM.

The superficial composition of the calcined and reduced Pd-based catalysts was determined by X-ray photoelectron spectroscopy (XPS). In all cases, the signal was corrected using the adventitious carbon in the C 1s core level spectra (284.8 eV), as reference, and the results are collected in Table 2. With regard to the O 1s core level spectra, it is noteworthy the presence of a single contribution ascribed to the presence of oxides species and zeolites. It is necessary to emphasize that for Al 2p contribution about 74.0 eV for the ZSM5 support, this binding energy value is shifted to higher values (74.5–74.8 eV) when Pd species are incorporated. This fact suggests that Pd species could increase their electronic density due to the interaction with aluminum after calcination. This is in agreement with the DRIFT spectra with deuterated acetonitrile, where a shift to higher wavenumbers was observed. The Pd 3d core level spectra displays a small contribution located about 336.6 eV, which

Table 2 Binding energies and Pd/Si + Al atomic ratio for calcined and reduced catalysts

Samples	Binding energy (eV)				Pd/Si + Al atomic ratio
	O 1s	Si 2p	Al 2p	Pd 3d	
ZSM5	531.8	103.0	74.0	–	–
1PdZSM5	531.7	103.2	74.6	336.7	0.0034
1PdZSM5 (red)	532.0	103.3	74.8	335.2	0.0021
2PdZSM5	531.8	103.1	74.5	336.7	0.0056
2PdZSM5 (red)	531.9	103.2	74.8	335.1	0.0047
4PdZSM5	531.9	103.1	74.6	336.7	0.0104
4PdZSM5 (red)	531.8	103.2	74.8	335.1	0.0072
2PdBEA	531.9	103.5	74.8	336.9	0.0030
2PdBEA (red)	531.9	103.2	74.8	335.1	0.0020
2PdSA	532.1	102.9	74.6	336.8	0.0022
2PdSA (red)	532.0	103.1	74.7	335.1	0.0011

is assigned to oxidized Pd species (Pd^{2+} and/or Pd^{4+}) for the catalytic precursor. After the reduction at 240 °C, the contribution ascribed to oxidized species disappears, arising another one between 335.0 and 335.2 eV, which is assigned to Pd^0, so the catalyst is fully reduced.

On the other hand, the surface Pd/Si + Al atomic ratio indicates that Pd content on the catalyst surface increases directly with the Pd content on ZSM5 support both in calcined precursor and in its corresponding reduced. In the case of catalysts with 2 wt% of Pd, the surface Pd content is similar for 2PdBEA and 2PdZSM5 catalysts. It is noteworthy that 2PdBEA catalyst exhibited the smallest particle size in the TEM micrograph. This fact should suppose a greater dispersion on the catalyst surface. However, it must be considered that BEA zeolite also presents mesopores and Pd species can be inside these mesochannels. XPS is a superficial characterization technique, a portion of these well dispersed Pd particles may not be detected. 2PdSA showed the lower Pd dispersion which is consistent with the TEM and CO-DRIFT data previously described.

For further comprehension of the catalytic activity, the catalysts used in the batch reactor and the solution after reaction have been studied and analyzed. The chemical analysis by total reflection X-ray fluorescence (S2 PicoFox TXRF spectrometer) of the reaction medium after reaction confirms that there is no Pd leaching in the medium. TEM is also a valuable tool to confirm that there is no sintering for 2PdZSM5 and 2PdSA catalysts, since average particle size does not change for fresh and used samples. However, for 2PdBEA, particle size increases significantly from fresh to used, indicating that sintering is taking place. 2PdZSM5 and 2PdSA show a higher stability against sintering than 2PdBEA.

Moreover the used catalysts have been studied by DRIFT spectroscopy. Figure 7a shows the spectra after adsorption of deuterated acetonitrile. The suffixes -u and –ur after the name of the catalyst means sample used in reaction and used and regenerated by calcination respectively. Both 2PdZSM5 and 2PdBEA active catalysts show that the strongest Lewis acid sites, at 2333 and 2327 cm^{-1}, respectively, disappear after reaction. In the case of 2PdBEA-u catalyst, weaker Lewis centers at 2317 cm^{-1} appear in their place. With this information, a regeneration process by calcination in air flow (50 ml min^{-1}) at 300 °C during 30 min was applied. The goal was to eliminate possible carbonaceous residues that could have been formed on the acid centers during the course of the reaction. In the case of 2PdZSM5-ur, these LA sites with high acid strength are recovered after this process, while in the case of 2PdBEA-ur no significant changes in the surface acidity of the used catalyst were observed after the regeneration process. Thus, it can be stated that the carbonaceous deposits could be removed for 2PdZSM5-u employing the calcination to recover its acidic properties, whereas this calcination process is not as effective for 2PdBEA-u catalyst.

Another region to analyze in the infrared spectra when considering carbonaceous deposits is the range at 3000–2800 cm^{-1}, that is, the C–H stretching region (Fig. 7b). It can be appreciated that, as expected, no band appears in this region for the fresh catalysts. However, for the used catalysts, bands at 2980, 2962, 2936 and 2877 cm^{-1} are present, which can be assigned to symmetric and asymmetric stretching vibrations of CH_2 and CH_3 [36, 37]. After

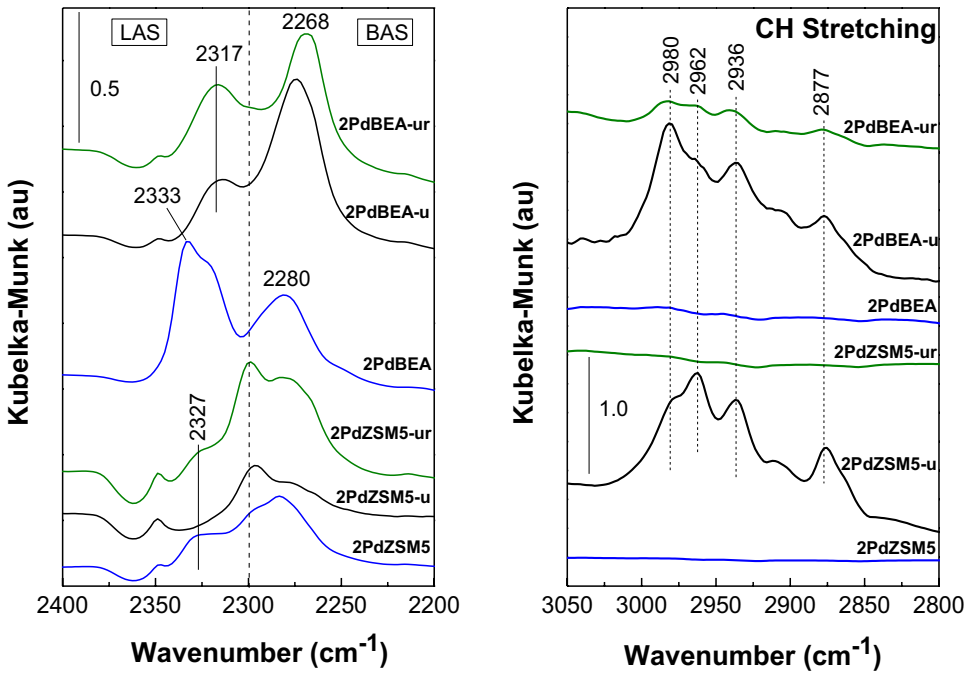

Fig. 7 DRIFT spectra of used catalysts in batch reactor and regenerated 2PdBEA and 2PdZSM5 catalysts (**a**) after adsorption of CD_3CN and (**b**) C–H stretching region

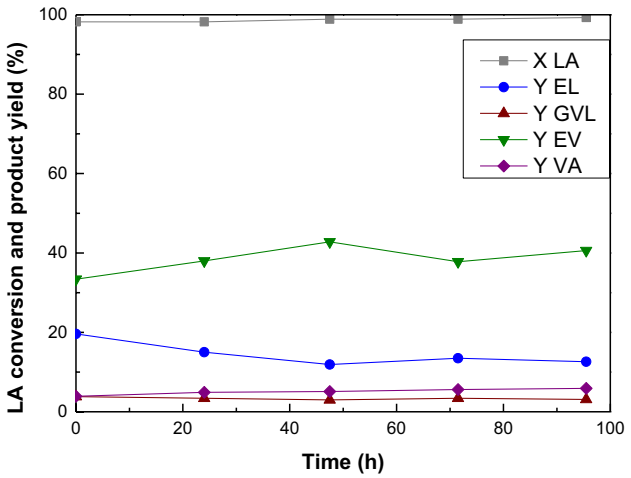

Fig. 8 Levulinic acid conversion and reaction product yields for the 2PdZSM5 in the fixed bed reactor. Reaction conditions: 10 wt% LA in ethanol, 0.25 g catalyst, WHSV = 2 h^{-1}, 250 °C and 3.0 MPa of H_2

calcination, 2PdZSM5-ur sample, these bands disappeared completely, while in the case of the 2PdBEA-ur sample, after applying this same procedure, these bands have significantly decreased their intensity, although they are not completely eliminated. This reveals that the carbonaceous residues are more difficult to remove in this last catalyst, with acid centers of greater strength than for ZSM5. This behavior may be due to the different nature or amount of carbonaceous deposits present on the 2PdBEA used catalyst.

3.3 Evaluation of the Stability of Catalysts

Tests carried out in batch conditions have allowed to discard leaching, since no Pd was detected in the chemical analysis of the reaction medium. However, the study of the surface acidity of the used catalysts by DRIFT shows fouling by carbonaceous deposit, which can be fully removed by calcination, at least for the 2PdZSM5 catalyst, as already explained. Besides, sintering for 2PdBEA used catalyst was also observed by TEM data, while 2PdZSM5 has a stable particle size. Since batch reactor had problems like quantitative recovering of the catalyst for reutilization cycles a suitable study of the stability of the catalyst must be conducted in a continuous system with a fixed-bed reactor. Besides when considering a hypothetical industrial application, flow reactor is the preferred option because it results in higher space time-yield (batch reactor involves shutting down the reactor and several steps for separating the catalyst from the reaction medium). Figure 8 displays the results of this experiment with the 2PdZSM5 catalyst, which was selected due to its best catalytic activity. It was placed in the reactor, where it was heated at 250 °C, pressurized at 3 MPa under H_2 and fed with an ethanolic solution of levulinic acid (10 wt%) at a WHSV = 2 h^{-1}. The yields for EV and VA in this case were around 40%. The difference between batch and flow results is due to the variation in reaction conditions. The mayor change is due to the working pressure for the batch reactor, provided by hydrogen and the autogenous pressure of the solvent at reaction temperatures (liquid phase), whereas that under the conditions of the continuous system the reagents are in the gas phase. Despite these differences between both systems it can be stated that, under these reaction conditions of the fixed-bed reactor, the 2PdZSM5 catalyst is stable for more than 90 h and it is valid to confirm its promising stability.

4 Conclusions

2PdZSM5 and 2PdBEA are active catalysts in the direct conversion of levulinic acid (ethanolic solution) into valeric biofuels (valeric acid and ethyl valerate). The reaction goes through the GVL intermediate and the ring opening was the rate determining step which has to be catalyzed by acid centers. The acidity required to obtain valeric biofuels has to be adequate in strength and amount. The acid sites of SA support are too weak to open the GVL ring ant thus, its activity for this reaction is low. On the other extreme, 2PdBEA shows acid sites too strong, giving rise to a poor yield due to the increasing of the amount of unknown products.

The best catalytic performance has been obtained for the 2PdZSM5 catalyst, which, after 8 h of reaction, a 92% yield of products of interest (ethyl valerate and valeric acid) was achieved. This behavior may be explained by the moderate acidity of the catalyst, both in strength and amount of acid sites. It has also been seen that the acidity of the support affects the Pd dispersion, but it is less relevant for its catalytic properties.

The stability of the 2PdZSM5 has been demonstrated in fixed-bed reactor, continuous system, for more than 90 h. However, the characterization of the batch used catalyst shows that surface acid sites are fouling by the formation of carbonaceous deposits. It has also been demonstrated that a simple calcination process is able to remove totally these deposits and regenerate the surface acidity of the catalyst.

Acknowledgements Financial support from Spanish Ministry of Economy and Competitiveness (CTQ2015-64226-C3-1-R and CTQ2015-64226-C3-3-R) is gratefully acknowledged.

References

1. Pileidis FD, Titirici MM (2016) Levulinic acid biorefineries: new challenges for efficient utilization of biomass. ChemSusChem 9:562–582

2. García-Sancho C, Fúnez-Núñez I, Moreno-Tost R, Santamaría-González J, Pérez-Inestrosa E, Fierro JLG, Maireles-Torres P (2017) Beneficial effects of calcium chloride on glucose dehydration to 5-hydroxymethylfurfural in the presence of alumina as catalyst. Appl Catal B 206:617–625
3. Lewkowsky J (2001) Synthesis, chemistry and applications of 5-hydroxymethylfurfural and its derivatives. Arkivoc. https://doi.org/10.3998/ark.5550190.0002.102
4. Yan K, Jarvis C, Gu J, Yan Y (2015) Production and catalytic transformation of levulinic acid: A platform for speciality chemicals and fuels. Renew Sust Energ Rev 51:986–997
5. Manzer LE (2013) Catalysis for the conversion of biomass and its derivatives (Max Planck Research Library for the History and Development of Knowledge.) Edited by Malte Behrens and Abhaya K. Datye. https://doi.org/10.1002/anie.201305619
6. Wang J, Jaenicke S, Chuah GK (2014) Zirconium–Beta zeolite as a robust catalyst for the transformation of levulinic acid to γ-valerolactone via Meerwein–Ponndorf–Verley reduction. RSC Adv 4:13481–13489
7. Serrano-Ruiz JC, West RM, Dumesic JA (2010) Catalytic conversion of renewable biomass resources to fuels and chemicals. Annu Rev Chem Biomol Eng 1:79–100
8. Yan K, Jarvis C, Lafleur T, Qiao Y, Xie X (2013) Novel synthesis of Pd nanoparticles for hydrogenation of biomass-derived platform chemicals showing enhanced catalytic performance. RSC Adv 3:25865–25871
9. Yan K, Lafleur T, Wu G, Liao J, Ceng C, Xie X (2013) Highly selective production of value-added gammavalerolactone from biomass-derived levulinic acid using the robust Pd nanoparticles. Appl Catal A 468:52–58
10. Horváth IT, Mehdi H, Fábos V, Boda L, Mika LT (2008) γ-valerolactone, a sustainable liquid for energy and carbon-based chemicals. Green Chem 10:238–242
11. Yan K, Yiyi Y, Chai J, Lu Y (2015) Catalytic reactions of gamma-valerolactone: a platform to fuels and value-added chemicals. Appl Catal B 179:292–304
12. De S, Saha B, Luque R (2015) Hydrodeoxygenation processes: advances on catalytic transformations of biomass-derived platform chemicals into hydrocarbon fuels. Bioresour Technol 178:108–118
13. Alonso DM, Wettstein SG, Dumesic JA (2013) Gamma-valerolactone, a sustainable platform molecule derived from lignocellulosic biomass. Green Chem 15:584–595
14. Alonso DM, Wettstein SG, Mellmer MA, Gurbuz EI, Dumesic JA (2013) Integrated conversion of hemicellulose and cellulose from lignocellulosic biomass. Energy Environ Sci 6:76–80
15. Lange JP, Price R, Ayoub PM, Louis J, Petrus L, Clarke L, Gosselink H (2010) Valeric biofuels: a platform of cellulosic transportation fuels. Angew Chem Int Ed 49:4479–4483
16. Dayma G, Halter F, Foucher F, Togbé C, Mounaim-Rouselle C, Dagaut P (2012) Experimental and detailed kinetic modeling study of ethyl pentanoate (ethyl valerate) oxidation in a jet stirred reactor and laminar burning velocities in a spherical combustion chamber. Energy Fuels 26:4735–4748
17. Luo W, Deka U, Beale AM, Van Eck ERH, Bruijnincx PCA, Weckhuysen BM (2013) Ruthenium-catalyzed hydrogenation of levulinic acid: influence of the support and solvent on catalyst selectivity and stability. J Catal 301:175–186
18. Luo W, Bruijnincx PCA, Weckhuysen BM (2014) Selective, one-pot catalytic conversion of levulinic acid to pentanoic acid over Ru/H-ZSM5. J Catal 320:33–41
19. Pan T, Deng J, Xu Q, Xu Y, Guo QX, Fu Y (2013) Catalytic conversion of biomass-derived levulinic acid to valerate esters as oxygenated fuels using supported ruthenium catalysts. Green Chem 15:2967–2974
20. Kon K, Onodera W, Shimizu KI (2014) Selective hydrogenation of levulinic acid to valeric acid and valeric biofuels by a Pt/HMFI catalyst. Catal Sci Technol 4:3227–3234
21. Lange JP (2011) US Patent 2011/0112326. Shell Int BV
22. Kumar VV, Naresh G, Deepa S, Bhavani PG, Nagaraju M, Sudhakar M, Chary KVR, Tardio J, Bhargava SK, Venugopal A (2017) Influence of W on the reduction behaviour and Brønsted acidity of Ni/TiO2 catalyst in the hydrogenation of levulinic acid to valeric acid: pyridine adsorbed DRIFTS study. Appl catal A 531:169–176
23. Xin L, Zhang Z, Qi J, Chadderdon DJ, Qiu Y, Warsko KM, Li W (2013) Electricity storage in biofuels: Selective electrocatalytic reduction of levulinic acid to valeric acid or γ-valerolactone. ChemSusChem 6:674–686
24. Qiu Y, Xin L, Chadderdon DJ, Qi J, Liang C, Li W (2014) Integrated electrocatalytic processing of levulinic acid and formic acid to produce biofuel intermediate valeric acid. Green Chem 16:1305–1315
25. Jung U, Elsen A, Li Y, Smith JG, Small MW, Stach EA, Frenkel AI, Nuzzo RG (2015) Comparative in operando studies in heterogeneous catalysis: atomic and electronic structural features in the hydrogenation of ethylene over supported Pd and Pt catalysts. ACS Catal 5:1539–1551
26. Chen J, Thomas JM, Sankar G (1994) IR spectroscopic study of CD_3CN adsorbed on ALPO-18 molecular sieve and the solid acid catalysts SAPO-18 and MeAPO-18. J Chem Soc Faraday Trans 90:3455–3459
27. Mariscal R, López-Granados M, Fierro JLG, Sotelo JL, Martos C, Van Grieken R (2000) Morphology and surface properties of titania-silica hydrophobic xerogels. Langmuir 16:9460–9467
28. Van Grieken R, Sotelo JL, Martos C, Fierro JLG, López-Granados M, Mariscal R (2000) Surface modified amorphous titanosilicate catalysts for liquid phase epoxidation. Catal Today 61:49–54
29. Wang Z, Wang L, Jiang Y, Hunger M, Huang J (2014) Cooperativity of Brønsted and lewis acid sites on zeolite for glycerol dehydration. ACS Catal 4:1144–1147
30. Zhang D, Yun-Peng Z, Fan X, Liu ZQ, Wang RY, Wei XY (2018) Catalytic hydrogenation of levulinic acid into gamma-valerolactone over Ni/HZSM-5 catalysts. Catal Surv Asia 22:129–135
31. Aylor AW, Lobree LJ, Reimer JA, Bell AT (1997) Investigations of the dispersion of Pd in H-ZSM-5. J Catal 172:453–462
32. Okumura K, Niwa M (2002) Control of the dispersion of Pd through the interaction with acid sites of zeolite studied by EXAFS. Top Catal 18:85–89
33. Shen Y, Bo X, Tian Z, Wang Y, Guo X, Xie M, Gao F, Lin M, Guo X, Guo X, Ding W (2017) Fabrication of highly dispersed/active ultrafine Pd nanoparticle supported catalysts: a facile solvent-free in situ dispersion/reduction method. Green Chem 19:2646–2652
34. Lear T, Marshall R, Lopez-Sanchez JA, Jackson SD, Klapötke TM, Bäumer M, Rupprechter G, Freund HJ, Lennon D (2005) The application of infrared spectroscopy to probe the surface morphology of alumina-supported palladium catalysts. J Chem Phys 123:174706
35. Agostini G, Pellegrini R, Leofanti G, Bertinetti L, Bertarione S, Groppo E, Zecchina A, Lamberti C (2009) Determination of the particle size, available surface area, and nature of exposed sites for silica—alumina-supported Pd nanoparticles: a multitechnical approach. J Phys Chem C 113:10485–10492
36. Mosqueda-Jiménez BI, Jentys A, Seshan K, Lercher JA (2003) On the surface reactions during NO reduction with propene and propane on Ni-exchanged mordenite. Appl Catal B 46:189–202
37. Ivanov P, Papp H (2000) FT-IR study of the isomerization of n-butene over different zeolites. Langmuir 16:7769–7772

3.2. Elucidating the roles of acid site nature and strength in the direct conversion of levulinic acid into ethyl valerate: the case of Zr-modified beta zeolite-supported Pd catalysts; Sustanaible Energy & Fuel, **6**, 1164-1174 (2022)

Sustainable Energy & Fuels

ROYAL SOCIETY OF CHEMISTRY

PAPER

Cite this: *Sustainable Energy Fuels*, 2022, **6**, 1164

Elucidating the roles of acid site nature and strength in the direct conversion of levulinic acid into ethyl valerate: the case of Zr-modified beta zeolite-supported Pd catalysts†

M. Muñoz-Olasagasti,[a] I. Martínez-Salazar,[a] M. López Granados,[a] C. López-Aguado,[b] J. Iglesias,[b] G. Morales[b] and R. Mariscal*[a]

The effects of the nature and strength of surface acid sites on the properties of the catalyst used for the one-pot conversion of levulinic acid to valeric biofuels have been investigated. The acid supports were prepared from a commercial beta zeolite (HBEA) modified by partial substitution of Al by Zr atoms. This procedure enables changes in the nature and strength of the acidic sites of the starting zeolite. A constant amount of Pd (2 wt%) was incorporated on these acid supports by the incipient wetness impregnation method. These catalysts were tested in liquid phase reactions and the Pd/HBEA catalyst showed the best catalytic performance, achieving an 80% yield of valeric biofuel after 2 h of the reaction. The fresh catalysts were characterized by DRIFT spectroscopy using pyridine, CD_3CN, and CO as probe molecules and by XRD to explain the differences in catalytic performance. The presence of strong Brønsted acid sites (BAS) was shown to be critical for reaching high ethyl valerate yields since the differences in catalytic behavior and the concentration of these acid sites parallel each other. Up to three types of Lewis acid sites (LAS) of different strengths were also identified. These LAS have also been shown to be active, although their intrinsic activities decrease as they are weaker. Reutilization tests of the Pd/HBEA catalyst were also carried out and mild deactivation was observed. The spent catalyst underwent a simple calcination treatment at 773 K and this was adequate for the recovery of the surface acidity, but the reducibility of the Pd species was affected. This prevented complete recovery of catalytic activity.

Received 13th November 2021
Accepted 7th January 2022

DOI: 10.1039/d1se01802g

rsc.li/sustainable-energy

1. Introduction

The high rate of consumption of petrochemical resources constitutes a current global concern. These resources are exploited for their use as fuels and as feedstocks for the synthesis of many chemicals. Biomass is capable of fulfilling both of these functions. First-generation biomass-derived biofuels, such as ethanol from corn or fatty acid methyl esters from plant oils, have the disadvantage of competing with human food needs.[1] Lignocellulosic biomass avoids this competition since it is nonedible, renewable, abundant and has a limited economic value.[2,3] Utilizing this feedstock requires prior processing to obtain platform molecules such as levulinic acid (LA) or furfural.[4–6] LA has great potential due to its functionality, since its keto and carboxylic acid groups are useful for multiple reactions used to upgrade it. Among the products derived from the hydrogenation of LA are 2-methyl tetrahydrofuran, 1,4-pentanediol, gamma-valerolactone (GVL) and valeric biofuels.[7–10]

By focusing on upgrading LA to valeric biofuels, valeric acid and valerate esters, many developments have been realized since Lange *et al.*[11] proposed the procurement of valeric biofuels from lignocellulose *via* LA in 2010. This process consists of a cascade reaction, in which every step requires specific catalytically active sites, as has been recently reported by Yu *et al.*[12] Fig. 1 shows a simplified scheme for the reaction pathway and detailed catalytic requirements. The first step is the conversion of LA to GVL, which proceeds *via* two steps and can follow two different routes: (i) when the reaction is conducted at 473 K the transformation proceeds *via* hydrogenation of LA (catalyzed by metal sites) to provide 4-hydroxyvaleric acid/ester, which is then dehydrated (catalyzed by acid sites) to produce GVL; and (ii) at temperatures above 473 K, the reaction proceeds *via* dehydration of LA (acid sites) to give angelica lactone and this is then hydrogenated (metal sites) to obtain GVL. In the third step, acid sites are required for the GVL ring-opening reaction to give pentenoic acid/ester, which is hydrogenated (at metal sites) to

[a]*Group of Sustainable Energy and Chemistry (EQS), Institute of Catalysis and Petrochemistry (IPC-CSIC), C/Marie Curie 2, Cantoblanco, 28049 Madrid, Spain. E-mail: r.mariscal@icp.csic.es*

[b]*Chemical and Environmental Engineering Group, Universidad Rey Juan Carlos, C/ Tulipán s/n, 28933 Móstoles, Madrid, Spain*

† Electronic supplementary information (ESI) available. See DOI: 10.1039/d1se01802g

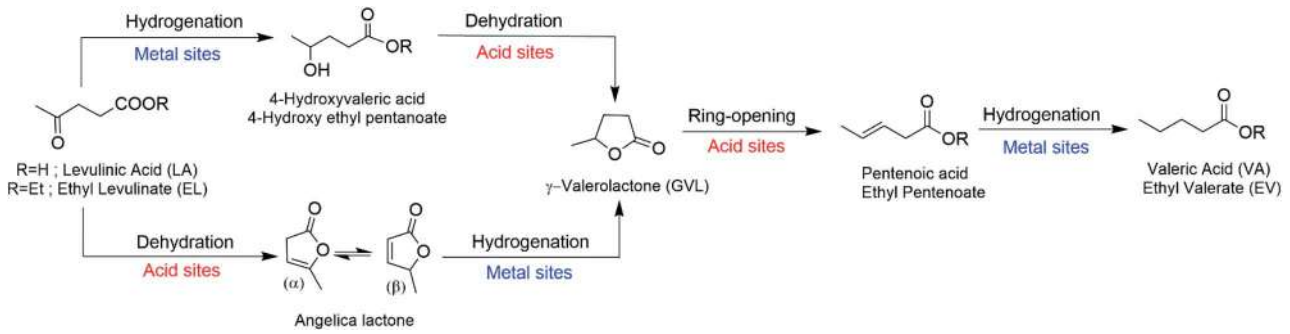

Fig. 1 Scheme of the reaction pathway for conversion of LA/EL into VA/EV in aqueous or ethanol solution (adapted from ref. 12).

valeric acid (VA) in the fourth and final step. If water is used as the solvent, an additional step converts VA into the corresponding valerate ester by acid-catalyzed esterification with alcohol, a reaction usually promoted by strong Lewis acidity.

Therefore, it is evident that a bifunctional catalyst with hydrogenating/metallic and acid functions is required to accomplish this reaction under one-pot conditions. Most of the work regarding the metallic function has studied the type of metal used, such as noble (Pt, Ru and Pd) and non-noble (Co, Ni and Cu) metals. At this point, some other investigations on the selective hydrogenation of levulinic acid to γ-valerolactone should also be emphasized like those based on Cu-ZrO_2,[13] supported Ru[14] and bimetallic Ru–Ni/MMT[15] catalysts.

The acid function has also been worthy of numerous studies because acidic sites have been identified as the active sites in the rate determining step, specifically the ring-opening reaction of GVL.[16] Recently, Yi *et al.*[17] reported that a metal can regulate the selectivity for conversion of LA into GVL or valeric biofuels using 1,4 dioxane as the solvent. The Ru/HZSM-5 catalyst produces a high yield (85.7%) of valeric biofuels, while the Ni/HZSM-5 catalyst achieves a GVL yield of 93.1% with a negligible formation of valeric acid or esters at 473 K and 3 MPa H_2. The introduction of Ru into HZSM-5 increased the number of strong acidic sites and enhanced the ring-opening reaction of the GVL intermediate.

The acid function is generally supplied by the oxide support and does not usually depend on the metal used. Pan *et al.*[18] reported the effects of different supports and acidity levels on the hydrogenation of LA to valerate esters with Ru-based catalysts. A 94% combined yield of ethyl valerate and valeric acid (EV + VA) was achieved after 10 h, using a Ru/SBA-SO_3H catalyst at 523 K and 4 MPa H_2 and ethanol as a solvent. The catalyst was primarily deactivated by leaching of sulfonic acid sites. The acid support most frequently used for the one-pot reaction has been the HZSM5 zeolite with different supported metals such as Pt,[19,20] Ru,[21] Pd[22] and Co[23] under distinct reaction conditions. Regulation of the acidity on the Ni/HZSM-5 catalyst and increases in the potassium content were also studied. Potassium decreased the acid strength and adjusted the ratio of the Brønsted/Lewis centers in the flow reactor at 513 K and with 3.0 MPa of H_2.[24] In general, all these studies show that a cooperative mechanism involving metal and strong BAS is required to carry out the GVL ring-opening reaction. While the role of LAS has been associated with their activity in another step of the tandem reaction, no clear role has been assigned in this essential step. Zhou *et al.*[25] reported for the first time that strong LAS are also active in the ring opening of GVL. These authors have described a dual catalyst consisting of Pd/C and $Hf(OTf)_4$ in *n*-octane solution. At a relatively low temperature of 423 K and with 5.0 MPa H_2, 92% VA selectivity and almost complete LA conversion were obtained. The recycling experiment showed that the catalysts continued to exhibit satisfactory activity after five uses. Recently Muñoz-Olasagasti *et al.*[26] reported the relevance of the LAS in the gas phase conversion of LA into EV using a continuous fixed-bed reactor and ethanol as the solvent for CoSBA-*x*Al catalysts. The best catalyst was that with the highest Al content, CoSBA-2.5Al, which reached an EV yield of up to 70%. This result is associated with the presence of LAS attributed to the presence of Co^{2+} surface species that, although with low intrinsic activity in the selective GVL ring-opening reaction, are highly concentrated in this sample.

Many of the studies described above have been conducted under H_2 pressure and autogenous solvent pressure in the liquid phase in a batch reactor. However, despite all of these studies, it is not clear whether, in the liquid phase, the BAS, LAS or both acid centers are responsible for the direct conversion of LA to EV. Moreover, the effects of the strengths of these acid sites on intrinsic activity also require attention.

This is precisely what we have addressed in this paper, in which we evaluate the effects of the acid site nature (B/L). In other words, it is important to identify the importance of Brønsted and Lewis sites (or both) and whether their different strengths affect their intrinsic activity in the direct conversion of LA to EV under liquid phase conditions. For this, we selected Pd as the reducting metal. Although it is more expensive than other metals such as Co and Ni, its choice is justified because it does not leach into the reaction medium.[22] Moreover, Pd has been described as an efficient metal for the catalytic hydrogenation of levulinic acid in γ-valerolactone[27] where the alloy of Ru–Pd on titanium dioxide favors the activity and stability of the catalyst. Yan *et al.*[28] have also reported a bifunctional Pd/HY catalyst that achieved a 60% yield of the biofuel pentyl valerate in one pot synthesis. However the acid support was the commercial beta zeolite (with an atomic ratio Si/Al = 22) which contains Brønsted and Lewis acid sites. The nature and strength of these centers can be controlled through the substitution of Al

atoms by Zr atoms.[29–31] In acidic zeolites, the negative charge induced by Al is neutralized with protons, creating Brønsted acid sites. After replacing Al by Zr, the Brønsted acidity provided by the former gives rise to Lewis acidity due to the latter. This approach allows us to change the acid function without modifying the structural properties and thermal stability of the support.[32]

This particular research is designed to correlate the nature and strength of acid sites in the catalyst with their catalytic behavior in the conversion of LA to EV. Hydrogenation functionality was achieved by incorporating consistent levels of Pd into the zeolite by impregnation, so the effect of such Pd loading can be ignored in the comparison study. Moreover, structural variations have also been eliminated by using the same beta zeolite structure for all materials, in which the only modification is the progressive substitution of Al by Zr. This showed a strong impact on the acidity of the zeolite but not on other relevant textural and structural properties[33] and is shown in Fig. S1 and S2.† This series of zeolites were tested in the reaction, and their acidic properties were characterized by diffuse reflectance infrared Fourier transform (DRIFT) spectroscopy to elucidate the correlation between acidity and activity. In this work, we found that strong BAS are required to perform the GVL ring-opening reaction. However, LAS also show activity in this reaction but to a lesser extent. Regarding the strength of LAS, the weaker the Lewis centers are, the less activity they exhibit for the LA to EV conversion. Interestingly, these weak acids associated with Zr are also less active in coke formation.

2. Experimental

2.1. Preparation of catalysts

Zr–Al-Beta zeolite acid supports were prepared by substitution of Al atoms with Zr atoms in a commercial Al-Beta zeolite (CP814C, Si/Al ratio = 19, Zeolyst International). An efficient and optimized two-step procedure was followed. Partial dealumination was carried out by treating the commercial zeolite in aqueous HNO_3 with concentrations in the range of 0.1–10 M (room temperature, 1 h, 20 mL g $^{-1}$). To achieve total dealumination, harsher conditions were needed (373 K, 20 h, 20 mL g $^{-1}$). After filtration and washing with deionized water until reaching the neutral pH, the material was dried overnight at 383 K. Dealumination was followed by post-synthetic grafting of Zr species into the generated vacancies. The zirconium precursor ($Zr(NO_3)_4$, Chemical Point) and water concentration for impregnation were optimized to achieve the highest Zr dispersion. Thus, the Zr precursor was suspended in deionized water (10 mL g $^{-1}$), and the corresponding amount of the zirconium salt was added. The resultant solid was heated under vacuum to remove the remaining water, and then it was dried overnight at 473 K. Finally, calcination in air at 823 K (for 6 h, with a heating ramp of 3 C min $^{-1}$) yielded the zeolites in the active form. More details of these preparations can be found in previous work.[30,31,34] The starting commercial beta zeolite was labeled HBEA and three Zr–Al-Beta supports were prepared and labeled ZAB-1.6, ZAB-0.1 and ZAB-0.0, where the number denotes the Al/Zr molar ratio.

Afterward, the incipient wetness impregnation method was used to incorporate 2 wt% Pd into the synthesized supports. An aqueous solution of $(NH_4)_2PdCl_4$ (Sigma-Aldrich, ≥99 995%) was used as the palladium precursor. Once impregnation with the palladium salt was completed, the solid was dried for 10 h at 393 K and then calcined at 823 K for 2 h. No further treatment was applied, as it is assumed that reduction of the metal occurred under the reaction conditions due to the temperature and hydrogen pressure used (513 K, 4 MPa of H_2). The resultant catalysts were labeled Pd/HBEA, Pd/ZAB-1.6, Pd/ZAB-0.1 and Pd/ZAB-0.0.

2.2. Activity measurements

For catalytic measurements, a stainless-steel autoclave (100 mL, Parr-series 4590 reactor) was loaded with 15 g of ethanol, 0.25 g of levulinic acid and 0.1 g of the catalyst. The autoclave was purged several times, first with nitrogen and then with hydrogen, to remove air and nitrogen, respectively. The system was pressurized with H_2 up to 4.0 MPa and then heated to the reaction temperature (513 K). Once the set temperature was reached, agitation was performed at 700 rpm. This time was considered as the time zero of the reaction.

The liquid reaction medium was analyzed by gas chromatography (Agilent 6890 N) using a capillary column (ZB-WAX: 30 m 0.32 mm 0.50 μm) equipped with a flame ionization detector (FID). The quantified products were ethyl levulinate (EL), gamma-valerolactone (GVL), ethyl valerate (EV) and valeric acid (VA). Signals attributed to ethanol (solvent) and other minor products, such as ethyl pentenoate isomers, were observed in the chromatogram, but they were not quantified due to their low abundances. An aliquot of the reaction medium was mixed with a known amount of cyclohexanol, which was employed as a standard for analysis during sample preparation. Eqn (1) shows that the conversion of LA is defined as the molar ratio of LA consumed in the reaction relative to the initial amount of LA. Yields are defined for every product as the molar ratio of the respective product relative to the initial amount of LA (eqn (2)).

$$\text{Conversion}\ (\%) = \frac{\text{consumed LA moles}}{\text{initial LA moles}} \quad 100 \qquad (1)$$

$$\text{Yield}\ (\%) = \frac{\text{formed product moles}}{\text{initial LA moles}} \quad 100 \qquad (2)$$

In reutilization tests, the catalyst was recovered after the reaction. The mother liquor was filtered, and the solid was rinsed several times with ethanol. The solid was dried overnight at 333 K, and when necessary, the fresh catalyst was added to compensate for losses in the recovery process. Reutilization reactions were carried out as previously described but with the recovered catalyst. After several reaction cycles, catalysts were reactivated by calcination employing a heating ramp of 1 min $^{-1}$ up to 773 K, and this temperature was maintained for 1 h. After cooling, the catalyst was retested under identical reaction conditions.

2.3. Catalyst characterization

Elemental analysis of the zirconium and aluminum contents of the modified supports was performed by inductively coupled plasma optical emission spectroscopy (ICP-OES) with a Varian Vista AX apparatus. Powder X-ray diffraction (XRD) patterns were recorded using an X'Pert Pro PANalytical diffractometer in the Bragg–Brentano reflection geometry with the CuKα radiation line ($\lambda = 1.54194$ Å) in the 2θ angle range from 4 to 90 (step size 0.0335)

DRIFT spectra were collected with a Nicolet 5700 spectrometer equipped with a high sensitivity Hg–Cd–Te cryo-detector operating in the spectral range of 4000–650 cm ^{1}. A diffuse reflectance accessory (Praying Mantis-Harrick Co.) was used as an optical mirror accessory. Approximately 30 mg of the previously ground sample was placed in a high-temperature catalytic reaction chamber (HVC-DRP Harrick Scientific Products, NY) that allows treatment *in situ* at high temperatures. To evaluate the surface acidity, pyridine (Py) and deuterated acetonitrile (CD_3CN) were used as complementary probe molecules. The sample was first dried at 393 K for 1 h under an Ar flow (50 mL min ^{1}) to clean the surface and then cooled to 298 K. Then, the probe molecule was added in sufficient quantity to saturate the sample. The physisorbed fraction was removed by flushing with an Ar flow (50 mL min ^{1}) at 393 and 298 K for 1 h and 15 min for Py and CD_3CN, respectively. To identify the state of oxidation and aggregation of the palladium surface species, carbon monoxide (CO) was also used as a probe molecule. Before CO adsorption, fresh or calcined catalysts were reduced under 10% H_2/Ar flow (50 mL min ^{1}) at 523 K for 30 min. After that, H_2 was replaced by Ar (50 mL min ^{1}) and the sample was cooled to room temperature. Then, 5% CO/He flow (30 mL min ^{1}) was fed for adsorption. Physisorbed CO was removed by flushing with Ar at this temperature for 2 min. The net spectrum was obtained by subtracting the reference spectrum of the solid catalyst. All spectra were recorded with 128 scans and a resolution of 4 cm ^{1}.

3. Results and discussion

3.1. Catalytic activity

Fig. 2 shows the catalytic behavior of these catalysts in the conversion of levulinic acid (LA) into valeric biofuels (EV + VA) after one hour of the reaction. Complete conversion of levulinic acid was observed for all catalysts under our reaction conditions. The Pd/HBEA catalyst exhibited the highest yield of valeric biofuels, achieving a remarkable value close to 60%; the rest of the series retained a more significant proportion of gamma-valerolactone (GVL), the main intermediate of the integrated reaction (see Fig. 1). Samples with a lower Al/Zr ratio gave worse yields of valeric biofuels, and the most unsatisfactory results were those obtained for the sample without aluminum (Pd/ZAB-0.0). This catalyst provided the highest yield of GVL instead. Therefore, the distribution products will depend on the Al/Zr atomic ratio of the bimetallic zeolitic supports where Al has been exchanged for Zr. As this exchange increases, the catalysts in our reaction present worse behavior.

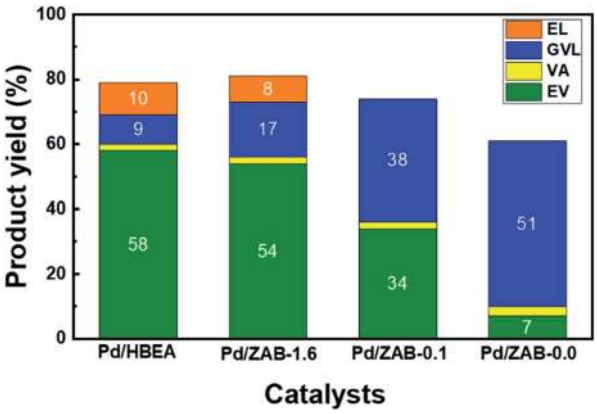

Fig. 2 Reaction product yields for the Pd/Zr–Al-Beta catalysts. Reaction conditions: 15 g ethanol, 0.25 g LA, 0.1 g catalyst, $T = 513$ K, 4.0 MPa H_2, 1 h and 700 rpm.

Accordingly, the Pd/HBEA catalyst is the sample with the best catalytic performance.

Notably, some additional small peaks were also present in the chromatograms, indicating the appearance of other byproducts. In this way, methyl tetrahydrofuran, 1-pentanol and ethyl pentenoate isomers were identified, representing less than 3–5% of the total products coming from starting LA, which is not enough to achieve the carbon balance. Therefore, carbonaceous coke-like products, which are undetectable by gas chromatography, were most likely formed during the reaction. Some reaction mixtures were analyzed with GC-MS to identify these products, but it was unsuccessful, indicating that they might be high-boiling or coke-like products, hard to detect by GC. Indeed, it is well known that coke can be formed when organic compounds are hydrotreated at temperatures above 500 K and in the presence of acidic sites.[35,36] As will be discussed below, these carbonaceous residues are partially responsible for the deactivation of the active centers in the catalyst by fouling.

According to the scheme displayed in Fig. 1, EL and GVL are intermediate products. These intermediates were present after one hour of the reaction (see Fig. 2), and therefore, these catalysts can continue to convert them into the products of interest (EV + VA) if they are allowed sufficient time to carry out the complete reaction. Thus, experiments with longer reaction times (2 h and 4 h) were conducted, and the results are shown in Fig. 3. All the catalysts improved the yields of valeric biofuels with an increased reaction time. Nevertheless, there were apparent differences in the progress of the reactions. For Pd/HBEA, an optimum value was reached at two hours, with a yield of 76% for the combined EV + VA. For the rest of the catalysts, the yield of valeric biofuels continued to increase after 4 h of the reaction. This result is attributed to the continued conversion of intermediates, which increased the yields accordingly.

As mentioned, this trend is different for the Pd/HBEA catalyst, which reached a maximum yield of target products after two hours on stream. After that time, not only did the yield of these products decrease, but the carbon balance also worsened. A similar decrease in the carbon balance was also observed for

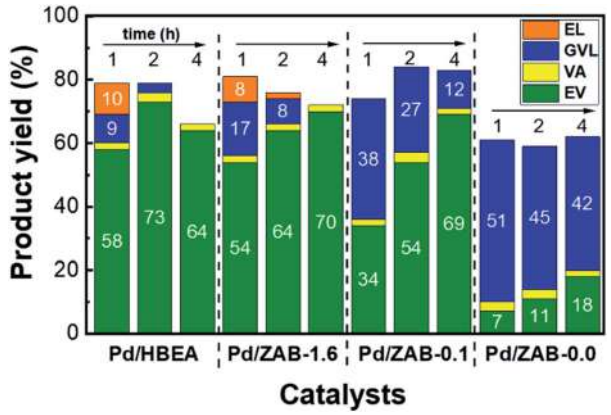

Fig. 3 Reaction product yields for the Pd/Zr–Al-Beta catalysts with reaction times of 1, 2 and 4 hours. The reaction conditions are the same as those shown in Fig. 2.

the Pd/ZAB-1.6 sample. The significant difference between these two catalysts is that over Pd/ZAB-1.6, the yield of valeric biofuels did not decrease after four hours, maintaining over 70%. Pd/ZAB-0.1 exhibited much slower reaction rates for the first two hours, but after that, it reached the same yield as Pd/ZAB-1.6 but with a better carbon balance. Finally, for the Pd/ZAB-0.0 catalyst, the carbon balance was much lower from the beginning (61%), but it remained stable. After the first hour, the only process underway was the conversion of intermediate GVL to EV. The maximum attainable yield of EV with this catalyst would be just 60%; after 4 hours of the reaction, it only reached 18%.

To evaluate the stability of the Pd/HBEA catalyst, reutilization tests were conducted. For these assays, a two hour reaction time was selected and the yield of the desired products (EV + VA) reached a maximum of 76%. Fig. 4 displays the results and shows a slight deactivation of the catalyst in each recycling step. Thus, the yield of combined VA and VE decreases from 76% with the fresh catalyst to 56% after three cycles. After the third cycle, the catalyst was calcined at 773 K for one hour, and then

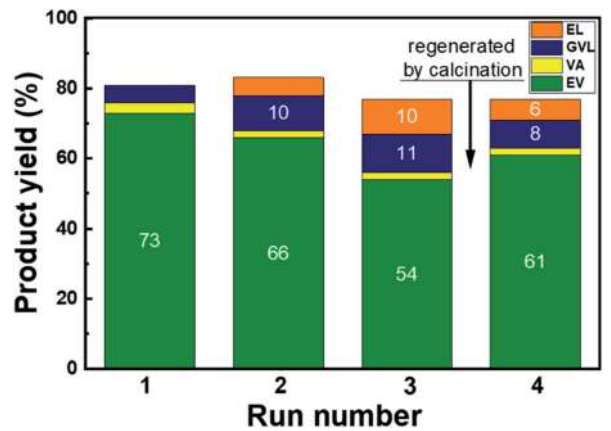

Fig. 4 Product yields during the reutilization tests of the Pd/HBEA catalyst. The time of the reaction was 2 h, and other conditions are the same as those shown in Fig. 2.

a further reutilization test was conducted. This calcination procedure changed the downward trend by significantly improving the yield up to 63%, but the initial activity was not recovered.

These results need further explanation and characterization experiments are designed to obtain additional information regarding the reason for the deactivation observed, potential approaches to avoid it and the impact of regeneration by calcination on the active sites.

3.2. Characterization of the catalysts

3.2.1. Chemical analysis of the supports. Different Zr–Al-Beta (ZAB) zeolitic acid supports were synthesized by tuning the Al/Zr molar ratio from infinite (zirconium-free, commercial beta zeolite HBEA) to zero, *i.e.*, the sample in which practically all of the aluminum atoms were extracted (ZAB-0.0). Table 1 compiles the elemental compositions of the synthesized supports determined by ICP-OES analysis. The Al/Zr atomic ratio was adjusted through the dealumination process with nitric acid and the subsequent incorporation of Zr species. This same synthetic procedure has been used previously, and the preservation of the zeolitic network and textural properties were confirmed.[33,34]

3.2.2. Surface acidity. To evaluate the surface acidity of the catalysts, DRIFT spectra with two complementary basic probe molecules, pyridine (Py) and deuterated acetonitrile (CD_3CN), were determined. Regarding the absorption of the Py probe molecule, the DRIFT spectra of the four Pd/ZrAl-Beta catalysts are shown in Fig. 5. All catalysts presented characteristic pyridine adsorption bands, and detailed assignments can be found elsewhere.[37] Here, we will describe the three most relevant Py bands indicated in Fig. 5. The first adsorption band centered at 1445 cm^{-1} was associated with Lewis acid sites (L), the second infrared band at 1490 cm^{-1} was attributed to both Lewis and Brønsted acid sites (L + B), and the third adsorption band at 1545 cm^{-1} was associated with Brønsted acid sites alone.[38,39] Although these spectra present some noise, the Py bands of interest are clearly distinguished.

After desorption at 393 K for one hour (thick lines shown in Fig. 5), some physisorbed/pseudo liquid Py remained, while at above 573 K for 30 min (thin lines), only chemisorbed pyridine was present. Al contributes to both Brønsted and Lewis acidity, while Zr only provides Lewis acid centers.[34] From Fig. 5, it can be concluded that the Pd/HBEA and Pd/ZAB-1.6 catalysts showed the most significant numbers of Brønsted acid sites (BAS), whereas this amount was reduced in Pd/ZAB-0.1 and non-existent in the Al-free Pd/ZAB-0.0 catalyst. This confirms the

Table 1 Chemical analysis of the acid supports by ICP-OES

Support	Al (wt%)	Zr (wt%)	Al/Zr (mol mol $^{-1}$)
HBEA	2.0	0.0	∞
ZAB-1.6	1.4	2.9	1.6
ZAB-0.1	0.2	6.9	0.1
ZAB-0.0	0.0	6.3	0.0

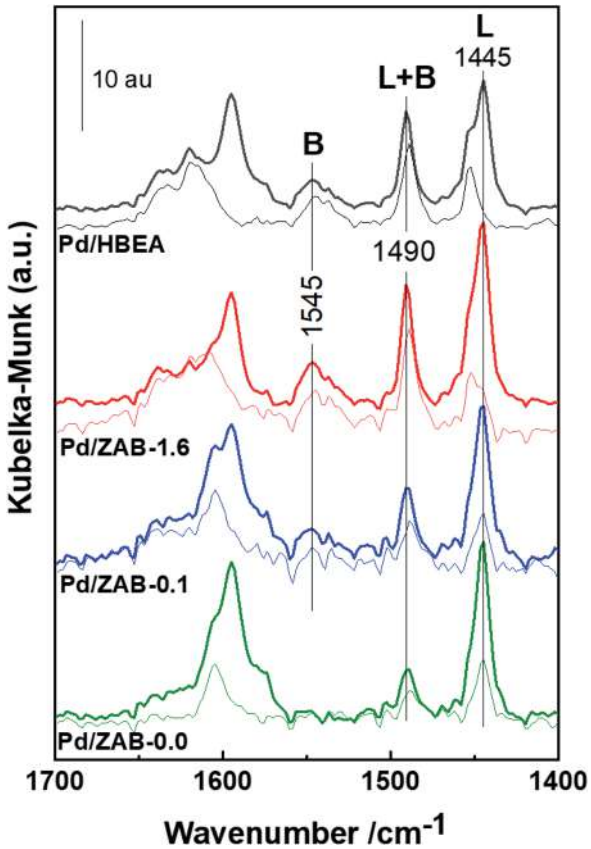

Fig. 5 DRIFT spectra of adsorbed Py on Pd/ZrAl-Beta catalysts. The thick and thin lines represent flushing with an Ar flow at 393 and 573 K, respectively.

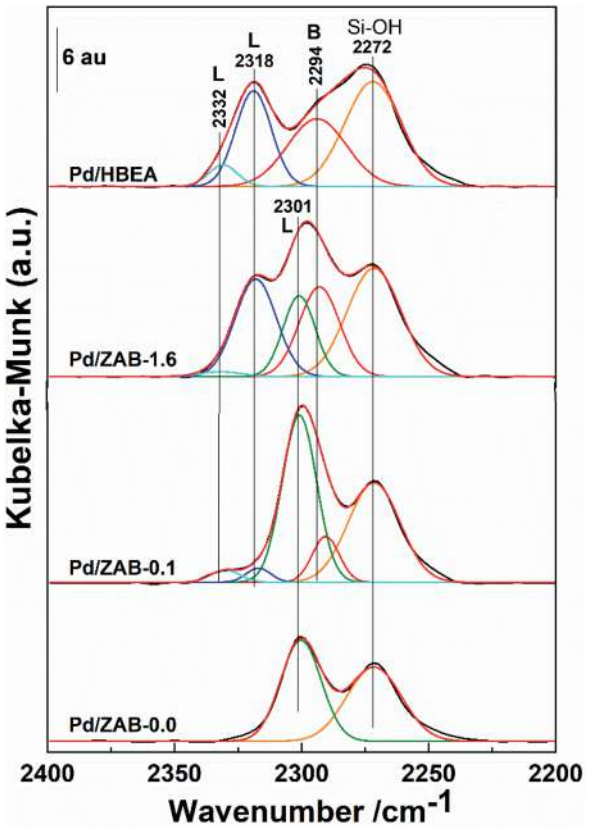

Fig. 6 DRIFT spectra of deuterated acetonitrile on Pd/ZrAl-Beta catalysts. Deconvolution in the infrared bands is also displayed.

complete removal of all the aluminum from this sample, as indicated by the elemental chemical analysis.

Next, the study of surface acidity was completed by using CD_3CN as a probe molecule. The corresponding DRIFT spectra of the different catalysts are shown in Fig. 6, where the deconvolution of the simple infrared bands is also included. Four infrared bands were observed for the Pd/HBEA catalyst, one small peak at 2332 cm $^{-1}$ and three broad intense peaks at 2318, 2294 and 2272 cm $^{-1}$. The replacement of Al by Zr atoms had a strong impact on the DRIFT spectra, in which the number and intensities of the absorption bands were modified. At the other end of the series, only two bands are observed for the Pd/ZAB-0.0 catalyst, at 2301 and 2272 cm $^{-1}$. In the intermediate catalysts Pd/ZAB-1.6 and Pd/ZAB-0.1, which contain both ions (Al and Zr), up to five infrared bands can be observed, representing a combination of the other two catalysts of the series. Two bands were identified in Pd/ZAB-0.0 at 2272 and 2301 cm $^{-1}$, but correct deconvolution required the inclusion of a band at 2294 cm $^{-1}$ and two bands at 2318 and 2332 cm $^{-1}$. These last three infrared bands were also present in the Pd/HBEA catalyst samples where the support only contained Al and the intensities of these three bands decreased with the dealumination of the supports.

Regarding the different CD_3CN absorption band assignments, it is known that when the band maxima are at frequencies $\geq$2300 cm $^{-1}$ they are associated with Lewis acid sites (LAS), while the other bands with maxima at frequencies <2300 cm $^{-1}$ are associated with Brønsted acid sites (BAS). Moreover, the higher the frequencies of these peaks are, the greater the strength of the indicated acid centers.[40–42] Concerning the Brønsted region, very weak BAS associated with silanol groups, with an IR peak at 2272 cm $^{-1}$, remains in all samples, consistent with the silicic nature of the zeolitic supports[29,34] On the other hand, the progressive removal of Al provides a concomitant reduction in the number of strong Brønsted acid sites, so the intensity of the 2294 cm $^{-1}$ adsorption band decreases throughout the series. Regarding the Lewis acid region, the peaks at 2332 cm $^{-1}$ and 2318 cm $^{-1}$ are attributed to strong Lewis acid sites.[22,40] Both peak intensities decreased with the replacement of Zr by Al in the catalyst support. Finally, when more Zr was incorporated, an infrared band at 2301 cm $^{-1}$, associated with weak LAS and the presence of Zr atoms,[34,43] prevailed.

The deconvolution shown in Fig. 6 was supported by the results obtained with the adsorption of Py as a probe molecule. Both molecules are complementary in indicating the evolution of surface acidity in terms of the nature and strength of the acid sites. Moreover, it is necessary to mention that the acidity of the catalytic supports was also studied prior to incorporation of Pd (spectra shown in Fig. S3†), and no significant differences were observed for the Pd/ZrAl-Beta catalysts. Therefore, we can

confirm that the incorporation of Pd did not affect the surface acidity of the support in this case.

The information regarding surface acidity for this series of catalysts, derived from DRIFT data obtained after absorption of Py and CD_3CN, can be summarized as follows: the substitution of Al by Zr in the acidic supports (HBeta zeolite) has consequences for the Lewis and Brønsted surface acid centers. In principle, a strong LAS band (2318 cm ^{1}) appears at a higher frequency (2332 cm ^{1}) with the generation of strong Lewis acid sites. However, when the level of substitution is sufficient, the LAS associated with zirconium atoms are very weak (infrared band centered at 2301 cm ^{1}). The strong BAS band at 2994 cm ^{1} decreased in intensity throughout the series and was no longer present when Zr had entirely replaced the Al in the parent zeolite. Finally, the weak Brønsted acid sites associated with the presence of silanol groups were essentially maintained throughout the series.

3.2.3. Surface Pd species. To analyze the Pd surface species and the possible modifications resulting when they were incorporated on the different zeolitic supports, a DRIFT study was carried out using carbon monoxide (CO) as a probe molecule. DRIFT spectra of the catalysts reduced at 523 K for 30 min were recorded and are depicted in Fig. 7. A broad and weak band was observed for the four catalysts at 2083 cm ^{1}, attributed to linearly adsorbed CO on isolated metallic Pd.[44,45] Below 2000 cm ^{1}, there was another broad and considerably more intense band, which can be the result of several overlapping bands. It is sufficiently documented that there are several bands that occur in the range of 2000–1900 cm ^{1}, including those for two-fold μ^2 bridged-CO bonded on Pd (100) faces and broad bands for μ^3 hollow bonded CO or two-fold bridge-bonded CO on the (111) planes of palladium particles.[45,46]

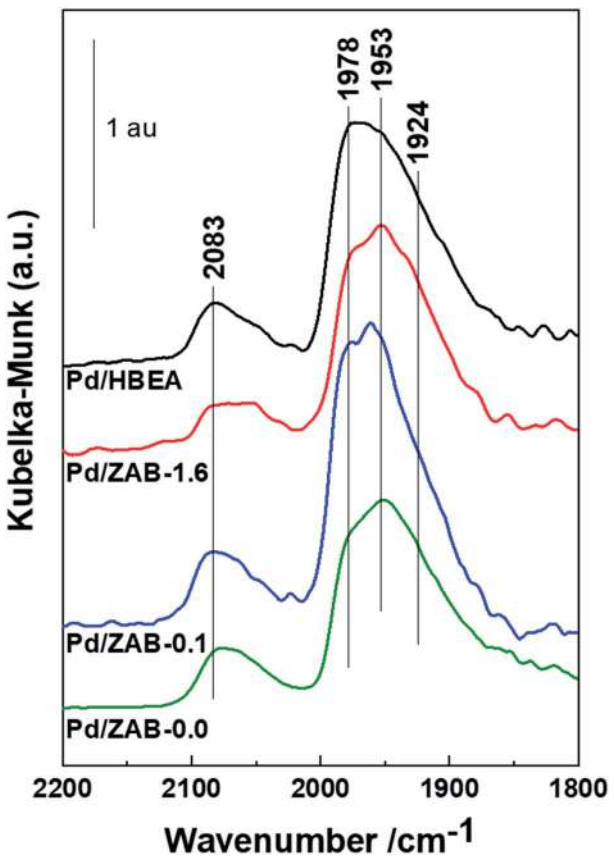

Fig. 7 DRIFT spectra of CO adsorbed on reduced Pd/ZrAl-Beta catalysts at room temperature.

The spectra of the different samples are similar in terms of the bands and intensities, and no significant changes were observed. Therefore, we can affirm that the Pd surface species generated after incorporation *via* impregnation were not affected by the different surface acidities of the supports. This suggests that the previously discussed differences observed in the catalytic comportment of the different materials must be attributed to the nature (Brønsted/Lewis) and strength of the surface acid centers rather than to the exposed metal Pd species.

Therefore, after analyzing the DRIFT spectra of the acid sites and the Pd metallic species, it can be established that neither the incorporation of Pd affects the acidity of the zeolitic support nor the different acidities of the prepared Zr–Al-Beta supports modify the Pd metallic species.

3.2.4. Characterization of the used and regenerated Pd/HBEA catalyst. DRIFT experiments were also conducted to explore the changes in the catalyst after the reaction and regeneration by calcination. As previously discussed, catalytic experiments were conducted to study reutilization, and a decrease in activity was observed after three cycles (see Fig. 4). After three consecutive reaction runs, the used Pd/HBEA catalyst was analyzed by DRIFT spectroscopy with three probe molecules (Py, CD_3CN and CO). The regeneration procedure was conducted by calcination in air at 773 K in the reaction chamber, and this regenerated Pd/HBEA sample was also studied by DRIFT spectroscopy. Additionally, carbonaceous deposits were also identified by observing the C–H stretching region at 3150–2700 cm ^{1}. The spectra of fresh, used and regenerated samples are compiled and shown in Fig. 8. Since the regeneration treatment at 773 K has shown that it is a sufficient temperature to eliminate the IR bands due to carbonaceous deposits, the temperature of regeneration was not increased further to avoid the sintering of the palladium particles in the regenerated sample.

DRIFT spectra in the C–H stretching region (3150–2700 cm ^{1}) are presented for the fresh, used and regenerated Pd/HBEA sample shown in Fig. 8a. The fresh catalyst does not present infrared bands in this region, as expected. In contrast, for the used sample, several absorption bands at 3118, 3083, 2978, 2935, 2910 and 2862 cm ^{1} can be attributed to carbonaceous species with unsaturated bonds (3118 and 3083 cm ^{1} infrared bands) and with saturated C–H bonds (the rest of the bands).[47,48] After exposing the used catalyst to regeneration by calcination, practically all the carbonaceous deposits were removed; see the spectrum of the regenerated catalyst in Fig. 8a.

Fig. 8b shows the spectra of the Pd/HBEA samples (fresh, used and regenerated) obtained by using Py as a probe molecule. In this case, the decreasing acidity for the used catalyst was mainly due to the superficial Lewis acid sites present in the

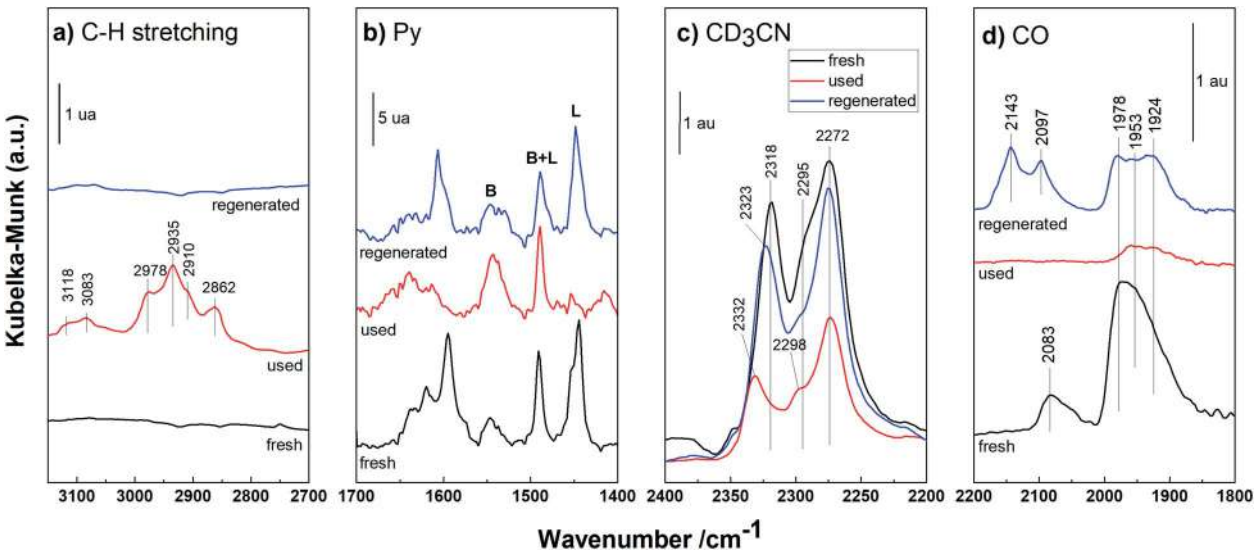

Fig. 8 DRIFT spectra of the fresh, used and regenerated Pd/HBEA. (a) C–H stretching region; (b) Py, (c) CD_3CN and (d) CO like probe molecules.

catalyst; once they underwent the regeneration process, they were largely recovered. This suggests that these centers are the main promoters for formation of carbonaceous residues fouling the catalyst surface. This same sequence of DRIFT experiments was also performed for another basic probe molecule, deuterated acetonitrile (CD_3CN), and the DRIFT spectra are compiled and shown in Fig. 8c. For the used Pd/HBEA catalyst, a strong drop in the intensity of the bands was observed (relative to the fresh catalyst), which was almost fully reversed after regeneration. Therefore, it can be surmised that the used Pd/HBEA sample underwent a drastic decrease in the number of exposed acid sites, as evidenced by the low intensities of the infrared bands. This is mainly due to the loss of LAS, as these centers can be fouled by carbonaceous species generated during the reaction. Such carbonaceous species can be removed with a high degree of efficiency with regeneration by calcination, as shown with both probe molecules (Py and CD_3CN).

On the other hand, the Pd surface species in used and regenerated catalysts have also been studied by DRIFT spectroscopy using CO as the probe molecule, and the spectra are shown in Fig. 8d. It is observed that the intensities of bands due to the Pd surface species diminished drastically because with the acid sites, the carbonaceous deposits also covered the metallic Pd. After the regeneration of this sample, a part of the isolated metallic Pd was recovered during calcination due to coke removal. However, partially oxidized Pd species (band at 2143 cm ^{1})[49] and slightly sintered Pd[46] species (the band at 1924 cm ^{1} is proportionally more intense) were also indicated.

Therefore, it can be concluded that the deactivation of the catalyst occurs mainly due to the fouling of its surface by carbon deposits, which affect both the acidic and metallic exposed active centers. After regeneration employing calcination in air, the surface acidity was practically recovered in its entirety, whereas the metallic Pd species were reoxidized. These reoxidized species were more resistant to reduction than the PdO species present in the precursor catalyst. This may be the main reason that the catalyst does not reach the valeric biofuel yield of the fresh catalyst after regeneration (see Fig. 4).

To investigate the causes of deactivation and the incomplete regeneration of the used catalyst, the samples were characterized by the XRD technique. The diffractograms of the Pd/ZAB catalysts are shown in Fig. 9.

The peaks corresponding to the PdO phase (JCPDS 006-0515) are observed for the fresh catalysts. The rest of the peaks are associated with the zeolitic support (see Fig. S2 in the ESI†). However, when we observe the spectrum of the used Pd/HBEA catalyst (uPd/HBEA), peaks corresponding only to metallic Pd (JCPDS 001-1201) are observed, which confirms that under the reaction conditions the palladium oxide is extensively reduced to Pd as expected. This is in accordance with the DRIFT technique after CO adsorption as shown in Fig. 8d. However, a part of the surface Pd may have been reoxidized during the handling of the sample after the reaction is finished. On the other hand, it should also be mentioned that diffraction peaks assigned to

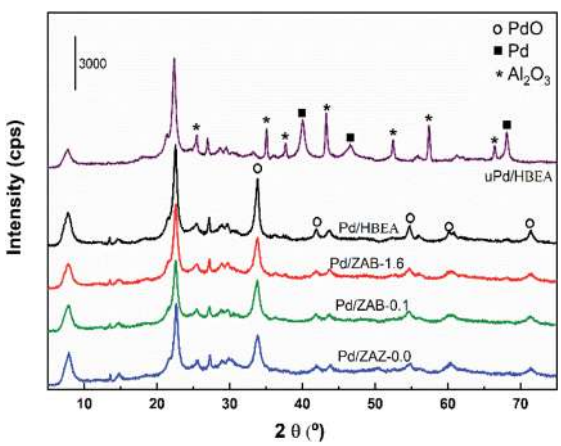

Fig. 9 XRD patterns of the fresh Pd/ZAB and used Pd/HBEA catalysts.

the crystalline phase Al_2O_3 (JCPDS 01-080-0786) are observed in the used catalyst, possibly since a partial extraction of the lattice aluminum occurs during the progress of the reaction. This fact together with the presence of carbonaceous residues is the most important cause of deactivation.

3.3. Impact of acid site nature and strength on catalytic performance and stability

This research is designed to find the direct relationship between the nature and strength of the surface acid sites and their catalytic behavior under liquid phase conditions. For this purpose, an acid support (H-beta zeolite) that was modified by progressively substituting Al for Zr atoms has been used. The correctness of this approach was confirmed by the analysis of DRIFT spectra. This indicated that the incorporation of Pd does not change the acidity of the supports. At the same time, the different acidities of the modified supports do not affect the dispersion and reducibility of the incorporated Pd. Therefore, the differences observed in the catalytic behaviors have to be fully attributed to the changes observed in the surface acidity of these bifunctional catalysts.

It is necessary to highlight the complexity of the challenge addressed. On the one hand, we have acid centers with different natures and strengths coexisting in the catalyst, and on the other hand, the acid centers catalyze various steps of the cascade reaction (see the scheme in Fig. 1). These acid sites will be more or less active depending on the step in which they participate (dehydration, GVL ring-opening, or even esterification), their nature and strength, and the reaction conditions.

The yield of valeric biofuels (EV + VA) follows the trend Pd/HBEA ≅ Pd/ZAB-1.6 > Pd/ZAB-0.1 > Pd/ZAB-0.0. This same qualitative tendency is indicated by the intensities of the IR bands for the strong BAS associated with Al sites on the surface of the catalysts (2294 cm^{-1} with CD_3CN and 1545 cm^{-1} with Py). Therefore, these results suggest that this type of acid site, associated with Al present in the catalysts, is mainly responsible for the best catalytic behavior. Such strong Brønsted centers are required for the GVL ring-opening reaction, which is the rate-determining step of the process.[16] This is consistent with the fact (see Fig. 2) that Pd/HBEA, Pd/ZAB-1.6 and Pd/ZAB-0.1 show Brønsted acid sites and gave up to 70% yields for valeric biofuels. However, Pd/ZAB-0.1 required 4 hours to reach this yield, possibly due to slower kinetics attributed to the low concentration of Brønsted acid sites in this sample relative to other samples. The performance is considerably poorer for the Pd/ZAB-0.0 catalyst that does not have strong BAS, even after 4 hours of the reaction. On the other hand, all the catalysts contain other types of weaker BAS associated with silanol groups (Si–OH, at 2272 cm^{-1} with the CD_3CN probe) whose presence and IR intensities do not change significantly in the series of supports. These weak acid sites are irrelevant for the catalytic conversion of LA into EV.[50]

Moreover, the roles of the LAS as related to their strengths should be analyzed. Three Lewis acid sites were identified from the DRIFT spectra, including the strongest with a band at 2332 cm^{-1}, another strong site shown at 2318 cm^{-1} and a weak site shown at 2301 cm^{-1} (see Fig. 6). It was observed that the weak LAS exhibited limited activity in opening the ring of the GVL: no active Brønsted sites were present in sample Pd/ZAB-0.0, which showed some GVL ring opening activity, but much less than the samples with strong BAS and an IR band at 2294 cm^{-1}. However, these centers were more active in the dehydration reaction giving the GVL intermediate. In the case of strong LAS (bands at 2332 and 2318 cm^{-1}), they are clearly more involved in this dehydration reaction and important in producing the intermediates (EL and GVL). Therefore, the capacity of the LAS for the dehydration reaction depends on their strength. On the other hand, the effect of the strong LAS (2332 and 2318 cm^{-1} bands with CD_3CN) on the ring opening reaction of the GVL is clear although the decrease in strong LAS, with the increase in the substitution of Al by Zr, is also accompanied by a reduction of the strong BAS. The presence of these strong LAS centers (together with the presence of strong BAS) is the main difference between the first three samples in the series and the Pd/ZAB-0.0 sample (see Fig. 5 and 6). This difference is critical in the activity of the Pd/ZAB-0.0 catalyst, since the absence of these LAS gives rise to more unknown products and less than 20% conversion to valeric biofuels even after four hours of the reaction. For the rest of the catalysts, even Pd/ZAB-0.1 provides 70% yield of the desired valeric products. In summary, weak and strong LAS are also active in the GVL ring-opening reaction but exhibit less intrinsic activity than BAS. Moreover, the activities of these centers for this reaction depend on their acid strengths.

The surface acid sites play an important role in determining the product distribution. Kumar *et al.*[51,52] investigated the vapor-phase hydrogenation of LA to VA on the Ni/TiO_2 catalyst. An improvement in catalytic behavior was observed after incorporating W and increasing the number of BAS due to the W interactions with Ni/TiO_2. These authors reported that under their conditions, 543 K and atmospheric pressure, sites other than LAS were mainly responsible for the high selectivity for GVL, whereas BAS were prone to enhance the GVL ring-opening reaction. We observed a similar behavior under liquid phase conditions and applied pressures, but we also observed the ability of LAS to carry out the ring-opening reaction of GVL, although with lower intrinsic activity than strong BAS.

Another aspect that should be mentioned is the role of the surface acid sites in the deactivation and selectivity of the intermediates and products of interest. The strong BAS, mostly present in the Pd/HBEA catalyst, were active in the subsequent transformation of EV into unidentified products; see the drop in the yield of EV after 4 hours of the reaction in Fig. 3. Therefore, these strong acid sites appear to be responsible for the unwanted progression of the reaction beyond the desired products at long reaction times, leading to worse performance at 4 h compared to 2 h. The causes of deactivation of the Pd/HBEA catalyst (Fig. 4) are the formation of carbonaceous residues that foul the acidic and metallic centers (see Fig. 8) on the catalyst surface and the slight formation of the Al_2O_3 phase (Fig. 9). Regarding regeneration by calcination in air at 773 K for 1 h, practically all the acid sites covered by these carbonaceous

residues were refreshed and re-exposed, but during the regeneration process some species of metallic Pd were oxidized to species more difficult to reduce than those in the fresh catalyst. The possible presence of oxidized Pd species in the regenerated catalyst could prevent the recovery of the initial activity. This is why the catalyst presents a partially reversible deactivation due to removal of the carbonaceous residues.

4. Conclusions

The combination of the catalytic activity and the DRIFT spectral data leads to the following conclusions concerning the nature and strength of surface acid sites in fresh catalysts. The importance of strong BAS in catalytic behavior is great because these centers are mainly responsible for the GVL open-ring reaction. However, these acid sites can also promote the undesirable reaction of EV to give other unidentified products at long reaction times. Concerning LAS, three different sites have been identified. Weak LAS associated with Zr species (infrared band at 2301 cm^{-1} for CD_3CN) exhibit low activity in the production of valeric biofuels, but they can be relevant in the deactivation process. When only weak Lewis acidity is present, the catalyst cannot accomplish the full transformation, attaining a limited EV yield. The dramatic difference in the performances of Pd/ZAB-0.1 and Pd/ZAB-0.0 indicates the crucial effects of strong LAS (infrared bands at 2318 and 2332 cm^{-1} for CD_3CN) in driving the reaction, although there are BAS centers also in this sample that can contribute. Consequently, both types of strong centers (BAS and LAS) are active in the cascade conversion of LA into EV. However, the intrinsic activity of the former is more significant because when their concentration is increased, less time is required to achieve expected yields of EV.

Regarding the deactivation and regeneration of Pd/HBEA, it was observed that the catalytic activity decreased slightly in each successive use, most likely due to the formation of carbonaceous deposits and the formation of the Al_2O_3 phase. After regeneration by calcination in air, the catalyst showed a partial recovery of the starting activity due to the full regeneration of acid sites, in agreement with the DRIFT results. However, Pd species were affected by the regeneration procedure and this prevented the catalyst from exhibiting its initial catalytic performance.

Conflicts of interest

There are no conflicts to declare.

Acknowledgements

Grants RTI2018-094918-B-C41 and RTI2018-094918-B-C42 by MCIN/AEI/10.13039/501100011033 and the Regional Government of Madrid (project S2018/EMT-4344) are kindly acknowledged for funding this research. MMO and IMS, due to the CSIC-UAM framework agreement, thank Ph.D. Program in Applied Chemistry, Doctoral School of Autonomous University of Madrid.

References

1 G. Dautzenberg, M. Gerhardt and B. Kamm, *Holzforschung*, 2011, **65**, 439–451.
2 C. Antonetti, D. Licursi, S. Fulignati, G. Valentini and A. Raspolli Galletti, *Catalysts*, 2016, **6**, 196.
3 J. C. Serrano-Ruiz, R. Luque and A. Sepúlveda-Escribano, *Chem. Soc. Rev.*, 2011, **40**, 5266–5281.
4 E. I. Gürbüz, S. G. Wettstein and J. A. Dumesic, *ChemSusChem*, 2012, **5**, 383–387.
5 F. D. Pileidis and M. M. Titirici, *ChemSusChem*, 2016, **9**, 562–582.
6 S. G. Wettstein, D. M. Alonso, Y. Chong and J. A. Dumesic, *Energy Environ. Sci.*, 2012, **5**, 8199–8203.
7 D. W. Rackemann and W. O. S. Doherty, *Biofuels, Bioprod. Biorefin.*, 2011, **5**, 198–214.
8 D. M. Alonso, S. Wettstein and J. A. Dumesic, *Green Chem.*, 2013, **15**, 584–595.
9 Z. Xue, Q. Liu, J. Wang and T. Mu, *Green Chem.*, 2018, **20**, 4391–4408.
10 J. Iglesias, I. Martínez-Salazar, P. Maireles-Torres, D. Martin Alonso, R. Mariscal and M. López Granados, *Chem. Soc. Rev.*, 2020, **49**, 5704–5771.
11 J. P. Lange, R. Price, P. M. Ayoub, J. Louis, L. Petrus, L. Clarke and H. Gosselink, *Angew. Chem., Int. Ed.*, 2010, **49**, 4479–4483.
12 Z. Yu, X. Lu, J. Xiong and N. Ji, *ChemSusChem*, 2019, **12**, 3915–3930.
13 A. M. Hengne and C. V. Rode, *Green Chem.*, 2012, **14**, 1064–1072.
14 A. M. R. Galletti, C. Antonetti, V. De Luise and M. Martinelli, *Green Chem.*, 2012, **14**, 688–694.
15 G. B. Kasar, R. S. Medhekar, P. N. Bhosale and C. V. Rode, *Ind. Eng. Chem. Res.*, 2019, **58**, 19803–19817.
16 W. Luo, U. Deka, A. M. Beale, E. R. H. Van Eck, P. C. A. Bruijnincx and B. M. Weckhuysen, *J. Catal.*, 2013, **301**, 175–186.
17 Z. Yi, D. Hu, H. Xu, Z. Wu, M. Zhang and K. Yan, *Fuel*, 2020, **259**, 3–6.
18 T. Pan, J. Deng, Q. Xu, Y. Xu, Q. X. Guo and Y. Fu, *Green Chem.*, 2013, **15**, 2967–2974.
19 K. Kon, W. Onodera and K. I. Shimizu, *Catal. Sci. Technol.*, 2014, **4**, 3227–3234.
20 X. M. Gu, B. Zhang, H. J. Liang, H. Bin Ge, H. M. Yang and Y. Qin, *J. Fuel Chem. Technol.*, 2017, **45**, 714–722.
21 W. Luo, P. C. A. Bruijnincx and B. M. Weckhuysen, *J. Catal.*, 2014, **320**, 33–41.
22 M. Muñoz-Olasagasti, A. Sañudo-Mena, J. A. Cecilia, M. L. Granados, P. Maireles-Torres and R. Mariscal, *Top. Catal.*, 2019, **62**, 579–588.
23 P. Sun, G. Gao, Z. Zhao, C. Xia and F. Li, *ACS Catal.*, 2014, **4**, 4136–4142.
24 P. Sun, G. Gao, Z. Zhao, C. Xia and F. Li, *Appl. Catal., B*, 2016, **189**, 19–25.
25 J. Zhou, R. Zhu, J. Deng and Y. Fu, *Green Chem.*, 2018, **20**, 3974–3980.

26 M. Muñoz-Olasagasti, M. López Granados, C. P. Jiménez-Gómez, J. A. Cecilia, P. Maireles-Torres, J. A. Dumesic and R. Mariscal, *Catal. Sci. Technol.*, 2021, **11**, 4280–4293.

27 W. Luo, M. Sankar, A. Beale, Q. He, C. Kiely, P. C. A. Bruijnincx and B. Weckhuysen, *Nat. Commun.*, 2015, **6**, 6540.

28 K. Yan, T. Lafleur, X. Wu, J. Chai, G. Wu and X. Xie, *Chem. Commun.*, 2015, **51**, 6984–6987.

29 M. M. Antunes, P. Neves, A. Fernandes, S. Lima, A. F. Silva, M. F. Ribeiro, C. M. Silva, M. Pillinger and A. A. Valente, *Catal. Sci. Technol.*, 2016, **6**, 7812–7829.

30 B. Hernández, J. Iglesias, G. Morales, M. Paniagua, C. López-Aguado, J. L. García Fierro, P. Wolf, I. Hermans and J. A. Melero, *Green Chem.*, 2016, **18**, 5777–5781.

31 J. A. Melero, G. Morales, J. Iglesias, M. Paniagua, C. López-Aguado, K. Wilson and A. Osatiashtiani, *Green Chem.*, 2017, **19**, 5114–5121.

32 T. Pang, X. Yang, C. Yuan, A. A. Elzatahry, A. Alghamdi, X. He, X. Cheng and Y. Deng, *Chin. Chem. Lett.*, 2021, **32**, 328–338.

33 J. A. Melero, G. Morales, J. Iglesias, M. Paniagua, C. López-Aguado, K. Wilson and A. Osatiashtiani, *Green Chem.*, 2017, **19**, 5114–5121.

34 M. Paniagua, G. Morales, J. A. Melero, J. Iglesias, C. López-Aguado, N. Vidal, R. Mariscal, M. López-Granados and I. Martínez-Salazar, *Catal. Today*, 2021, **367**, 228–238.

35 D. M. Bibby, R. F. Howe and G. D. McLellan, *Appl. Catal., A*, 1992, **93**, 1–34.

36 I. Van Zandvoort, Y. Wang, C. B. Rasrendra, E. R. H. Van Eck, P. C. A. Bruijnincx, H. J. Heeres and B. M. Weckhuysen, *ChemSusChem*, 2013, **6**, 1745–1758.

37 G. A. H. Mekhemer, A. K. H. Nohman, N. E. Fouad and H. A. Khalaf, *Colloids Surf., A*, 2000, **161**, 439–446.

38 S. Jolly, J. Saussey and J. C. Lavalley, *J. Mol. Catal.*, 1994, **86**, 401–421.

39 F. Cabello Galisteo, R. Mariscal, M. López Granados, M. D. Zafra Poves, J. L. G. Fierro, V. Kröger and R. L. Keiski, *Appl. Catal., B*, 2007, **72**, 272–281.

40 A. G. Pelmenschikov, R. A. Van Santen, J. Jänchen and E. Meijer, *J. Phys. Chem.*, 1993, **97**, 11071–11074.

41 D. Fuentes-Perujo, J. Santamaría-González, J. Mérida-Robles, E. Rodríguez-Castellón, A. Jiménez-López, P. Maireles-Torres, R. Moreno-Tost and R. Mariscal, *J. Solid State Chem.*, 2006, **179**, 2182–2189.

42 D. T. Bregante, A. Y. Patel, A. M. Johnson and D. W. Flaherty, *J. Catal.*, 2018, **364**, 415–425.

43 V. L. Sushkevich, A. Vimont, A. Travert and I. I. Ivanova, *J. Phys. Chem. C*, 2015, **119**, 17633–17639.

44 Y. Shen, X. Bo, Z. Tian, Y. Wang, M. Xie, F. Gao, M. Lin, X. Guo, X. Guo and W. Ding, *Green Chem.*, 2017, **19**, 2646–2652.

45 T. Lear, R. Marshall, J. A. Lopez-Sanchez, S. D. Jackson, T. M. Klapötke, M. Bäumer, G. Rupprechter, H. J. Freund and D. Lennon, *J. Chem. Phys.*, 2005, **123**, 174706.

46 G. Agostini, R. Pellegrini, G. Leofanti, L. Bertinetti, S. Bertarione, E. Groppo, A. Zecchina and C. Lamberti, *J. Phys. Chem. C*, 2009, **113**, 10485–10492.

47 B. I. Mosqueda-Jiménez, A. Jentys, K. Seshan and J. A. Lercher, *Appl. Catal., B*, 2003, **46**, 189–202.

48 P. Ivanov and H. Papp, *Langmuir*, 2000, **16**, 7769–7772.

49 H. Tiznado, S. Fuentes and F. Zaera, *Langmuir*, 2004, **20**, 10490–10497.

50 G. Novodárszki, H. E. Solt, G. Lendvay, R. M. Mihályi, A. Vikár, F. Lónyi, J. Hancsók and J. Valyon, *Catal. Today*, 2019, **336**, 50–62.

51 V. V. Kumar, G. Naresh, M. Sudhakar, J. Tardio, S. K. Bhargava and A. Venugopal, *Appl. Catal., A*, 2015, **505**, 217–223.

52 V. V. Kumar, G. Naresh, S. Deepa, P. G. Bhavani, M. Nagaraju, M. Sudhakar, K. V. R. Chary, A. Venugopal, J. Tardio and S. K. Bhargava, *Appl. Catal., A*, 2017, **531**, 169–176.

Supplementary Information

Elucidating the roles of acid site nature and strength on the direct conversion of levulinic acid into ethyl valerate: the case of Zr-modified Beta zeolite-supported Pd catalysts

M. Muñoz-Olasagasti[a], I. Martínez-Salazar[a], M. López Granados[a], C. López-Aguado[b], J. Iglesias[b], G. Morales[b], Mariscal[a†]

1) Textural properties of the ZAB supports were evaluated from argon adsorption–desorption isotherms, which were recorded at 87 K using an AutoSorb equipment (Quantachrome Instruments).

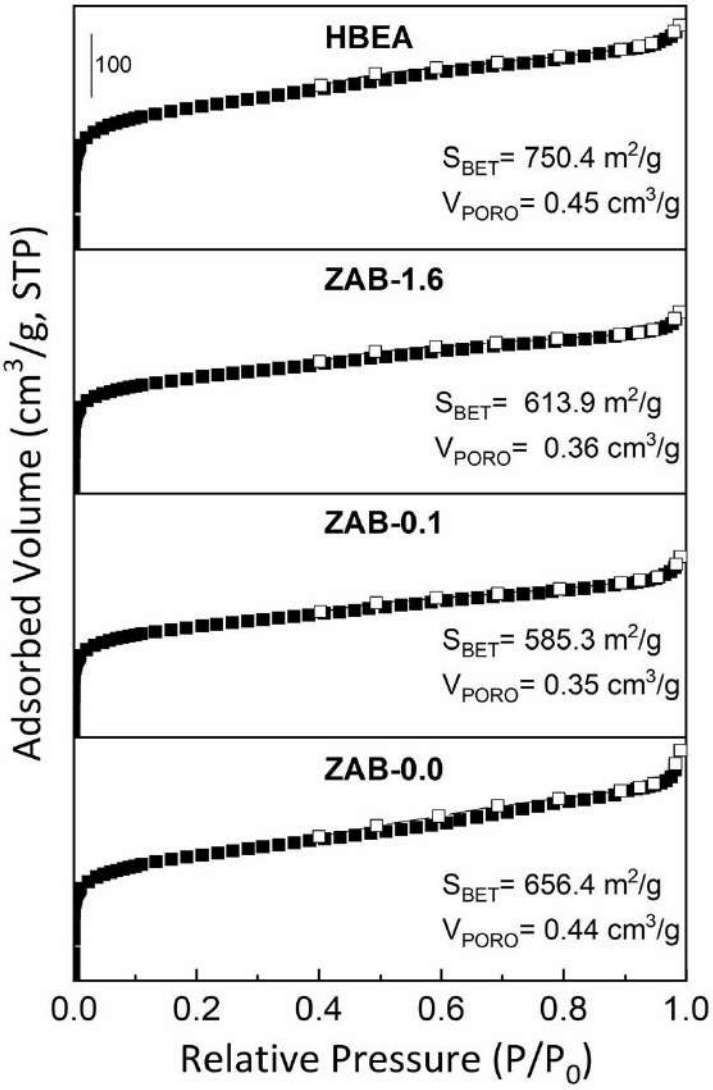

Figure S1. Argon adsorption-desorption isotherms of the ZAB zeolites.

2) Characterization of the ZAB supports using the XRD technique.

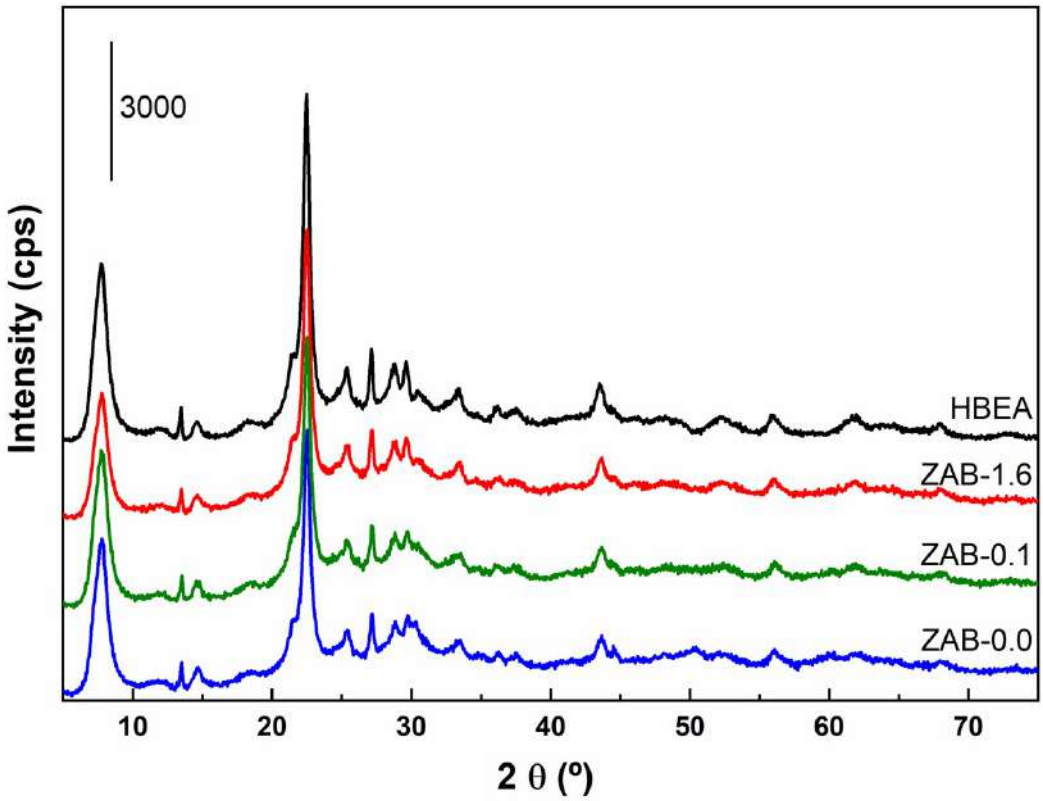

Figure S2. XRD patterns of the ZAB supports.

3) DRIFT spectra of ZAB acid supports using CD_3CN as probe molecule.

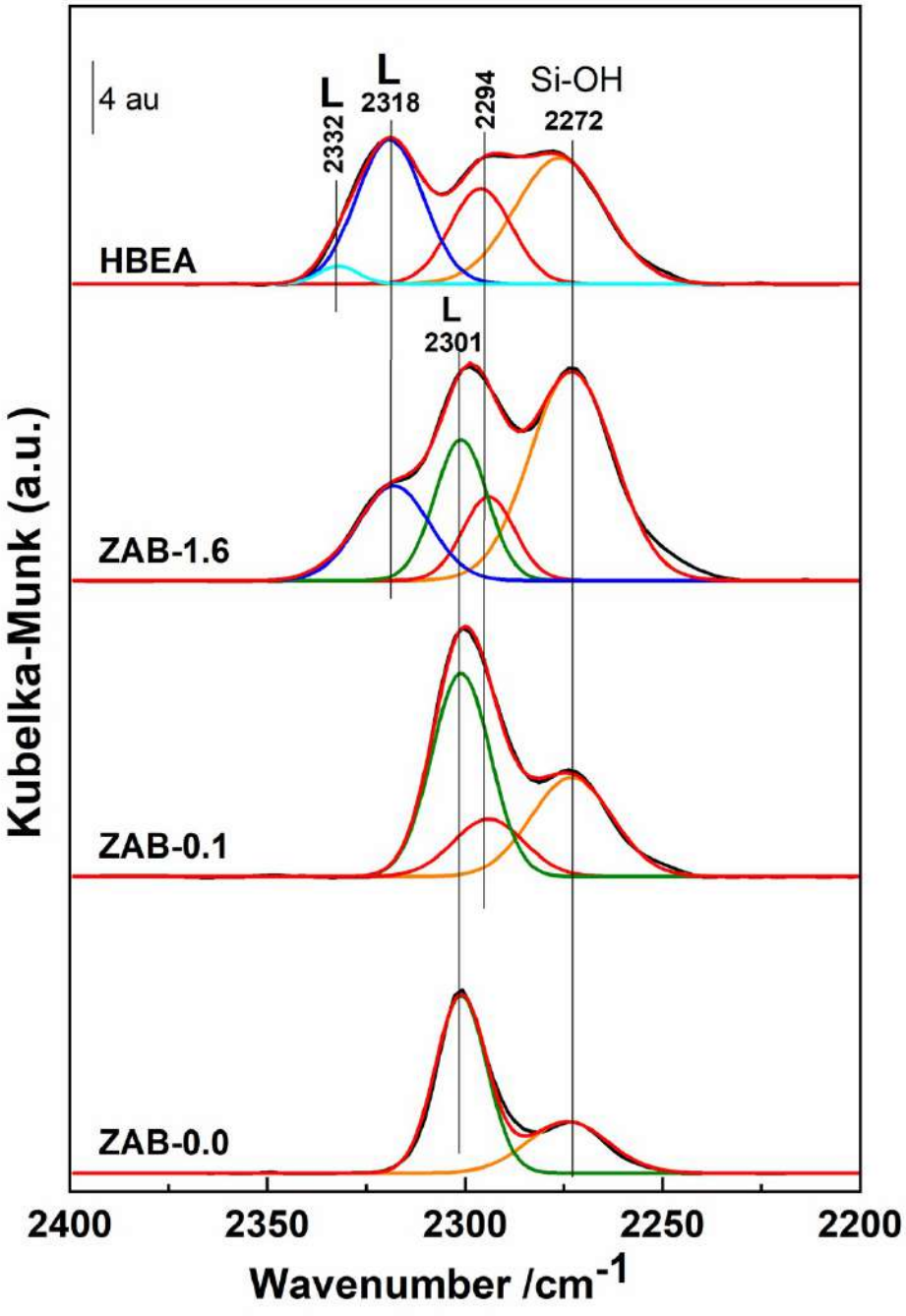

Figure S3. DRIFT spectra of the ZAB zeolites after adsorption of CD_3CN probe molecule.

3.3. The relevance of Lewis acid sites on the gas phase reaction of levulinic acid into ethyl valerate using CoSBA-xAl bifunctional catalysts; Catalysis Science & Technology **11**, 4280-4293 (2021)

Catalysis Science & Technology

ROYAL SOCIETY OF CHEMISTRY

PAPER

The relevance of Lewis acid sites on the gas phase

are the following: Pt/HMFI catalyst,[5] with which 99% yield to VA was reached in a solvent-free reaction due to a cooperative mechanism of Pt and the Brønsted acid sites (BAS). Pt/HZSM-5 catalyst, which was prepared after five atomic layer deposition (ALD) cycles, was considered a highly active bifunctional catalyst with a satisfactory stability for the reaction processes and an excellent VA yield of 91.4% in aqueous solution.[6] Ru/HZSM-5 also gave a high VA yield of 91.3% in dioxane after 10 h.[7] Pan *et al.*[8] reported the effects of different supports and acidity levels on the hydrogenation of LA to valerate esters on Ru-based catalysts. A 94% yield of ethyl valerate and valeric acid (EV + VA) was achieved over the Ru/SBA-SO_3H catalyst using ethanol as solvent. The loading of catalysts was high, 43 wt% (referred to LA), and the catalyst was mainly deactivated by leaching of sulphonic sites. Pd/ZSM-5 also demonstrated an excellent performance, with high VA and EV yields (92%) after an 8 h reaction using ethanol as solvent.[9] Recently, it has also been reported that the metal selected can modulate the selectivity of LA into GVL or valeric biofuels using 1,4 dioxane as solvent. Thus, Ru/HZSM-5 catalysts exhibit a high yield (85.7%) of valeric biofuels, whereas Ni/HZSM-5 catalysts achieve a GVL yield of 93.1% with negligible formation of valeric acid or esters. It is found that the introduction of Ru into HZSM-5 would increase the number of strong acidic sites and enhance the ring opening of the GVL intermediate.[10] Many of these studies have been conducted at moderate temperatures and under H_2 pressure (473–523 K and 1–4 MPa H_2) together with an autogenous ethanol pressure under liquid phase conditions in a batch reactor.

The former noble metal-based catalysts are expensive and commonly suffer from deactivation by coke formation and deposition. Consequently, alternative catalysts based on low-cost non-noble metals that are resistant to deactivation are required. The latter implies the study of the stability in long-term experiments in a fixed bed continuous flow reactor. Co catalysts have shown activity in cascade reactions involved in the transformation of LA to EV. In this way, the Co/SBA-15 system has demonstrated excellent behavior under mild conditions. Specifically, GVL yields up to 78% were obtained at 423 K with 5.0 MPa H_2 and 2 h in a batch reactor.[11] Additionally, Sun *et al.*[12] reported a 97% yield of VA + EV in a batch reactor at 513 K with 3.0 MPa H_2 after 3 h of reaction using catalysts based on cobalt nanoparticles embedded in HZSM-5. Slow deactivation of the best catalyst was observed in a fixed-bed reactor under continuous conditions. The activity was entirely restored after regeneration *via* calcination followed by reduction of the catalysts, suggesting that the cause of deactivation was the deposition of coke formed in the surface acid sites. A non-noble metal catalyst based on Nb–Cu/Zr-doped porous silica (ZPS) catalyst has been recently described.[13] Under mild reaction conditions, 423 K and 3 MPa H_2 for 4 h in aqueous medium, a VA yield of 99.8% was reached. The Lewis acid sites of ZPS enhanced the adsorption of LA on the catalyst surface, and both the Lewis and Brønsted acidity associated with Nb_2O_5 and the metallic Cu^0 sites promoted catalysis of the tandem reaction. Nb_2O_5 avoids metal leaching and coke formation, which are serious issues in liquid phase reaction conditions. In summary, the hydrogenating function has been extensively studied, especially the nature of the supported metal. The reducing function of the bifunctional catalysts is required in two steps: the hydrogenation of LA to GVL and the reduction of ethyl pentenoate isomers into EV. Both reactions are not considerably challenging under these reaction conditions.

The role of the acid function has also been worthy of numerous studies in liquid and vapor phase systems. Even more, it has been reported that the rate-determining step of the reaction is the ring opening of the GVL driven by acid sites.[14] In the aforementioned studies, the acid function is mainly based on HZSM5 or SBA-15 functionalized by SO_3H groups, where strong BAS have been described as those with the highest intrinsic activity for the GVL ring opening. Sun *et al.*[15] studied the acidity regulation on the Ni/HZSM-5 catalyst by increasing the potassium content. Potassium decreases the acid strength together with an adjustment of the Brønsted/Lewis centers ratio in the flow reactor. More recently, Zhou *et al.*[16] have reported for the first time that strong Lewis acid sites (LAS) are also active for the ring opening of GVL. These authors have described a dual catalyst of Pd/C and $Hf(OTf)_4$ in a solution in *n*-octane. Under a relatively low temperature of 423 K and 5.0 MPa H_2, 92% VA selectivity at almost complete LA conversion was obtained.

In a different non-noble metal approach and using GVL as a substrate, the key intermediate in our cascade reaction, Ravasio *et al.*[17] have studied GVL transformation with a catalyst based in a non-noble metal supported on amorphous weakly acidic material, specifically Cu–SiZr systems. Using pentanol as the solvent, pentyl valerate can be obtained in one pot with GVL conversions of 90% and selectivity up to 83%. Liu *et al.*[18] have described a highly dispersed Cu/ZrO_2 catalyst due to a strong interaction between CuO and ZrO_2 in the precursor could lead to enhanced Cu dispersion and the formation of Cu^+ active centers. This catalyst presents low acidity and exhibited 85.4% conversion of GVL and 98% selectivity for pentyl valerate at 503 K and 1.5 MPa H_2 pressure. The success of these catalytic systems based on weakly acidic oxides opens an exciting alternative to noble metal–zeolite catalysts because they demonstrated that weak LAS are active in the GVL ring-opening reaction. Moreover, the weaker acid strength of these systems can prevent the deactivation of the catalyst by fouling with coke, which may prolong the practical life of the catalyst. A trade-off in the support acidity properties should be necessary to develop an efficient and stable bifunctional catalyst.

However, despite these efforts, a study for the direct reaction of LA to give EV with a bifunctional catalyst without strong BAS or LAS has not yet been conducted. The support oxide usually provides the acid function. Our approach to conduct such study has been to prepare a series of catalysts based on Co supported on Al-modified SBA-15 supports. The

Co concentration (metal hydrogenation function) was kept constant, whereas the Al content in the support SBA-15 was varied to change the nature, strength and concentration of the acid sites. The investigation presented here allows us to demonstrate that both Al^{3+}- and Co^{2+}-based LAS are capable of conducting the key acid-catalyzed reactions. Especially relevant are the latter, those defined by Co^{2+} sites stabilized by the incorporated Al oxide. Their relative weak strength, capable of performing the GVL ring-opening reaction, does not catalyze the formation of coke-like deposits that may prevent the deactivation by fouling.

2. Experimental procedure

2.1. Preparation of the CoSBA-*x*Al bifunctional catalysts

The synthesis of acid catalytic supports was conducted in two stages. First, SBA-15 mesoporous silicate was prepared following the method described by Gómez-Cazalilla *et al.*[19] 25 g of Pluronic was incorporated in 1 L of a 0.4 M sulfuric acid solution, and this mixture was gently stirred for one day at room temperature. Then, 1 g of sodium hydroxide was added along with a sodium silicate solution (66.4 mL of sodium silicate + 920 mL of distilled water), which was added dropwise under moderate agitation at room temperature. The resulting mixture (gel appearance) was stirred for five days at room temperature. The solid was recovered *via* vacuum filtration and washed several times with distilled water. Subsequently, it was dried in an oven at 353 K for 12 h and was finally calcined at 823 K for 6 h at a heating rate of 2 K min^{-1}. Second, to provide acidity over the catalyst support, aluminum was incorporated into SBA-15. The procedure was conducted by mixing different volumes of a 1.2 M $AlCl_3{\cdot}6H_2O$ aqueous solution with tetramethylammonium hydroxide (TMAOH, 25 wt%), keeping a TMAOH/Al ratio = 2.5 for all preparations. The volume of the solution was adjusted to obtain final Si/Al molar ratios of 40, 20, 10, 5 and 2.5. This mixture was then heated at 353 K for 1 h to ensure that the aluminum precipitated properly, where the mixture was previously diluted with H_2O until it reached pH 3.7. Next, it was left to cool at room temperature and solid SBA-15 was added. The temperature was then increased again to 353 K and held constant for 3 h. Finally, the solid was filtered, dried and calcined at 873 K for 4 h (heating rate of 1 K min^{-1}).

To provide the catalysts a hydrogenation function, a non-noble metal, such as cobalt, was selected for the catalytic process. Thus, the different Al-modified SBA-15 supports with variable amounts of aluminum were impregnated with an aqueous solution of $Co(NO_3)_2{\cdot}6H_2O$ salt. The incipient wet volume of SBA-15 was 3 mL of H_2O per g support and, accordingly, a cobalt nitrate solution to obtain a Co metallic concentration of 10 wt% was prepared. Finally, the impregnated solid was dried at 393 K for 12 h and calcined at 773 K for 5 h in an oven (heating ramp 1.5 K min^{-1}). These calcined samples were activated by H_2 reduction before measuring their catalytic activity, as will be explained in more detail below. The acid supports and catalysts were labeled as SBA-*x*Al and CoSBA-*x*Al, where *x* refers to the nominal Si/Al molar ratio.

2.2. Techniques of characterization

The chemical analysis of the calcined catalysts was performed with inductively coupled plasma atomic emission spectroscopy (ICP-AES) using a Perkin-Elmer Optima 3300 DV instrument. Prior to the analysis, the samples were solubilized in a mixture of HF, HCl, HNO_3 and H_3PO_4 and homogenized in a high-pressure microwave oven (Multiwave 3000 Anton Paar) for 2 h. The resulting solutions were diluted to 50 mL using Milli-Q deionized water.

The textural parameters were evaluated from nitrogen adsorption–desorption isotherms at 77 K, as determined using an automatic ASAP 2020 system from Micromeritics. Prior to the measurements, the samples were outgassed at 473 K and 10^{-4} mbar overnight. The surface areas were determined by using the Brunauer–Emmett–Teller (BET) equation, assuming a cross section of 16.2 $Å^2$ for the nitrogen molecule. The pore size distribution, the average pore diameter (D_p), and the total pore volume (V_p) were calculated from the isotherm desorption branch using the non-local density functional theory.

The TPR profiles were registered using a semiautomatic Micromeritics TPD/TPR 2900 apparatus. Before the reduction experiment, the calcined sample (*ca.* 80 mg loaded in a U-shaped reactor) was heated at 393 K under a He flow (35 mL min^{-1}) for 45 min to remove the physically adsorbed H_2O. After the sample cooled to room temperature, the TPR profile was recorded by heating the sample from 323 K to 973 K in an Ar/H_2 flow (48 mL min^{-1}, 10 vol% H_2) at a heating rate of 10 K min^{-1}. The water formed in the reduction reaction was trapped by passing the exit flow through a cold trap immersed in a liquid N_2/isopropyl alcohol bath (193 K).

X-ray photoelectron spectra (XPS) were collected using a Physical Electronics PHI 5700 spectrometer with non-monochromatic Al Kα radiation (300 W, 15 kV, and 1486.6 eV) with a multichannel detector. The spectra of the samples were recorded in the constant pass energy mode at 29.35 eV using a 720 mm diameter analysis area. Charge referencing was measured against adventitious carbon (C 1s at 284.8 eV). The Co 3d, Al 2p, Si 2p, C 1s and O 1s regions were scanned a sufficient number of times to obtain high signal-to-noise ratios. A PHI ACCESS ESCA-V6.0F software package was used for acquisition and data analysis. A Shirley-type background was subtracted from the signals. The recorded spectra were always fit using Gaussian–Lorentzian curves to determine the binding energies of the different element core levels more accurately. Reduced catalysts were stored in sealed vials in an inert solvent (cyclohexane). The sample preparation was performed in a dry box under a N_2 flow, where the solvent was evaporated before its introduction into the analysis chamber and directly analyzed without any previous treatment.

Aluminum coordination was evaluated by ^{27}Al MAS NMR spectra recorded with a Bruker AV-400 (9.4 T) spectrometer (Rheinstetten, Germany) using a BL-4 probe with zirconia rotors. The spectra were obtained using a spinning speed of ν_R = 10 kHz, a pulse width of 1 μs (corresponding to π/12 rad pulse length), a relaxation delay of 1 s, and typically 1200 scans.

The total acidity was measured using temperature-programmed desorption of ammonia (NH_3-TPD). The *in situ* reduced catalysts (0.1 g) were pretreated at 773 K for 1 h and then cooled to 373 K under a 50 mL min^{-1} Ar flow to remove the adsorbed surface species. Then, a flow of 5 vol% NH_3/He at 50 mL min^{-1} was passed through the sample bed for 1 h at 373 K, and subsequent flushing with an Ar flow at the same temperature was used to remove the physisorbed ammonia. The NH_3 desorption was performed from 373 to 1073 K at a heating rate of 10 K min^{-1}. The TPD analyses were registered using a Balzer Prisma™ quadrupole mass spectrometer (QMS 200) following the fragments m/z = 16 (NH_2^+), m/z = 17 (NH_3^+ and H_2O^+), m/z = 18 (H_2O^+), m/z = 28 (N_2^+ and CO^+), m/z = 30 (NO^+), m/z = 40 (Ar^+), m/z = 44 (N_2O^+), and m/z = 46 (NO_2^+) to follow the desorption of ammonia and to discard the oxidation of NH_3 to nitrogen oxides. The quantitative analysis of the desorbed ammonia was based on the m/z = 16 signal by integrating the area under this desorption curve. Previous calibration of this signal was properly conducted by passing streams with different NH_3 concentrations.

Diffuse reflectance infrared Fourier transform (DRIFT) spectra were collected with a Nicolet 5700 spectrometer equipped with a Hg–Cd–Te cryodetector with high sensitivity and working in the spectral range of 4000–650 cm^{-1}. A diffuse reflectance accessory (Praying Mantis-Harrick Co) was used as an optical mirror accessory. Approximately 30 mg of previously ground samples were placed in a high-temperature catalytic reaction chamber (HVC-DRP Harrick Scientific Products, NY) that allows treatment *in situ* at high temperatures. Before introducing the probe molecule, the solid sample was pretreated with a flow of 20% (v/v) O_2/Ar while being heated at 573 K, which was then left for 1 h to clean the surface of the supports or catalysts. In the case of catalysts containing cobalt, reduction under a 10% H_2/Ar flow at 723 K for 1 h was conducted. Afterward, the temperature was decreased to 298 K under an Ar flow; once at 298 K, the Ar was circulated across a bubbler with deuterated acetonitrile for 10 min. The fraction of physically or more weakly adsorbed CD_3CN was removed by flushing the reaction chamber with Ar (bypassing the bubbler). The DRIFT spectra of the deuterated acetonitrile were recorded at 128 scans with a resolution of 4 cm^{-1} at different temperatures and times during flushing with Ar.

2.3. Activity measurements

Fixed-bed continuous-flow catalytic studies were conducted in a 1/4″ tubular stainless-steel reactor at 523 K with 3 MPa H_2 controlled by a back-pressure regulator. The catalyst (0.25 g) was loaded between two end plugs of quartz wool. Prior to the reaction, the catalyst was reduced with an H_2 flow (50 mL min^{-1}) at 773 K with a heating rate of 2 K min^{-1} until the temperature reached 573 K. Once this temperature was reached, the heating ramp was changed to 1 K min^{-1} until it reached 773 K, where it was held for 10 h. Finally, it was cooled to the reaction temperature (523 K). Then, 10 wt% LA/ethanol solution was pumped into the reactor at different contact times, and the H_2 flow was adjusted to 20 mL min^{-1}. Although a liquid LA/ethanol solution is fed to the reactor, under the actual reaction conditions, the simulation with Advanced System for Process Engineering (ASPEN) software indicated that the reaction in the catalyst bed takes place in the gas phase, which is desired to avoid leaching of the cobalt and coke formation, which may have a lesser impact on deactivation during long-term continuous experiments. Downstream of the catalyst bed zone, at room temperature, the reaction mixture goes back to the liquid phase.

The product samples were analyzed in a gas chromatograph (Shimadzu GS2010) equipped with an SHRXI-5MS capillary column (30 m × 0.25 mm × 0.25 μm) and a flame ionization detector. Before the GC analysis, the samples were prepared by adding cyclohexanol (*ca.* 0.1 g) as an internal standard to an aliquot of the reaction products. LA conversion is defined as the ratio between the outlet molar flow of LA consumed in the reaction to the molar flow of LA initially fed in the reactor. The yield is defined as the ratio of the amount of molar flow of the product formed to the total molar flow of LA initially present. The selectivity is defined as the result of dividing the yield value by the LA conversion. The identification of different products was conducted in a GC-MS (Shimadzu QP2010S) equipped with an SHRXI-5MS capillary column as well.

3. Results and discussion

3.1. Characterization of the CoSBA-*x*Al catalysts

Table 1 compiles the experimental chemical analysis data of the calcined catalysts using inductively coupled plasma atomic emission spectroscopy (ICP-AES) technique. The empirical content of Co is quite close to the theoretical nominal value (10 wt%) for all samples. However, in terms of the Al content, its actual incorporation is lower than intended, which is more evident for samples with a higher aluminum content (a lower Si/Al ratio), indicating that part of the Al used in the preparation was not incorporated in the precursor. In any case, the empirical and nominal aluminum content follows the same trend: the Al concentration in each sample is roughly doubled in successive samples of the series. Therefore, these catalysts are suitable for conducting a study on the role of the Al content or surface acidity of these bifunctional catalysts on the catalytic properties.

The N_2 adsorption/desorption isotherms of the calcined CoSBA-*x*Al catalysts exhibit a type IV isotherm with an H2 hysteresis loop (Fig. S1a in the ESI†). The presence of a pore filling step with a narrow range of P/P_0, along with its

Table 1 Chemical analysis (ICP-AES) and textural properties of the CoSBA-*x*Al catalysts

	ICP-AES		N_2 isothermal (textural properties)				
Catalysts	Co (%)	Si/Al	S_{BET} ($m^2\ g^{-1}$)	t_{plot} ($m^2\ g^{-1}$)	V_{pore} ($cm^3\ g^{-1}$)	V_{mic} ($cm^3\ g^{-1}$)	D_{pore} (nm)
CoSBA	10.3	∞	392	123	0.340	0.028	4.8
CoSBA-40Al	10.2	47.6	325	118	0.295	0.048	4.4
CoSBA-20Al	9.7	24.5	293	86	0.281	0.035	4.3
CoSBA-10Al	9.4	12.2	196	26	0.212	0.009	4.6
CoSBA-5Al	9.7	7.5	183	29	0.191	0.011	4.4
CoSBA-2.5Al	9.6	5.2	139	17	0.160	0.005	4.4

reversibility, is consistent with the presence of mesoporous with highly ordered cylindrical pores of uniform size interconnected by intrawall micropores.[19,20] In terms of the surface area, Table 1 collects the S_{BET} associated with the total porosity of the samples, where the area associated exclusively to micropores, which was determined by method *t*, has also been compiled. In both cases, an increase in the aluminum content in the series results in a decrease in the surface area. This same trend is determined for the pore volume. In terms of the mesopore size distribution, no significant differences are observed throughout the series (see the last column on Table 1 and Fig. S1b†). It can be concluded that although the incorporation of aluminum and cobalt on SBA-15 decreases its surface area and pore volume, it does not significantly affect the structural properties of the starting SBA-15, as confirmed by small-angle powder XRD analysis (see Fig. S2†). All these results indicate that pores are blocked *via* incorporation of oxide species.[21]

To study the effect of the aluminum content on the reducibility of cobalt species, hydrogen temperature-programmed reduction (H_2-TPR) experiments were conducted. The Co_3O_4 spinel phase was the only Co crystalline phase identified by X-ray powder diffraction (see Fig. S3†) in the calcined CoSBA-*x*Al samples. Fig. 1 shows the TPR profiles of the calcined CoSBA-*x*Al samples. The Al-free CoSBA sample displays two peaks in the range of 500–700 K, with maxima at 580 and 609 K. These two reduction peaks are widely accepted to be associated with the two reduction steps of the Co_3O_4 spinel phase, first to the CoO phase and then to metallic cobalt (Co_3O_4 → CoO → Co^0). These two reduction processes have also been described for the Co_3O_4 phase supported on SBA-15.[11,21,22] For the Al-containing samples, these two reduction peaks are also observed in this same range of temperatures. In general, a slight shift to lower temperatures in both reduction peaks was observed for the samples with aluminum contents up to that of the CoSBA-10Al sample, specifically at 546 and 584 K. In contrast, for the samples with higher aluminum contents (CoSBA-5Al and CoSBA-2.5Al) these peaks shift to higher temperatures (at exactly 597 and 632 K).

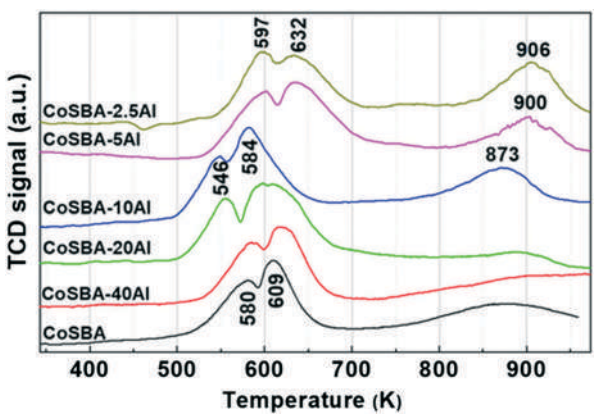

Fig. 1 TPR profiles of different calcined CoSBA-*x*Al samples.

It is known that cobalt dispersion, heterogeneity in particle size and support texture can modify the TPR profile.[23] It should be mentioned that these peaks are asymmetrical and challenging to fit into a single peak, suggesting that each of them is the result of two or more contributions. Thus, the reduction temperature is often directly related to the dispersion of the cobalt oxide species and the strength of its interaction with the support. Therefore, these data suggest that at low or moderate aluminum contents, the reducibility of the cobalt spinel is slightly favored by the presence of aluminum, while for a high aluminum content, the reducibility is more complicated, possibly because the interaction between the cobalt spinel and the support increased as the Al concentration increased.

Moreover, an additional reduction peak emerges in the temperature range of 850–975 K in the CoSBA-10Al, CoSBA-5Al and CoSBA-2.5Al samples, but this peak is incipient in the rest of the samples. Since this third reduction peak cannot be associated with cobalt aluminate ($CoAl_2O_4$) species, which require much higher temperatures of above 1073 K,[24] this peak can be better attributed to the reduction of another mixed phase of cobalt–aluminum oxide, nonstoichiometric aluminate.[25,26] After observing the reduction profiles of the calcined samples, the activation temperature of 773 K was chosen to reduce the most easily reducible species of cobalt; it was assumed that after this activation, only the Co^{2+} species that interact strongly with the support remain, which are mainly present in the samples with higher aluminum contents. Activating the samples at a temperature higher than 773 K to reduce all the Co^{2+} to Co^0 could imply the destruction of the mesoporous structure of the support. In summary, the TPR experiments show that incorporating Al affects the reducibility of the supported Co species.

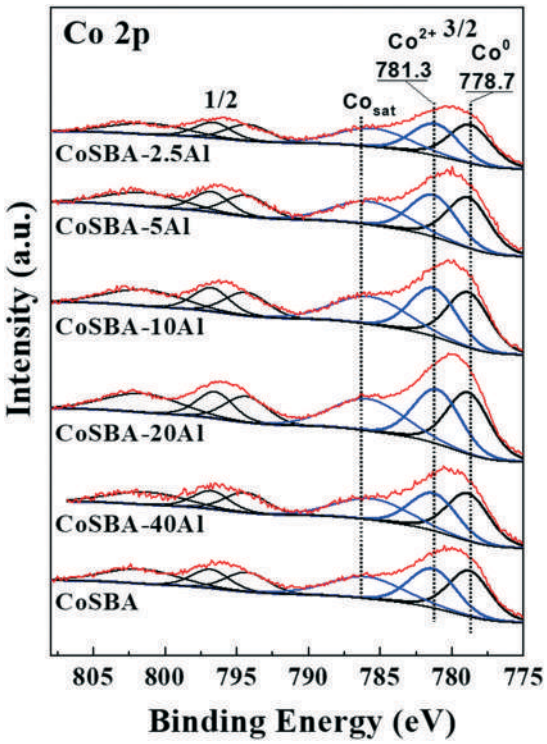

Fig. 2 XPS spectra of Co 2p core level for the CoSBA-*x*Al catalysts.

The oxidation state and chemical composition on the surface of the catalysts were analyzed *via* X-ray photoelectronic spectroscopy (XPS). Previous to this analysis, the samples were reduced following the same activation procedure performed in the reactor (up to a temperature of 773 K under H_2 with a flow rate of 50 mL min^{-1} for 10 h). Fig. 2 shows the XPS spectra of the Co 2p level, but we will only pay attention to the Co $2p_{3/2}$ component. The BE values are located at *ca.* 778.7 and 781.3 eV and assigned to the Co^0 and Co^{2+} ion species, respectively, whereas a third weak peak at *ca.* 786 eV represents the shake-up peak (Co_{sat}) due to the presence of cobalt ions.[27,28] Si 2p, Al 2p and O 1s core levels exhibit BE values expected for these mesoporous materials; the values are compiled in Table 2. According to the TPR results, after the reduction process at 773 K, Co^{2+} ions were only expected in the three catalysts with the highest aluminum contents, which showed a third species of cobalt that was reducible at temperatures above 850 K. However, Co^{2+} ions are observed on the surface of all catalysts in the series. The presence of Co^{2+} species can also be explained by the transferring of the samples from the reactor where the reduction is conducted to the XPS chamber. It may have resulted in the oxidation of the outermost layer of some of the metallic Co particles driven by the unavoidable contact with traces of ambient air. This could be the reason why the Co^{2+}/Co^0 ratio is similar for all samples.

Table 2 also shows that the Si/Al atomic ratio on the surface decreased as the aluminum content increased, which agrees with the bulk values determined by chemical analysis (see Table 1). Moreover, the Co/(Si + Al) atomic ratio derived from the XPS analysis was used as an indication of the dispersion of cobalt species on the surface; with some limitations this ratio has also been used previously for Co supported catalysts.[28–30] This atomic ratio increases with the aluminum content, indicating that the dispersion of Co is favored by the presence of aluminum (even though the incorporation of Al causes a decrease in the surface area). This increase in the dispersion of Co species is an evidence of the influence of Al oxide on Co oxide and strongly suggests the existence of an interaction between the cobalt and aluminum oxide species.[30] Summarizing, the XPS results evidence that incorporating Al favors the dispersion of the Co species.

The coordination of Al atoms in the catalysts was evaluated by ^{27}Al MAS NMR. The spectra of the catalysts after the incorporation of cobalt are similar (see, for example, CoSBA-20Al in comparison to SBA-20Al), and therefore the information extracted for the Al coordination by this technique is valid for both the supports and the catalysts. The spectra of the SBA-*x*Al supports are shown in Fig. 3. In general, the samples present two contributions: a peak at δ = 53 ppm ascribed to the framework aluminum species in tetrahedral coordination (Al^{IV}), and peaks at δ ranging from 0 to 6 ppm assigned to the extra-framework aluminum species in octahedral coordination (Al^{VI}).[19,31] When the Al content is low (Si/Al >10), the tetrahedral Al sites predominate and only a few species of octahedral Al are observed. For samples with

Table 2 Characterization data of the CoSBA-*x*Al catalysts

Catalyst	Binding energies (eV) and atomic ratios by XPS						NH_3-TPD μmol g^{-1}
	Al 2p	Si 2p	O 1s	Co $3p_{3/2}$	Si/Al	Co/Si + Al	
CoSBA		103.5	532.7(95%) 529.8 (5%)	778.7(53%) 781.3(47%)		0.197	29
CoSBA-40Al	74.7	103.6	532.8(89%) 530.2(11%)	778.5(56%) 781.4(44%)	73.60	0.223	73
CoSBA-20Al	74.8	103.1	532.5(91%) 529.7 (9%)	778.8(54%) 781.0(46%)	23.44	0.259	167
CoSBA-10Al	75.0	103.3	532.5(93%) 529.7 (7%)	778.8(52%) 781.3(48%)	14.14	0.255	262
CoSBA-5Al	74.9	103.2	532.4(88%) 529.8(12%)	778.8(54%) 781.2(46%)	6.78	0.267	382
CoSBA-2.5Al	75.0	103.2	532.5(85%) 530.1(15%)	778.7(55%) 781.1(45%)	3.99	0.299	436

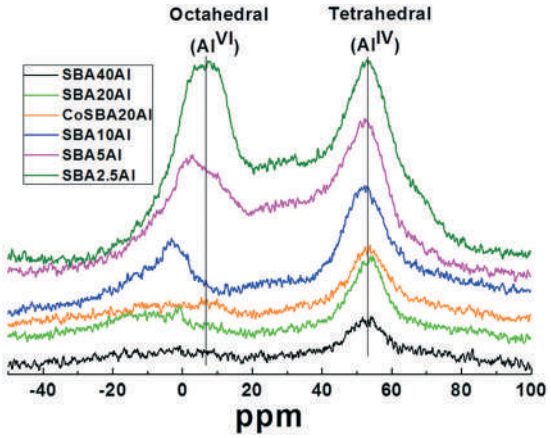

Fig. 3 ^{27}Al MAS NMR spectra of the SBA-*x*Al supports.

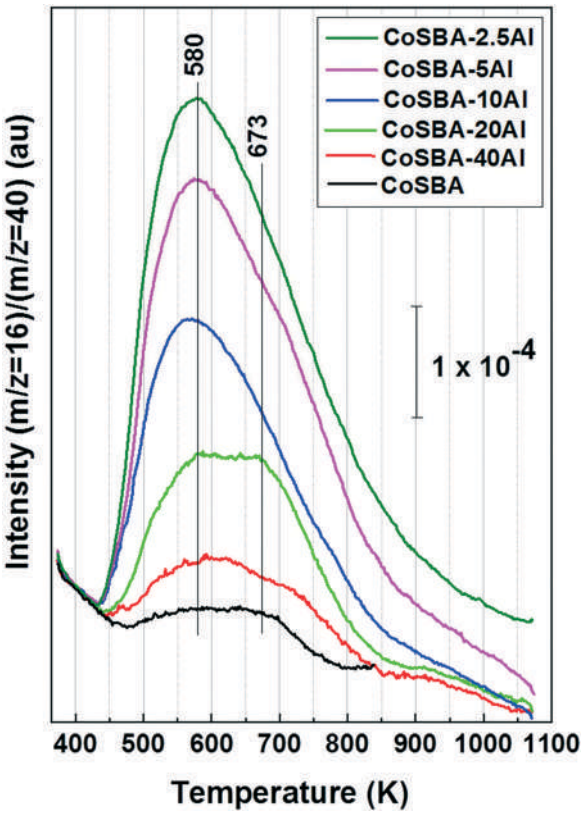

Fig. 4 NH_3-TPD profiles of the CoSBA-*x*Al catalysts.

higher Al concentrations (Si/Al ≤10), although the concentration of tetrahedral sites increases, there is a faster relative increase in the concentration of octahedral sites, whose presence in the SBA-2.5Al sample is as significant as that of the tetrahedral sites. Therefore, at low aluminum contents, Al is predominantly incorporated into the SBA framework as tetrahedral Al, but when the aluminum content increases, the SBA framework is no longer capable of incorporating successive amounts of Al and extra-framework octahedral Al appears. Consequently, for Si/Al <20, the number of tetrahedral sites remains quite constant, whereas the concentration of octahedral (extra-framework) Al sites increases. The presence of distorted tetrahedral or five-coordinated aluminum cannot be disregarded due to the low-intensity signal observed at approximately 30 ppm.[32] In summary, although the number of Al sites increases, the ratio of Al_{tetra}/Al_{octa} decreases with the decrease in the Si/Al ratio, indicating that samples with lower Al content possess the largest relative percentage of Al incorporated in an SBA framework.

To evaluate the total amount and the strengths of the acid sites on the catalyst surface, temperature-programmed desorption of ammonia (NH_3-TPD) was performed for the reduced catalysts. Fig. 4 displays the desorption profiles of ammonia. A broad peak of desorption is observed between the 440 and 923 K interval. Two peaks can be clearly discerned at 580 and 673 K for the CoSBA-40Al and CoSBA-20Al samples, those with a lower aluminum content, whereas in the remaining samples the contribution peaking at 673 K is only observable as a shoulder of the main peak at 580 K. However, an exact assignment cannot be made since in these catalysts this broad and intense peak is the result of the contribution of acid centers of different nature and strength (as will be observed below) associated with the presence of aluminum ions in tetrahedral and octahedral coordination, Co^{2+} ions and silanol groups.

The total number of acid centers increases with the aluminum content. In terms of quantification, it is possible to calculate the total number of μmol of ammonia desorbed per gram of catalyst. The values obtained are shown in last column of Table 2. The surface acidity of the samples is mainly associated with the presence of Al. As the Al content in the catalyst increases, the number of acid centers increases as well, although the proportion is not exactly linear. At higher aluminum contents, the surface acidity does not grow at the same rate as the Al content.

The Brønsted/Lewis nature and strength of the acid sites were also studied employing the diffuse reflectance infrared Fourier transform (DRIFT) technique using deuterated acetonitrile as the probe molecule. If CH_3CN is used the *ν*CN band is overshadowed by the Fermi resonance between the *ν*CN and the combination of $\delta_s(CH_3)$ + *ν*C–C frequencies. Therefore, the use of CD_3CN facilitates the assignment of infrared bands.[33,34] Moreover, the dynamic diameter of this molecule is small, so diffusion problems within the channels of SBA-15 are not expected. Acetonitrile chemisorbed on Lewis acid sites (LAS) displays a *ν*CN vibration distinguishable (>2300 cm^{-1}) from that assigned to acetonitrile chemisorbed on Brønsted acid sites (BAS, <2300 cm^{-1}).[35]

Fig. 5 shows the different infrared spectra of the supports and catalysts. Fig. 5A shows the spectra obtained for the various SBA-*x*Al supports after deuterated acetonitrile (CD_3-CN) adsorption and subsequent flushing with Ar at 373 K for 5 min. (see Fig. S4A and B† as examples of how the intensity of the bands in SBA-10Al and CoSBA-10Al samples, respectively, evolves during the entire process of CD_3CN

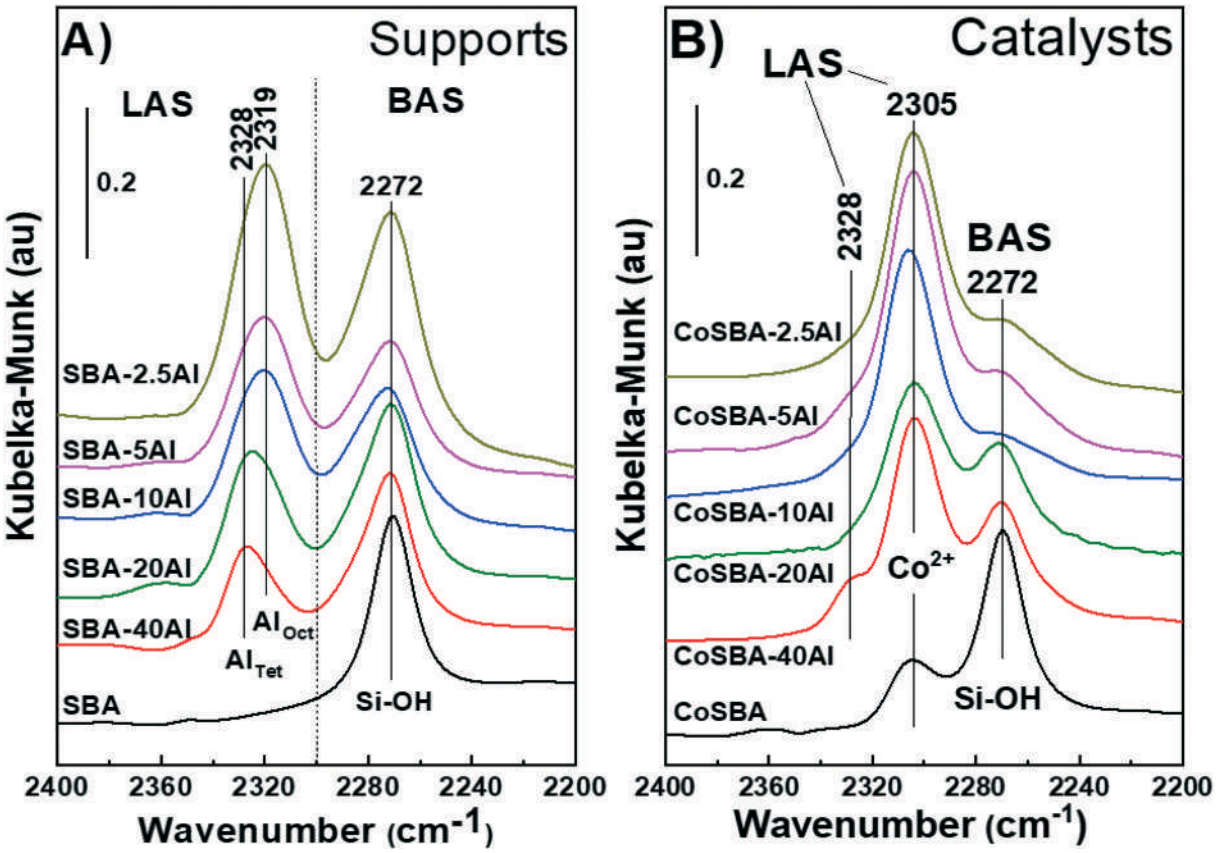

Fig. 5 DRIFT spectra after adsorption of deuterated acetonitrile of the CoSBA-*x*Al samples. (A) Supports and (B) reduced catalysts.

adsorption and subsequent Ar flushing at different temperatures and times). In Fig. 5A, two adsorption bands are shown. One is at 2272 cm^{-1}, which is associated with CD_3CN adsorption on the surface Brønsted acid sites (BAS), essentially due to silanol groups.[36,37] This assignation was confirmed by the fact that when the CD_3CN was outgassed by flushing at different temperatures and times, an increase in the intensity of the free silanol groups at 3740 cm^{-1} was also observed (this is not shown in the figure for the sake of simplicity). The second band has a maximum adsorption centered at 2328 cm^{-1}, which is associated with tetrahedral aluminum sites (SBA-40Al sample), centers responsible for high strength Lewis acid sites (LAS).[35–37] When this peak maximum was observed in more detail, a shift up to 2319 cm^{-1} was observed upon increasing the aluminum content, indicating the presence of a higher proportion of octahedral Al (SBA-2.5Al sample), as has been followed above by ^{27}Al NMR-MAS analysis. This shift is explained by the fact that the lower the frequency, the lower the acid strength of the acid centers. A displacement in the same direction has been described for LAS to coordinate tetrahedral and octahedral aluminum in zeolites.[35]

Fig. 5B shows the spectra obtained for the different calcined Co-containing SBA-*x*Al catalysts. The incorporation of cobalt drastically changes the surface acidity of the supports, though the bands associated with silanol groups (2272 cm^{-1}) and Al$_{tet}$ (2328 cm^{-1}) are also observed. For catalysts with a lower aluminum content (CoSBA-40Al), the band at 2328 cm^{-1}, which represents the stronger Lewis acid sites associated with tetrahedral Al sites, is still clearly observed (in the rest of the samples, the latter band is observed as a shoulder of the main 2305 cm^{-1} peak). After incorporating cobalt, a prominent band at 2305 cm^{-1}, associated with weak LAS, is generated clearly in those catalysts containing Al. The wavenumber of the 2305 cm^{-1} band is considerably low to be associated with tetrahedral and octahedral aluminum for zeolites.[35] While an infrared band in the range 2310–2305 cm^{-1} has been previously associated with the presence of Co^{2+} ions supported on zeolites by several groups,[36,38] the fact that the appearance of this band is related to the vanishing of the Al$_{oct}$ band at 2319 cm^{-1} suggests that Co^{2+} species are preferentially related to previously existing octahedral aluminum. Therefore, it can be concluded that aluminum oxide stabilizes the formation of weak LAS centers *via* the cobalt ions on the surface.[31,33] A similar effect has been observed for supported Cu/SiO_2 catalysts where the interaction of the oxide precursor with the support generates weak Lewis acid sites by the presence of surface Cu^{2+} ions.[39,40]

Summarizing, regarding the surface acidity of the catalysts, all the catalysts present weak BAS due to the presence of silanol groups. The incorporation of aluminum generates up to three types of LAS with different strengths.

Two types of strong or moderate LAS are due to the presence of Al in tetrahedral and octahedral coordination, respectively. In addition, extra-framework aluminum oxide induces the formation of another weak LAS center associated with Co^{2+} ions.

3.2. Catalytic activity

Fig. 6 shows the yield of the reaction products *versus* time on stream (TOS) for the different CoSBA-*x*Al catalysts; the applied weight-hourly space velocity (WHSV) is also

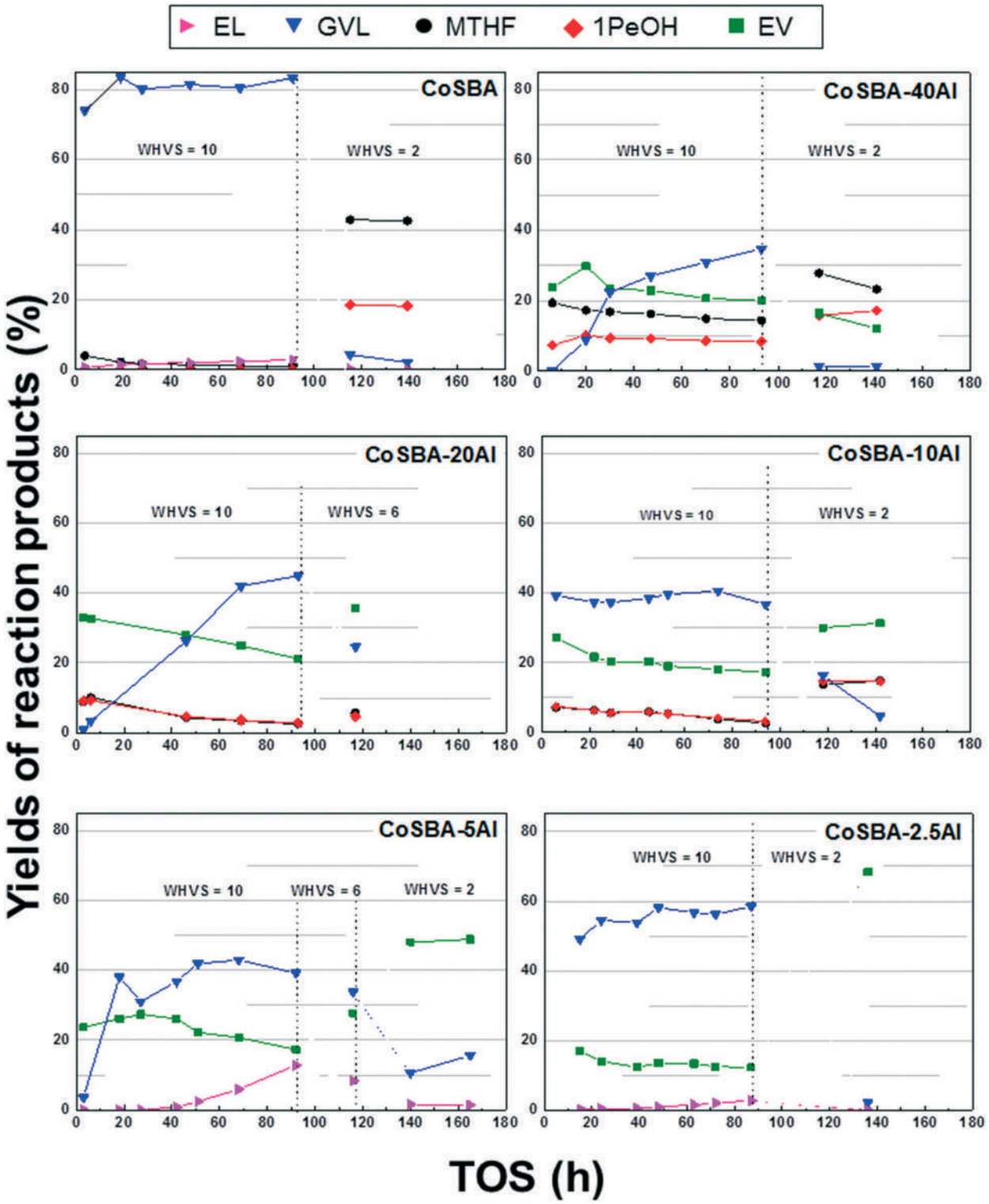

Fig. 6 Product yields *versus* time on stream (TOS) for the CoSBA-*x*Al catalysts. Reaction conditions: 10 wt% LA in ethanol, 0.25 g catalyst, 513 K and 3.0 MPa H_2.

indicated. The experimental procedures for all the catalysts were similar, starting the reaction at WHSV = 10 h^{-1} for approximately 90 h and then decreasing the WHSV by reducing the LA ethanol solution flow rate, which increases the contact time. The LA conversion is complete for all the catalysts of the series, and therefore it is not shown in the figure. The reaction product yields depend on the composition of the tested catalyst. The yields of the main products, such as ethyl levulinate (EL), gamma-valerolactone (GVL), methyl tetrahydrofuran (MTHF), 1-pentanol (1PeOH) and ethyl valerate (EV), are shown. However, other minor products, such as valeric acid (VA), pentenoic acid and ethyl pentenoate isomers, and ethyl pentyl ether (EPE), are also detected by GC-MS analysis, but with yields of less than 3%. In any case, the carbon balance did not close and therefore, other products that are not detected by gas chromatography can be formed during the reaction. It is well known that coke-like products can be formed when hydrotreating organic compounds at temperatures above 500 K in the presence of acidic sites[41,42] that can account, at least partially, for the lack of carbon balance. These carbonaceous coke-like residues can have their relevance in the deactivation by fouling the active centers in the catalyst, as will be mentioned below.

To facilitate the description of Fig. 6, the widely accepted LA catalytic hydrodeoxygenation reaction pathways[7,43] are presented in Fig. 7. Ethyl levulinate (EL) is the first product of the reaction and it can even be formed thermally under our reaction conditions; EL was identified as the main reaction product in a blank test using an inert bed (sieved quartz). GVL is the pivotal intermediate compound in this reaction. There are two competitive transformations of GVL, which will depend on the catalyst and, more specifically, on the balance between the reducing and acid centers on the surface of the catalyst.

GVL transformation can proceed (i) *via* a non-selective hydrogenation route on the reduction centers (metallic cobalt) to obtain mainly MTHF, 1PeOH and even ethyl pentyl ether (EPE); the latter can be formed after etherification on acid sites of 1PeOH with the ethanol solvent; and (ii) the selective route on acid centers with the ring opening of GVL occurring in the bond between the furan oxygen and the carbon with the methyl group, giving ethyl pentenoate (or pentenoic acid) isomers which can be subsequently reduced to obtain ethyl valerate (or valeric acid in aqueous medium).

As shown in Fig. 6, the Al-free catalyst (CoSBA), which hardly presents acidity, mainly forms GVL at WHSV = 10 h^{-1}. This indicates that the catalyst has sufficient reducing ability to allow for the hydrocyclisation of LA/EL to GVL (first step of the reaction). Moreover, this catalyst was considerably stable after 90 h under these reaction conditions. The modification of the space velocity to WHSV = 2 h^{-1} resulted in an evident change in the reaction of the GVL intermediate: GVL practically disappears and follows the so-called non-selective route, forming methyl tetrahydrofuran (MTHF) and 1-pentanol (1PeOH), which are identified and stable along the time on stream. This same reaction pathway, in the absence of surface acidity, has already been reported for the Co/SiO_2 catalyst.[43]

For the rest of the catalysts, which contain different proportions of aluminum on the support, the catalytic course of the reaction changes significantly. In the case of the CoSBA-40Al catalyst, the presence of acid sites *via* the incorporation of Al species on the support modifies the

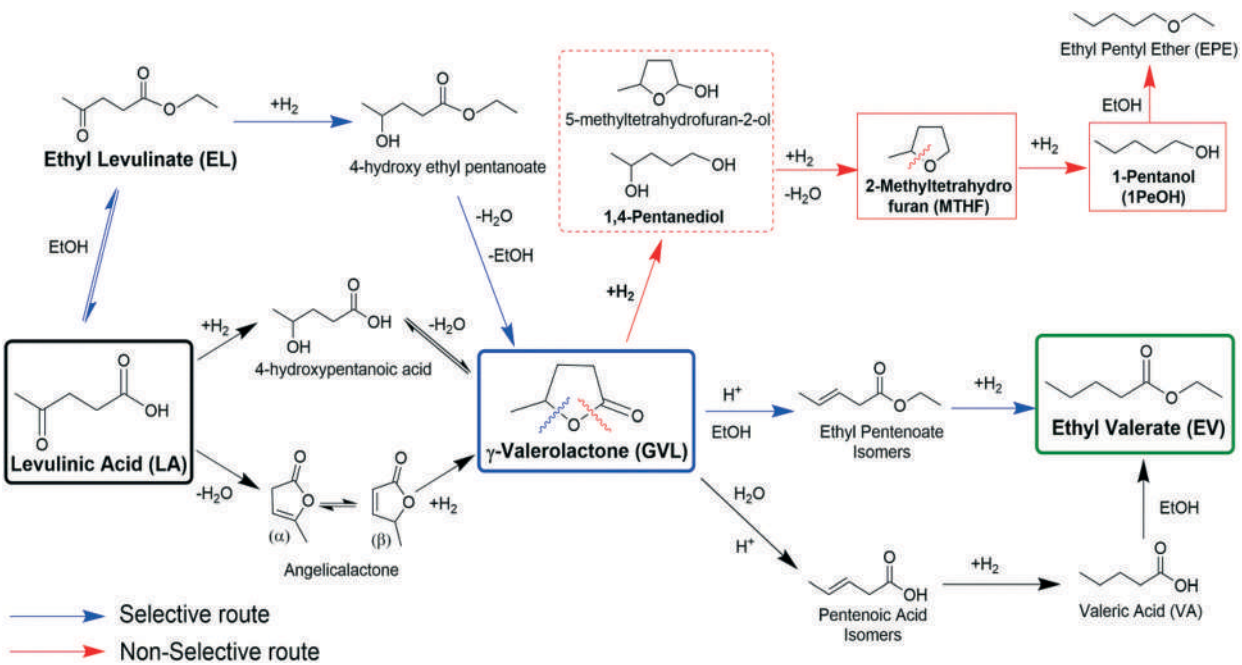

Fig. 7 Reaction pathways of levulinic acid (LA) transforming into ethyl valerate (EV). Adapted from Luo *et al.*[7]

behavior of the catalyst and favors the ring opening of GVL, yielding EV, whose yield is between 20% and 30% at WHSV = 10 h^{-1}. The GVL yield is initially considerably low, but after 30 h on stream, GVL becomes the major product without significantly affecting the EV yield. This transient behavior of GVL is not related to the dead volume effects of the reactor because the rest of the products remain quite constant along the experiment. It is clear that, regarding GVL formation, there is a conditioning period of the catalyst. MTHF and 1PeOH coming from the non-selective route of GVL are also obtained. Additionally, some amount of ethyl pentyl ether (EPE) has also been detected due to the etherification reaction between 1PeOH and the ethanol solvent. These findings suggest that the reducing capacity of this catalyst is higher than for the CoSBA catalyst *via* the presence of aluminum. The presence of acid sites at the surface of the support modifies the reducibility and dispersion of Co species due to a possible interaction between both metals,[44] which can enhance the hydrogenating characteristics of the cobalt particles and the promotion of the non-selective hydrogenation route. Similarly to the previous free aluminum catalyst, when the WHSV was decreased to 2 h^{-1}, GVL disappears by transformation *via* non-selective paths (formation of MTHF and 1PeOH and other non-detected products), which also decreases the EV yield.

Next, the behavior of the CoSBA-20Al catalyst is discussed. At WHSV = 10 h^{-1}, the catalytic performance is quite similar to that of the CoSBA-40Al system, with an initial transient behavior for GVL formation, becoming the most important product after some time on stream, and the formation of EV and other products such as MTHF and 1PeOH. The latter two products have lower yields than in the CoSBA-40Al case. In both CoSBA-20Al and the next catalyst of the series, CoSBA-10Al, the yield values for MTHF and 1PeOH are similar and therefore the two lines overlap. At longer contact times (WHSV = 2 h^{-1}), the GVL yield decreases at the expense of the formation of more EV. Lower amounts of MTHF and 1PeOH are also formed. In the CoSBA-10Al catalyst, no transient behavior is observed for GVL, and no EPE was detected.

Concerning the series of catalysts with higher Al contents, it is expected that the existence of a higher proportion of acid sites will provide greater importance to the selective GVL ring-opening route. Thus, the CoSBA-5Al catalyst essentially leads to GVL, EV when setting the conditions for longer contact times (moving from WHSV = 10 h^{-1} to 6 h^{-1}), while the products of the non-selective route are not detected. When WHSV was further reduced to 6 h^{-1} and 2 h^{-1} (longer contact times), the EV yield increases due to the enhanced transformation of intermediate products, such as EL and GVL into EV, which is now promoted by the larger concentration of acid sites. A similar behavior is also observed for the CoSBA-2.5Al catalyst (see Fig. 6); actually, a higher yield of EV was observed at WHSV = 2 h^{-1}, close to 70%, which is the largest yield of all the catalyst series. EV is essentially the unique product identified under these conditions.

All the above results can be discussed in the context of the critical question: the fate of the GVL intermediate when the aluminum oxide is incorporated into the support and how it evolves when increasing the aluminum content. At a WHVS of 10 h^{-1}, for the aluminum-free catalyst (CoSBA), the reaction only gives GVL: GVL conversion is not allowed under our operating conditions. However, when catalysts with low and moderate aluminum contents (CoSBA-40Al, CoSBA-20Al and CoSBA-10Al) are tested, the GVL reaction progresses *via* both competitive routes. Then, GVL can be partially transformed *via* the non-selective way to give MTHF and 1PeOH, and simultaneously another fraction of GVL is converted to EV by the selective route. Therefore, the presence of aluminum in the catalyst is critical to favor both routes. In our opinion, the particular pathway to give EV is promoted by the presence of Al due to the acidity that it directly provides to the catalyst by the presence of tetrahedral and octahedral Al sites, and indirectly provides by the stabilization of cobalt ions after the incorporation of aluminum.

To complete the picture, it is necessary to analyze the reaction when the WHVS is decreased to 2 h^{-1}. The contact time is then longer and the reaction can proceed further. For the catalyst without aluminum, CoSBA, the catalyst can now convert GVL to MTHF and 1PeOH (non-selective route). The catalysts with low or moderate amounts of aluminum (CoSBA-40Al, CoSBA-20Al and CoSBA-10Al) can conduct the two GVL conversion routes. Finally, in catalysts with a higher aluminum content (CoSBA-5Al and CoSBA-2.5Al) that already gave the selective route at high WHVS (low contact time), now at WHSV = 2 h^{-1} selectively transforms GVL to EV.

Summarizing, these bifunctional CoSBA-*x*Al catalysts are active and selective in the cascade conversion of LA to EV in ethanol. GVL is the main reaction intermediate, which is formed, and then two competitive reactions, the non-selective GVL route to MTHF and 1PeOH and the selective GVL ring-opening route to EV, occur. Which route predominates will depend on the concentration of the acid site on the surface on the catalyst and the contact time selected. All these results essentially agree with the mechanism already proposed in the literature. We will discuss next the relevance of Lewis acid sites in the cascade reaction.

3.3. Role of the surface acidity on the catalytic properties

First, it should be mentioned that the incorporation of aluminum in the support, in addition to providing acidity to the support, affects the reducibility and dispersion of the surface species of cobalt. In the catalysts with a higher proportion of aluminum, the stabilization of Co^{2+} ions is clearly observed. This means that as the aluminum content in the support increases, the hydrogenating capacity decreases. The relative proportion of metallic species of Co is lower. This is an advantage for catalysts with high Al content since a high hydrogenating capacity favors the conversion of LA to undesirable products (MTHF and 1PeOH).

On the other hand, it is known that the acid centers are required in different stages of the cascade reaction to transform LA to EV[4] and that the rate-determining step is the GVL ring-opening reaction.[14] Therefore this function gains greater relevance within the context of our CoSBA-*x*Al systems. It should be remembered that these bifunctional catalysts do not present strong BAS. Only considerably weak silanol groups are observed and are in practice quite inactive in the ring-opening reaction, as can be deduced from the negligible selectivity to EV when using the CoSBA catalyst. This catalyst has mainly silanol groups. According to our results, under our operating conditions (gas phase), the LAS must catalyze this reaction. In this CoSBA-*x*Al system, we have reported three LAS types of different strengths: tetrahedral and octahedral Al^{3+} and Co^{2+} ions. Their different acid strengths, and therefore their intrinsic activity in the acid-driven reactions, together with their relative concentration in the catalysts, explains the catalytic behavior of the catalysts studied in this work. The acid strength of the three LAS centers identified in our catalysts follows the trend $Al_{tet} > Al_{oct} > Co^{2+}$. The tetrahedral Al predominates at low Al content. When more Al is incorporated, both Al_{tet} and Al_{oct} become more concentrated but Al_{oct} concentration grows faster and practically outweighs the Al_{tet} concentration in the CoSBA-2.5Al. A weaker acidity corresponds to its lower intrinsic activity in the GVL ring-opening reaction. With the increasing of Al content, a higher fraction of Co^{2+} species, resistant to reduction, is stabilized on the surface of the activated catalyst. According to the results presented in this article, these weak LAS are also selective for the ring-opening reaction of the GVL. These weak LAS acid centers are capable of opening the ring of GVL; their less intrinsic activity is compensated for by the higher concentration of these centers. Recently, Velisoju *et al.*[45] have described the formation of Ni^{2+}/Ni^0 in Ni/ZSM5 catalysts promoted by the incorporation of Mo. They suggested that the Ni^{2+} species stabilized by interaction with Mo can perform the GVL opening ring by cracking the C–O bond on the methyl group side of the GVL molecule. Although these authors have used γ-valerolactone instead of levulinic acid as the substrate, these findings support our results since there is an explicit parallelism between the presence of Ni^{2+} species described by them and the stabilized Co^{2+} species described in our catalysts, especially in supports with high Al content.

In summary, although it is not surprising that the incorporation of Al provides LAS in our bifunctional catalysts, the catalytic results indicate that these LAS are active in the direct reaction from LA to EV. It must also be stressed that even the weak LAS centers associated with Co^{2+} ions are active and considerably selective under our reaction conditions. These weak LAS reach the highest concentration in the sample with the highest Al content, which is quite selective to EV, the product of interest.

To further evaluate the intrinsic activity of the acid centers and their deactivation, Fig. 8 shows the rate of EV formation per gram of CoSBA-*x*Al catalysts for WHSV = 10 and 2. This allows us to properly evaluate the possible deactivation of the different catalysts. We have conducted the reaction under

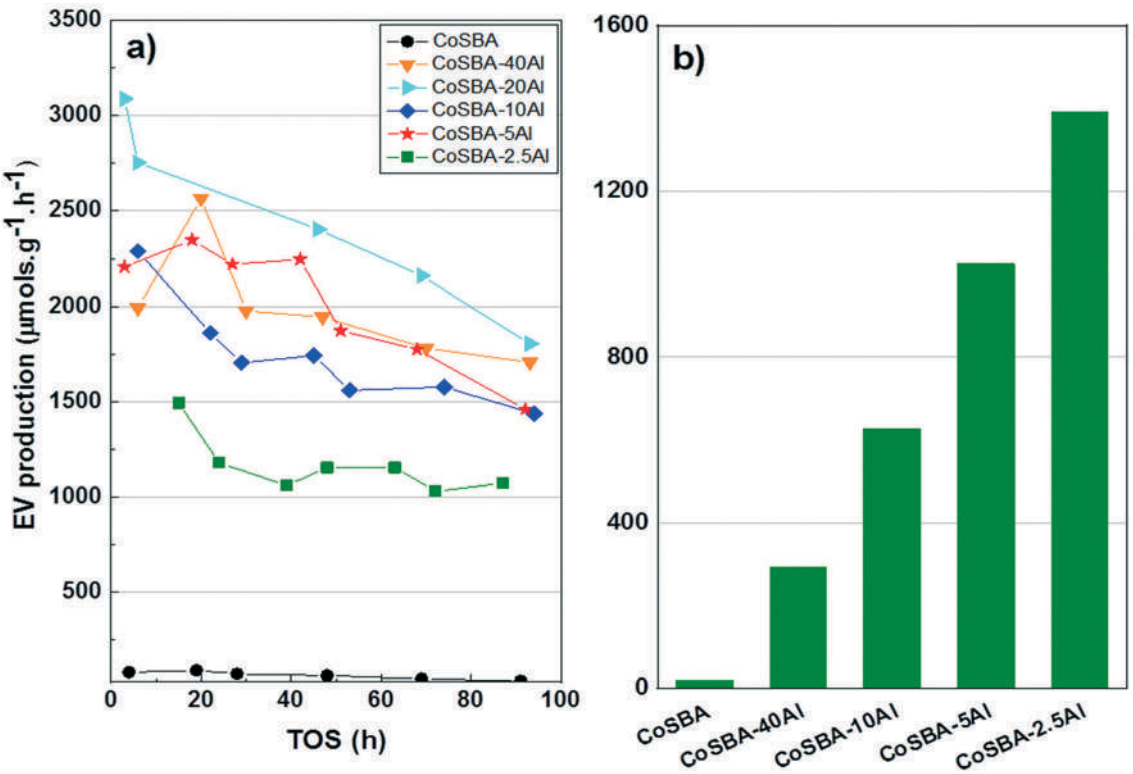

Fig. 8 EV productivity for the different CoSBA-*x*Al catalysts under the following conditions: (a) WHSV = 10 h^{-1} and (b) WHVS = 2 h^{-1}.

WHSV = 10 h^{-1} to detect the slow deactivation processes (see Fig. 8a), where the production of EV is displayed against the TOS. All the bifunctional catalysts present a slight deactivation with time on stream. The observed trend is that the higher the aluminum concentration, the more stable the catalyst is, although the productivity and yield of EV are lower. If we take into account that the aluminum concentration approximately doubles in two consecutive samples of the series, it can be deduced that the intrinsic activity in EV of the LAS associated with Al_{tet} (predominant in the first samples of the series) is higher than that of Al_{oct} and Co^{2+} that are proportionally in greater quantity in the samples of the series with more aluminum content.

In the case of WHSV = 2 h^{-1} (see Fig. 8b where the values have been derived from the average value when there is more than one point in these conditions), it is observed that the higher the concentration of aluminum in the catalyst, the higher the productivity and yield of EV due to the higher surface concentration of acid centers, as found by the TPD of ammonia (see Fig. 4). For the CoSBA-2.5Al catalyst we have reported an EV productivity of 1391 μmol g^{-1} h^{-1}, which is one of the highest values reported in the bibliography. This data has more value if we consider that it has been obtained after it has been subjected to a total of 140 h, at WHSV = 10 and 2 h^{-1} for around 90 and 50 hours, respectively, of reaction.

In general, samples with less Al initially produce more EV; but they are deactivated; the cascade of reactions is stopped in GVL and, consequently, less EV is formed. It seems that in samples with less Al, aluminum centers in tetrahedral and octahedral coordination (LAS) predominate, which are very active in the GVL ring-opening reaction but are also involved in the formation of coke deposits. The coke formation could explain the worse carbon balance in these samples. The fouling of the catalyst by the formed coke in practice decreases the number of acid centers exposed to the surface. In contrast, in samples with a high Al content, LAS Co^{2+} ions are also more concentrated. They are weaker and therefore less active in the GVL ring-opening reaction but the lower strength makes them even more stable because they are also less effective for coke production and less prone to fouling (deactivated).

In summary, the catalyst with the largest amount of aluminum (CoSBA-2.5Al) presents the highest EV yield. This performance is derived from the lower proportion of metallic Co species decreasing the hydrogenating capacity of this catalyst. This decrease is a positive result because it prevents GVL hydrogenation to undesired products. The Co^{2+} surface ions have been stabilized by incorporation of the aluminum into the support, modifying the reducibility and dispersion of cobalt species. The presence of LAS associated with these Co^{2+} species that, although with low intrinsic activity in the selective GVL ring-opening reaction, are highly concentrated in this sample and also possess less activity in the undesirable and deactivating formation of coke.

These results allow for expanding the possibilities of these bifunctional catalysts. It has been observed that both functions (hydrogenating and acidity) are modulated with the aluminum content present in the acid support. The selectivity and, consequently, the yield of the reaction products will depend on the reaction conditions, where the balance between the metallic centers and the amount and strength of the Lewis acid centers plays an essential role. Different cobalt contents and higher aluminum concentrations need to be explored for these systems. At this point, we have to mention that the micro or mesoporous nature of the support is also essential in the catalytic behavior along with the aluminum content, as has been previously reported.[9]

4. Conclusions

Bifunctional CoSBA-*x*Al catalysts are active for the direct conversion of levulinic acid to ethyl valerate in the gas phase using a solution of levulinic acid in ethanol in a continuous system. Once the intermediate product γ-valerolactone has been formed, it can follow two competitive routes: (i) non-selective, giving methyl tetrahydrofuran and 1-pentanol, and (ii) selective, giving ethyl valerate, for which the presence of Al is required. With an increase in the aluminum content in the series, a progressive conversion of γ-valerolactone towards the particular path to ethyl valerate is observed, to the detriment of the non-selective way.

The originality of this work is derived from these bifunctional CoSBA-*x*Al catalysts, except for the inactive weak silanol groups, which only present LAS that are active in the cascade reaction of levulinic acid to ethyl valerate, including determining the γ-valerolactone ring-opening step. Specifically, three types of Lewis acid sites are identified: tetrahedral and octahedral Al ions join with a fraction of non-reduced cobalt (Co^{2+} ions) stabilized by the incorporated Al in the support.

The best and most stable catalyst is the one with the highest concentration of aluminum (CoSBA-2.5Al), where an ethyl valerate yield of 70% is reached at longer contact times (WHSV = 2 h^{-1}). This behavior is due to the presence of a weaker, and consequently lower, intrinsic activity than Al ions, and higher density of acid centers associated with the presence of Co^{2+} ions, which are capable of selectively activating to give the corresponding ethyl pentenoate and allow for a subsequent reduction in ethyl valerate, avoiding its deactivation by coke fouling. Simultaneously, the higher Co^{2+}/Co^{0} ratio on the surface of this catalyst (see DRIFT spectra in Fig. 5B) decreases its hydrogenating capacity. It prevents the hydrogenation reactions of the γ-valerolactone intermediate, giving undesired products, such as methyl tetrahydrofuran and 1-pentanol, and increasing the ethyl valerate yield instead. This catalyst also showed promising stability in a 140 h on-stream run.

Conflicts of interest

There are no conflicts to declare.

Acknowledgements

Financial support from the Spanish Ministry of Economy and Competitiveness (RTI2018-94918-B-C41/C43) is gratefully acknowledged. R. M. also thanks the Ministry of Education, Culture and Sports for a "Salvador de Madariaga" grant (PRX16/00167) and the Fulbright Commission in Spain for co-financing his stay at UW-Madison.

References

1 F. D. Pileidis and M. M. Titirici, *ChemSusChem*, 2016, **9**, 562–582.
2 Z. Xue, Q. Liu, J. Wang and T. Mu, *Green Chem.*, 2018, **20**, 4391–4408.
3 J. P. Lange, R. Price, P. M. Ayoub, J. Louis, L. Petrus, L. Clarke and H. Gosselink, *Angew. Chem., Int. Ed.*, 2010, **49**, 4479–4483.
4 Z. Yu, X. Lu, J. Xiong and N. Ji, *ChemSusChem*, 2019, **12**, 3915–3930.
5 K. Kon, W. Onodera and K. I. Shimizu, *Catal. Sci. Technol.*, 2014, **4**, 3227–3234.
6 X. M. Gu, B. Zhang, H. J. Liang, H. Bin Ge, H. M. Yang and Y. Qin, *Ranliao Huaxue Xuebao*, 2017, **45**, 714–722.
7 W. Luo, P. C. A. Bruijnincx and B. M. Weckhuysen, *J. Catal.*, 2014, **320**, 33–41.
8 T. Pan, J. Deng, Q. Xu, Y. Xu, Q. X. Guo and Y. Fu, *Green Chem.*, 2013, **15**, 2967–2974.
9 M. Muñoz-Olasagasti, A. Sañudo-Mena, J. A. Cecilia, M. López Granados, P. Maireles-Torres and R. Mariscal, *Top. Catal.*, 2019, **62**, 579–588.
10 Z. Yi, D. Hu, H. Xu, Z. Wu, M. Zhang and K. Yan, *Fuel*, 2020, **259**, 3–6.
11 M. Audemar, C. Ciotonea, K. De Oliveira Vigier, S. Royer, A. Ungureanu, B. Dragoi, E. Dumitriu and F. Jérôme, *ChemSusChem*, 2015, **8**, 1885–1891.
12 P. Sun, G. Gao, Z. Zhao, C. Xia and F. Li, *ACS Catal.*, 2014, **4**, 4136–4142.
13 N. Karanwal, D. Verma, P. Butolia, S. M. Kim and J. Kim, *Green Chem.*, 2020, **22**, 766–787.
14 W. Luo, U. Deka, A. M. Beale, E. R. H. Van Eck, P. C. A. Bruijnincx and B. M. Weckhuysen, *J. Catal.*, 2013, **301**, 175–186.
15 P. Sun, G. Gao, Z. Zhao, C. Xia and F. Li, *Appl. Catal., B*, 2016, **189**, 19–25.
16 J. Zhou, R. Zhu, J. Deng and Y. Fu, *Green Chem.*, 2018, **20**, 3974–3980.
17 C. E. Chan-Thaw, M. Marelli, R. Psaro, N. Ravasio and F. Zaccheria, *RSC Adv.*, 2013, **3**, 1302–1306.
18 S. Liu, G. Fan, L. Yang and F. Li, *Appl. Catal., A*, 2017, **543**, 180–188.
19 M. Gómez-Cazalilla, J. M. Mérida-Robles, A. Gurbani, E. Rodríguez-Castellón and A. Jiménez-López, *J. Solid State Chem.*, 2007, **180**, 1130–1140.
20 R. Zhang, D. Shi, N. Liu, Y. Cao and B. Chen, *Appl. Catal., B*, 2014, **146**, 79–93.
21 M. Kondeboina, S. S. Enumula, V. R. B. Gurram, R. R. Chada, D. R. Burri and S. R. R. Kamaraju, *J. Ind. Eng. Chem.*, 2018, **61**, 227–235.
22 Y. Yang, G. Lv, L. Deng, B. Lu, J. Li, J. Zhang, J. Shi and S. Du, *Microporous Mesoporous Mater.*, 2017, **250**, 47–54.
23 B. Ernst, A. Bensaddik, L. Hilaire, P. Chaumette and A. Kiennemann, *Catal. Today*, 1998, **39**, 329–341.
24 W. J. Wang and Y. W. Chen, *Appl. Catal.*, 1991, **77**, 223–233.
25 G. Jacobs, T. K. Das, Y. Zhang, J. Li, G. Racoillet and B. H. Davis, *Appl. Catal., A*, 2002, **233**, 263–281.
26 P. Arnoldy and J. A. Moulijn, *J. Catal.*, 1985, **93**, 38–54.
27 H. Zhou, J. Song, H. Fan, B. Zhang, Y. Yang, J. Hu, Q. Zhu and B. Han, *Green Chem.*, 2014, **16**, 3870–3875.
28 A. Boix, E. E. Miró, E. A. Lombardo, M. A. Bañares, R. Mariscal and J. L. G. Fierro, *J. Catal.*, 2003, **217**, 186–194.
29 R. Balzer, L. F. D. Probst, V. Drago, W. H. Schreiner and H. V. Fajardo, *Braz. J. Chem. Eng.*, 2014, **31**, 757–769.
30 A. Y. Khodakov, W. Chu and P. Fongarland, *Chem. Rev.*, 2007, **107**, 1692–1744.
31 S. Chen, J. Li, Y. Zhang, Y. Zhao and J. Hong, *Catal. Sci. Technol.*, 2013, **3**, 1063–1068.
32 T. H. Chen, B. H. Wouters and P. J. Grobet, *Eur. J. Inorg. Chem.*, 2000, 281–285.
33 S. Jolly, J. Saussey and J. C. Lavalley, *J. Mol. Catal.*, 1994, **86**, 401–421.
34 R. Mariscal, M. López-Granados, J. L. G. Fierro, J. L. Sotelo, C. Martos and R. Van Grieken, *Langmuir*, 2000, **16**, 9460–9467.
35 A. G. Pelmenschikov, R. A. Van Santen, J. Jänchen and E. Meijer, *J. Phys. Chem.*, 1993, **97**, 11071–11074.
36 J. Chen, J. M. Thomas and G. Sankar, *J. Chem. Soc., Faraday Trans.*, 1994, **90**, 3455–3459.
37 M. Paniagua, G. Morales, J. A. Melero, J. Iglesias, C. López-Aguado, N. Vidal, R. Mariscal, M. López-Granados and I. Martínez-Salazar, *Catal. Today*, 2020, **367**, 228–238.
38 O. Bortnovsky, Z. Sobalík and B. Wichterlová, *Microporous Mesoporous Mater.*, 2001, **46**, 265–275.
39 N. Scotti, M. Dangate, A. Gervasini, C. Evangelisti, N. Ravasio and F. Zaccheria, *ACS Catal.*, 2014, **4**, 2818–2826.
40 F. Zaccheria, N. Scotti, M. Marelli, R. Psaro and N. Ravasio, *Dalton Trans.*, 2013, **42**, 1319–1328.
41 D. M. Bibby, R. F. Howe and G. D. McLellan, *Appl. Catal., A*, 1992, **93**, 1–34.
42 I. Van Zandvoort, Y. Wang, C. B. Rasrendra, E. R. H. Van Eck, P. C. A. Bruijnincx, H. J. Heeres and B. M. Weckhuysen, *ChemSusChem*, 2013, **6**, 1745–1758.
43 G. Novodárszki, H. E. Solt, J. Valyon, F. Lónyi, J. Hancsók, D. Deka, R. Tuba and M. R. Mihályi, *Catal. Sci. Technol.*, 2019, **9**, 2291–2304.
44 R. Munirathinam, D. Pham Minh and A. Nzihou, *Ind. Eng. Chem. Res.*, 2018, **57**, 16137–16161.
45 V. K. Velisoju, D. Jampaiah, N. Gutta, U. Bentrup, A. Brückner, S. K. Bhargava and V. Akula, *ChemCatChem*, 2020, **12**, 1341–1349.

Supplementary Information

The relevance of the Lewis acid sites on one-pot gas phase reaction of levulinic acid into ethyl valerate using CoSBA-xAl bifunctional catalysts

M. Muñoz-Olasagasti[a], M. López Granados[a], C. P. Jiménez-Gómez[b], J. A. Cecilia[b], P. Maireles-Torres[b], J. A. Dumesic[c], R. Mariscal[a*]

1) N_2 adsorption-desorption isothermal and pore distribution of calcined CoSBA-xAl samples

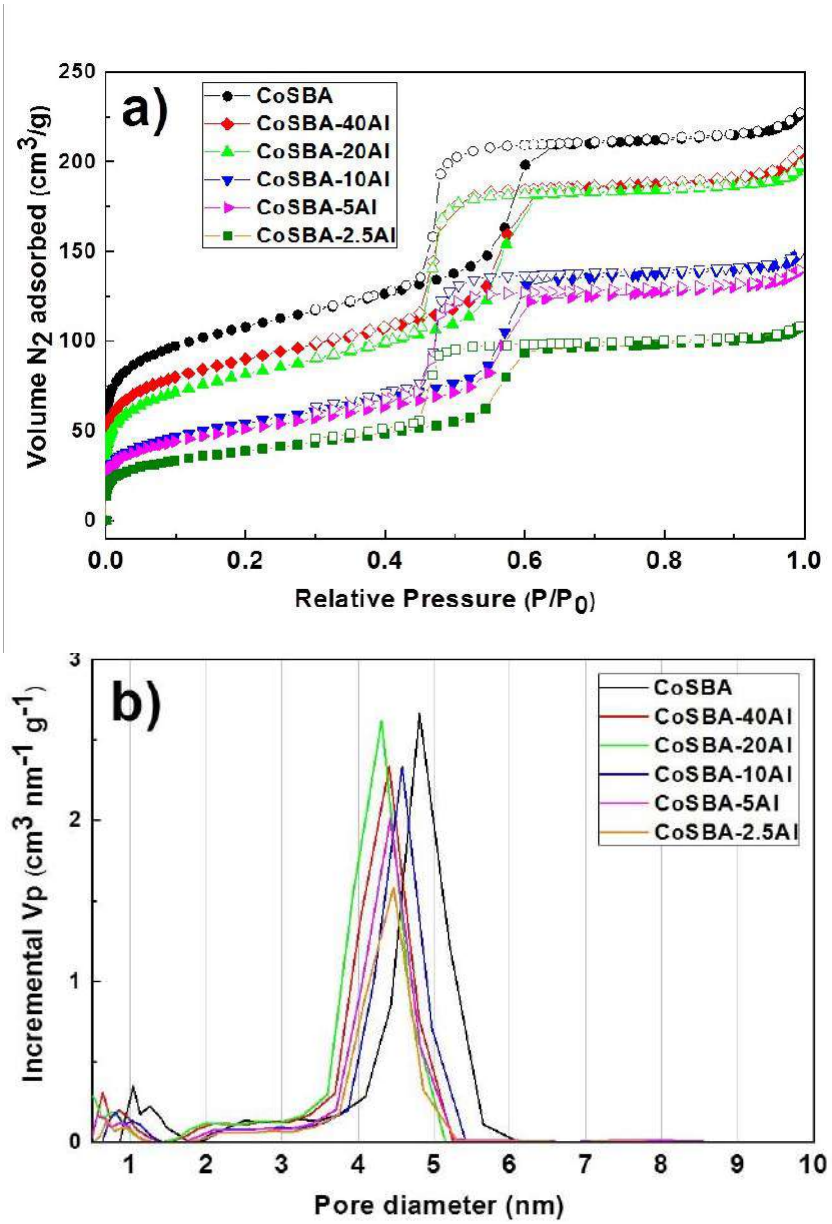

Figure S1. Textural properties of CoSBA-xAl bifunctional catalysts. a) N_2 adsorption-desorption isotherms and b) Pore size distribution.

2) Small-angle XRD patters of the SBA, SAB-2.5Al and CoSBA-2.5Al samples

The small-angle powder XRD patterns of calcined aluminum-free SBA-15 (SBA), the support with the highest aluminum content (SBA-2.5Al) and this support incorporating the cobalt (CoSBA-2.5Al) are shown in Fig. 2S. All samples exhibit three well-resolved diffraction peaks at 2θ values at around 1.08, 2.06, and 2.74, indexed to the (100), (110) and (200) reflections of the hexagonal space group p6mm [1]. It suggests the preservation of the SBA-15 structure after the incorporation of Al and Co species. The decrease in the intensity of diffraction peaks for the latter sample can be attributed to the decline in the difference between the channel walls of the matrices. The shift in the reflections of SBA-2.5Al and CoSBA-2.5Al samples towards slightly higher 2θ angles is due to the oxide monolayer coating the inner walls of SBA-15.[2]

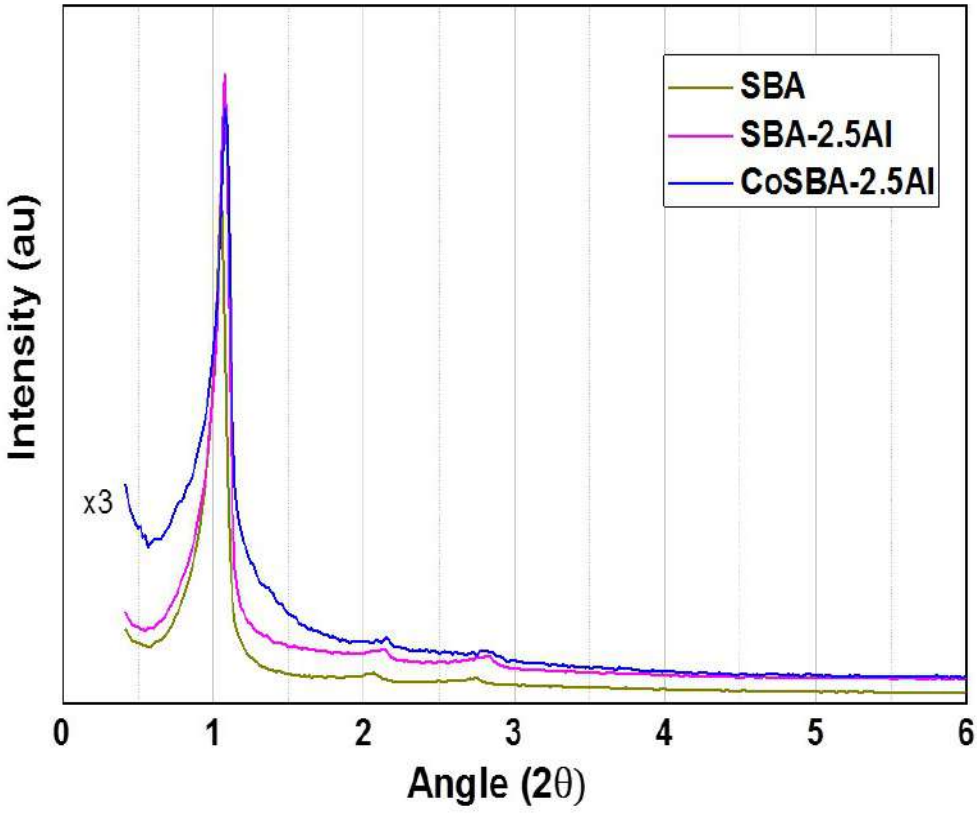

Figure S2. Small angle XRD for SBA, SBA-2.5Al and CoSBA-2.5Al samples

3) XRD patterns of the calcined CoSBA-xAl samples

Powder X-ray diffraction (XRD) patterns were recorded in the 10–90º 2θ range in the scan mode (0.04°, 500 s accumulation) using an X'Pert Pro PANalytical diffractometer with Cu $K_{\alpha 1,2}$ (λ = 0.15418 nm) radiation. The calcined sample diffractograms are shown in Figure S3, where for simplicity three diffraction patterns of the series have been displayed. Several diffraction peaks are observed, the most intense at 2θ = 31.2, 36.9, 59.2, and 63.2, which are associated with the Co_3O_4 spinel (1, JCPDS 00-001-1152) formed during the calcination in air.

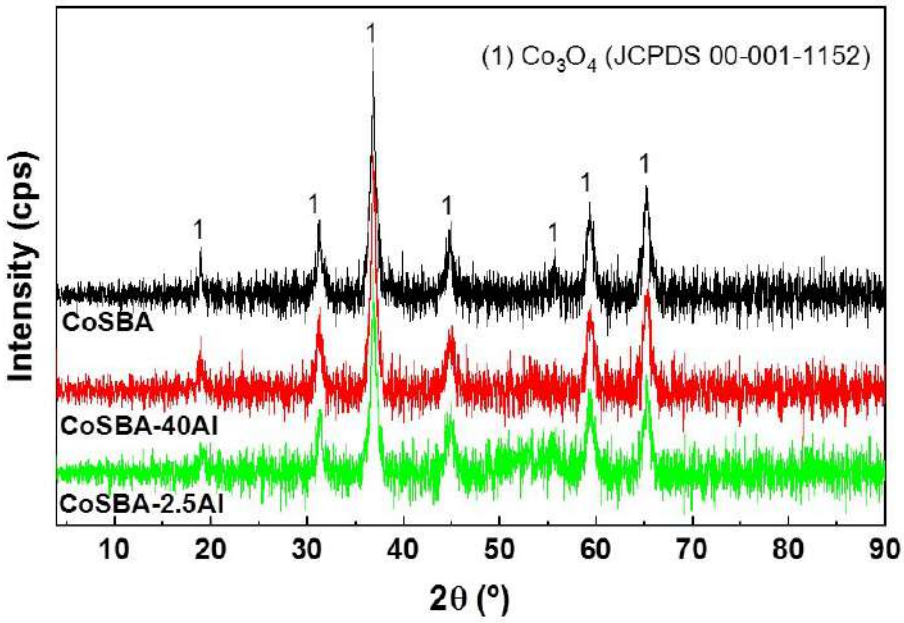

Figure S3. XRD patterns of calcined CoSBA-xAl samples

4) <u>DRIFS spectra after CD_3CN adsorption of the SBA-10Al acid support and reduced CoSBA-10Al catalyst</u>

Fig. S4A shows SBA-10Al spectra as an example of the band intensity evolution during the entire operation of CD_3CN adsorption and subsequent flushing with Ar at different temperatures and times. In addition to the two bands already assigned in the manuscript, a new band at lower frequencies 2266 cm^{-1} was observed, whereas a CD_3CN flow was going through the sample that is associated with the physisorbed CD_3CN [3,4]. After 5 minutes of flushing with a flow of Ar at room temperature this band disappears completely. The band assigned to adsorption on silanol groups (2272 cm^{-1}) rapidly decreases with the increase of the temperature and the flushing time. In contrast, the band associated with stronger acidity was maintained or even increases during the followed procedure**.**

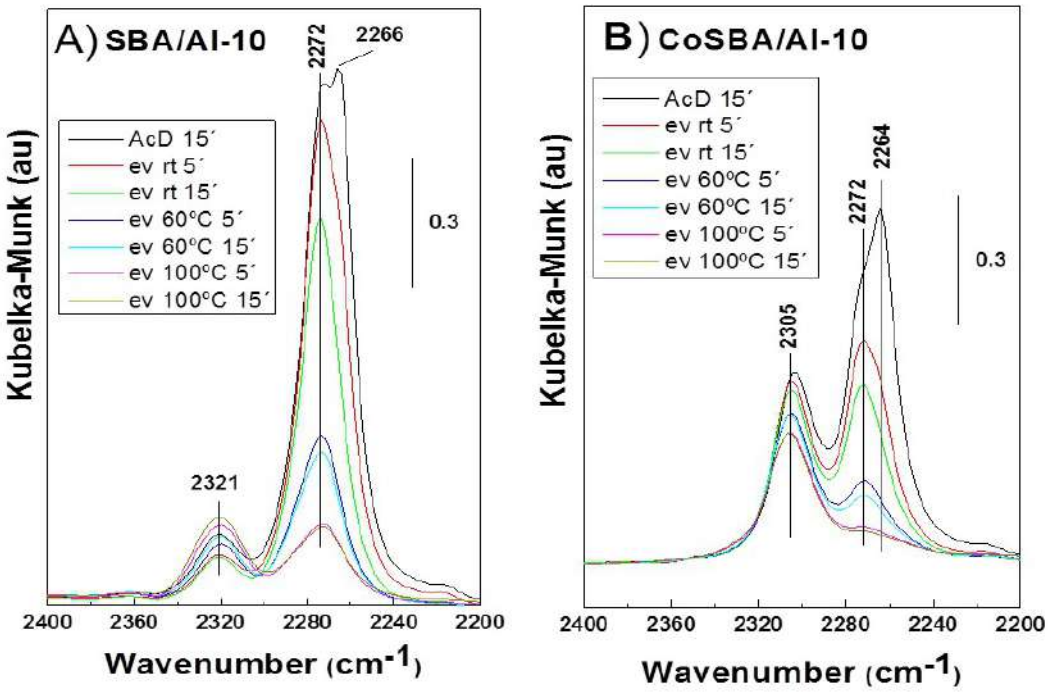

Figure S4. DRIFT spectra during the removal process of physiadsorbed AcD. A) SBA-10Al support and B) CoSBA-10Al catalysts

Parallel to the supports, Figure S4B shows the spectra obtained with CoSBA-10Al reduced catalyst where the band intensity evolution during the CD_3CN adsorption and subsequent flushing at different temperatures and times process is also collected. The intensity of the band associated with CD_3CN adsorbed on silanol groups (2272 cm^{-1}) is lower, whereas the band at 2305 cm^{-1} is more intense than the band 2321 cm^{-1} described previously on the support.

References

1 M. Gómez-Cazalilla, J. M. Mérida-Robles, A. Gurbani, E. Rodríguez-Castellón and A. Jiménez-López, *J. Solid State Chem.*, 2007, **180**, 1130–1140.

2 M. Kondeboina, S. S. Enumula, V. R. B. Gurram, R. R. Chada, D. R. Burri and S. R. R. Kamaraju, *J. Ind. Eng. Chem.*, 2018, **61**, 227–235.

3 R. Mariscal, M. López-Granados, J. L. G. Fierro, J. L. Sotelo, C. Martos and R. Van Grieken, *Langmuir*, 2000, **16**, 9460–9467.

4 D. Jamroz, J. Stangret and J. Lindgren, *J. Am. Chem. Soc.*, 1993, **115**, 6165–6168.

4. CONCLUSIONES

El presente trabajo se ha centrado en el estudio de la conversión directa del ácido levulínico en combustibles valéricos empleando catalizadores bifuncionales (función hidrogenante y ácida) para lograr la reacción en un único reactor (*one-pot*). Aunque el enfoque de esta Tesis Doctoral se ha dirigido principalmente a estudiar el papel de la función ácida, aportada normalmente por el soporte, las familias de catalizadores estudiados pueden agruparse de acuerdo con el metal hidrogenante seleccionado.

Catalizadores basados en Pd. Se ensayaron en fase líquida, en un reactor tipo *batch*, empleando una temperatura de reacción de 473 K y una presión de H_2 de 4 MPa con etanol como disolvente. En el primer trabajo se soportó un 2 % en peso de Pd sobre tres soportes comerciales: zeolitas beta, ZSM5 y una sílica-alúmina no cristalina (2PdBEA, 2PdZSM5, 2PdSA). Mientras que para un segundo artículo se sintetizó una serie de soportes en los que se modulaba las propiedades ácidas sustituyendo parcial o totalmente el Al de una zeolita tipo beta comercial por Zr. Tras la incorporación igualmente de un 2 % en peso de Pd, se obtenía una familia de catalizadores de acidez decreciente al incrementarse el grado de sustitución del Al por Zr, en proporción creciente de Zr: Pd/HBEA, Pd/ZAB-1.6, Pd/ZAB-0.1 y Pd/ZAB-0.0. De los ensayos realizados con estas dos series de catalizadores se concluye que:

- Tanto el 2PdBEA como el 2PdZSM5 han demostrado ser activos en la conversión directa del ácido levulínico a combustibles valéricos. Sin embargo, la acidez insuficiente del 2PdSA hace que no sea activo en la reacción. En el extremo opuesto, la acidez excesiva del 2PdBEA provocaba una mayor descomposición de los productos de interés. Se mostraba así que la acidez era un parámetro esencial en el comportamiento catalítico de los catalizadores bifuncionales.
- El 2PdZSM5 mostró ser el mejor de los 3 catalizadores ensayados proporcionando unos resultados prometedores, alcanzándose un **rendimiento a combustibles valéricos del 92 % transcurridas 8 horas de reacción**. Este catalizador demostró además ser estable en un reactor en flujo durante **más de 90 horas**. Sin embargo, en los catalizadores usados en *batch* se observó la presencia de depósitos carbonosos que mediante la calcinación eran eliminados.

- En el segundo trabajo, tanto de los resultados de actividad catalítica como de la caracterización de los catalizadores Pd/ZAB, se puede afirmar que los **centros ácidos Brønsted fuertes son los principales responsables de la reacción de apertura del anillo GVL,** etapa limitante de la reacción. Sin embargo, estos centros promueven también la descomposición de los productos de interés a tiempos más largos, por lo que es necesario un **compromiso para optimizar el rendimiento a combustibles valéricos**. En estos catalizadores se han identificado 3 diferentes centros ácidos de tipo Lewis: centros débiles asociados a Zr (2301 cm^{-1}) y centros moderados/fuertes asociados a Al (2318 y 2332 cm^{-1}) que son también responsables de la apertura del anillo de la GVL, pero con menor actividad intrínseca a medida que su fortaleza disminuye, y en cualquier caso siempre menor que los centros ácidos Brønsted fuertes.
- En cuanto a la estabilidad, la reutilización en *batch* (fase líquida) del mejor catalizador de la serie (Pd/HBEA) mostró un rendimiento a combustibles valéricos decreciente tras cada ciclo, pasando del **76 % en el primer ciclo, al 56 % en el tercero**. Esta caída se recuperaba solo parcialmente tras la calcinación, logrando un 63 % de rendimiento. **La presencia de Pd oxidado** podría explicar la **regeneración incompleta del catalizador junto con la identificación de una fase Al_2O_3 en el catalizador usado.**

Catalizadores basados en Co. *S*e empleó como soportes una serie de SBA-15 en la que se ha llevado a cabo la incorporación de Al por la sustitución parcial de los átomos de Si en proporción creciente: CoSBA, CoSBA-40Al, CoSBA-20Al, CoSBA-10Al, CoSBA-5Al y CoSBA-2.5Al. La ventaja de estos catalizadores es que evitan el uso del Pd, un metal noble, sustituyéndolo por el Co que es mucho más barato. Los ensayos de actividad de estos catalizadores se han llevado a cabo en un reactor en flujo en condiciones de fase gas. Los resultados experimentales obtenidos permiten concluir:

- Los catalizadores bifuncionales CoSBA-xAl han demostrado ser **activos en la conversión directa** del ácido levulínico en combustibles valéricos.

Además de esta ruta, una vez se ha formado el intermedio de gamma-valerolactona, la reacción puede dar lugar a una vía no selectiva con la que se obtiene 2-metiltetrahidrofurano y 1-pentanol**. La vía selectiva se ve favorecida a mayores contenidos de Al.** La presencia de Al en posiciones octaédricas y tetraédricas así como los iones Co^{2+} dan lugar a centros ácidos Lewis de diferente fortaleza en estos catalizadores y la proporción de los diferentes tipos de centros se ve afectada por el contenido de Al.

- El catalizador con mayor contenido en Al, el CoSBA-2.5Al, es el que da lugar a mejores rendimientos a valerato de etilo**, alcanzándose un 70 %** cuando el tiempo de contacto es el mayor de los empleados, 2 h^{-1}. Esta mayor actividad y selectividad es atribuida a la mayor densidad de Co^{2+} en la superficie del catalizador que aportan la acidez adecuada para la vía selectiva. A su vez, la mayor relación Co^{2+}/Co restringe la capacidad hidrogenante del catalizador, lo que resulta beneficioso para evitar la hidrogenación de la gamma-valerolactona que daría lugar a la vía no selectiva. Este catalizador ha mostrado una estabilidad prometedora a lo largo de más de 140 horas de reacción en flujo.

Se ha logrado así, a lo largo de los diferentes ensayos realizados, mostrar diversos catalizadores capaces de llevar a cabo la reacción de conversión directa del ácido levulínico en valerato de etilo y ácido valérico. Se ha analizado además diferentes variables entre las que cabe destacar el efecto de la acidez de los soportes en la actividad y selectividad del sistema catalítico. Se ha demostrado que la acidez es necesaria y que debe existir un compromiso entre acidez y capacidad reductora para llevar a cabo de manera óptima la reacción estudiada.

ANEXO I: Análisis de las muestras mediante cromatografía de gases

En el presente anexo, se describe el proceso para el análisis de los productos de reacción obtenidos en los ensayos de actividad catalítica, tanto en el reactor en flujo como en *batch*. Para ello se ha empleado un cromatógrafo de gases (Agilent 6890 N) con una columna capilar (ZB-WAX: 30 m x 0.32 mm x 0.50 µm) y un detector de ionización de llama (FID).

Antes de llevar a cabo el análisis de las muestras, se puso a punto el método cromatográfico con el que separar los diferentes analitos que podía encontrarse en la muestra. Modificando las variables cromatográficas, se logró un procedimiento para separar todas ellas obteniéndose un cromatograma como el de la figura siguiente.

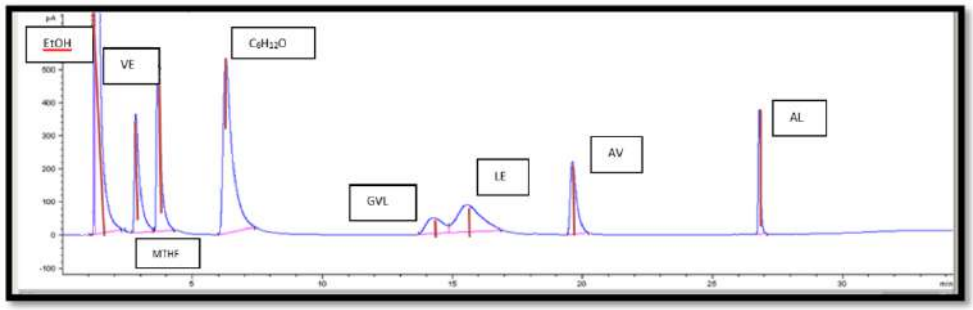

Como puede verse, la muestra patrón empleada para la puesta a punto del método contenía ácido levulínico (AL), levulinato de etilo (LE), gamma-valerolactona (GVL), ácido valérico (VA), valerato de etilo (VE), 2-metiltetrahidrofurano (MTHF) además del disolvente, etanol en este caso (EtOH) y el patrón interno elegido, el ciclohexanol ($C_6H_{12}O$). Tras ello, se prepararon diferentes patrones con concentración conocida de cada uno de los

analitos para determinar el factor de respuesta y poder cuantificar así en las muestras que se analizasen posteriormente.

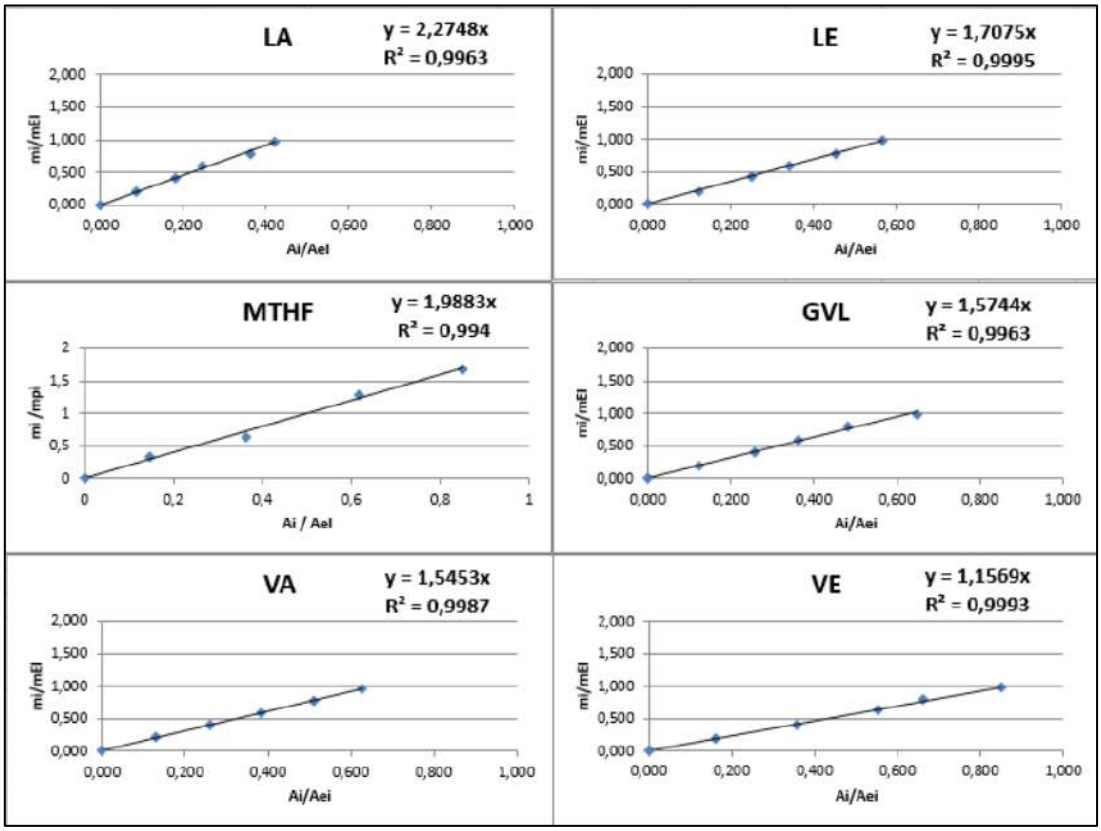

El cálculo del factor de respuesta se llevaba a cabo representando la relación de las masas del analito respecto de la del estándar interno (m_i/m_{EI}) frente a la relación de las áreas obtenidas para el analito frente al estándar interno (A_i/A_{EI}). La pendiente de la recta así obtenida se emplea para calcular, en muestras de concentración desconocida, el contenido en el analito una vez se conoce las áreas del mismo y del estándar interno así como la masa del estándar interno en la muestra.

Con esto, se estaba en condiciones de realizar análisis de las muestras desconocidas.

En cada reacción llevada a cabo, se tomó aproximadamente 4 gramos del líquido de reacción previamente filtrado con una jeringa acoplada a un filtro con diámetro de poro 0.22 µm de Millipore. Sobre esta alícuota, se añadió el patrón interno, en este caso, ciclohexanol, en cantidad aproximada de 0.05 gramos. 0.5 µL de la muestra así obtenida se inyectaba directamente en un cromatógrafo de gases con una microjeringa.

La identificación de los diferentes productos se llevaba a cabo en base al tiempo de elución al que se registraban en el cromatograma, mientras que el área del pico era empleada para calcular la cantidad del producto en cuestión que había en la muestra.